UNIVERSITY OF INSUBRIA

Department of Biotechnology and Life Sciences

Ph.D. Course in:

Analysis, Management and Protection of the Biodiversity Resources

XXVII cycle

COMPARATIVE TOXICOLOGICAL ANALYSIS OF IRON, COBALT AND NICKEL NANOPARTICLES IN THREE DIFFERENT *IN VITRO* MODELS

Coordinator: Prof. Flavia Marinelli

Tutor: Prof. Gianluca Molla

External supervisors: Dr. Federico Benetti

Dr. Enrico Sabbioni

Dissertation of:

Silvia Gabriella Ciappellano

2011/2014

TABLE OF CONTENTS

INTRODUCTION

1 Nanomaterials

1.1 Definition

Nanomaterials (NMs) are defined as materials having at least one dimension in the nanoscale range and, likewise, nanoparticles (NPs) consist of materials with all three dimensions in the nanoscale range (Buzea et al., 2007). According to the European Commission, NMs are constituted by material with 50 % or more of the particles in the number size distribution having one or more external dimensions in the range of 1-100 nm (European Commission, 2011). However, in nanomedicine the useful dimensional range is reported to fall within 5-250 nm (Garnett and Kallinteri, 2006).

1.2 Sources

NMs derive from natural or anthropogenic sources (Christian *et al.*, 2008; Dhawan and Sharma, 2010). They are produced in many natural processes, including photochemical reactions, volcanic eruptions, forest fires and simple erosion. These natural phenomena are estimated to generate 90% of nanoparticulate matter in air, while the remaining 10% ensues from human activity (Buzea *et al.*, 2007). Anthropogenic NMs can be divided into two categories: incidental and engineered/manufactured (Dhawan and Sharma, 2010). Incidental NMs, which are produced unintentionally, can derive from combustion and food cooking, chemical manufacturing, welding, combustion in vehicle and airplane engines, combustion of coal and fuel oil for power generation (Buzea *et al.*, 2007). Engineered NMs, according to their physico-chemical properties, are applicable in many fields and already present in market (Buzea *et al.*, 2007). This increasing development of nanotechnology (i.e. the design, synthesis, and application of engineered NMs) causes accidental or intended release of new materials in the environment (Christian *et al.*, 2008).

1.3 Engineered NMs

Engineered NMs can be categorized by their composition into organic, metallic, carbon-based, silicon-based and composite NMs (Christian *et al.*, 2008; Abhilash, 2010; Stone *et al.*, 2010).

Organic NMs include polymers, dendrymers and liposome NPs, and find many applications in nanomedicine, such as drug delivery (Abhilash, 2010).

Metal-based NMs, according to their physico-chemical properties, have widespread medical and industrial applications, as summarized in Table 1 (Schrand *et al.*, 2010).

TABLE 1. Examples of applications of metal-based NMs (from Schrand *et al.,* 2010).

Nanoparticle	Application
Silver (Ag)	Antimicrobial, photography, batteries, electrical
Aluminum (Al)	Fuel additive/propellant, explosive, wear resistant coating additive
Gold (Au)	Cellular imaging, photodynamic therapy
Cerium (CeO_2)	Polishing an computer chip manufacturing, fuel additive to decrease emissions
Copper (Cu)	Antimicrobial, nanocomposite coating, catalyst, lubricants, inks, filler materials for enhanced conductivity and wear resistance
Iron (Fe, Fe_3O_4, Fe_2O_3)	Magnetic imaging, environmental remediation
Manganese (Mn)	Catalyst, batteries
Nickel (Ni)	Conduction, catalyst, battery manufacturing, printing inks
Titanium dioxide (TiO_2)	Photocatalyst, antibacterial coating, sterilization, paint, cosmetics, sunscreens
Zinc (Zn, ZnO)	Skin protectant, sunscreens

Fullerenes and carbon nanotubes are the main carbon-based NMs (Christian *et al.*, 2008; Abhilash, 2010). The first are potentially useful in optics, superconductors and for drug delivery (Oberdörster *et al.*, 2007); the latter show important applications in energy storage and as nanoprobes and sensors in biological and chemical investigations (Ajayan and Zhou, 2001).

Silicon-based NMs, such as SiO_2 NPs, have great importance in industrial (such as the fabrication of electric and thermal insulators) and medical applications (as drug carrier, catalyst support and gene delivery) (Abhilash, 2010; Schrand *et al.*, 2010).

Composite NMs are a heterogeneous group comprising multi-component NMs (Stone *et al.*, 2010). Among them, quantum dots are fluorescent semiconductor nanocrystal with many biological applications, such as fluorescence labeling both in cellular and *in vivo* imaging (Michalet *et al.*, 2005).

1.4 Properties

The particular interest in NMs is related to the peculiar physico-chemical properties, which differ from their bulk counterpart (Nel *et al.*, 2006). The small size confers to these materials an exceptionally high surface area to volume ratio: as the particle size decreases, its surface area increases (Fig. 1) allowing a greater proportion of its atoms or molecules to be displayed on the surface rather than the interior of the material (Nel *et al.*, 2006; Christian *et al.*, 2008).

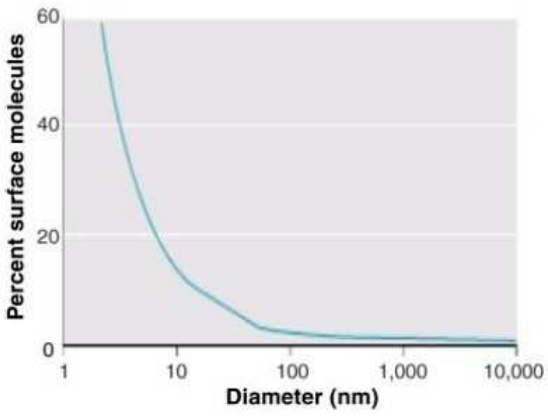

FIGURE 1. Inverse relationship between particle size and number of surface expressed molecules (from Nel et al., 2006).

The increased surface-to-volume ratio is responsible for enhanced NM reactivity (Christian *et al.*, 2008; Jones and Grainger, 2009) and their use in many application fields as catalysts and contrast agents. NM surfaces can also be modified with a wide range of molecules for biomedical purposes. For example, NPs can link specific markers and drugs for diagnostic and drug delivery (Jain, 2008; Dothager and Piwnica-Worms, 2011). Since NMs can bind and adsorb molecules, they are often stabilized with a range of small molecules (e.g. citrate), surfactants (e.g. sodium dodecyl sulphate, SDS) or polymers (e.g. polyvinylpyrrolidone, PVP, and polyethylene glycol, PEG) that are used for stabilizing them or to prevent opsonization (i.e. the binding of molecules, such as antibody, on the surface of NMs to enhance phagocytosis) in biomedical applications (Christian *et al.*, 2008; Pachón and Rothenberg, 2008).

Metal-based NPs, such as Pb, In, Hg, Sn, Cd, Ag and Au, exhibit size-dependent light absorption through excitation of the metal's plasma band electrons by incident photons and scattering of incident beam (Jones and Grainger, 2009). The plasmonic absorbance peak reflects NP size since decreases in intensity and red shifts are related to increase in NP diameter (Fig. 2).

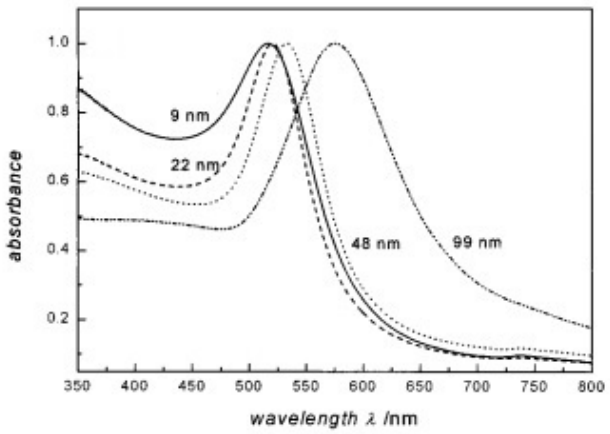

FIGURE 2. Uv-vis absorption spectra of 9, 22, 48 and 99 nm AuNP in water. All spectra are normalized at their maximum absorbance maxima (modified from Link and El-Sayed, 1999).

In addition, engineered NMs can be synthesized with different shape (e.g., spherical, rope-shaped, wire-shaped, rod-shaped etc.). Shape is important in determining the interaction with cells and in the development of NM-based targeting strategies for

therapeutic applications (Yang *et al.*, 2009; Fadeel and Garcia-Bennett, 2010; Sharifi *et al.*, 2012).

2 Nanotoxicology

The increased use of NMs and their consequent release in the environment give rise to many concerns regarding their fate in biological systems and their potential effects on human health and ecosystems. For these reasons, nanotoxicology was proposed as a branch of toxicology to address the potential toxic impacts of NMs on biological and ecological systems (Donaldson *et al.*, 2004).The peculiar physico-chemical properties of NMs differentiating them from bulk materials can influence their interaction with biological systems and pose challenges to classical toxicological assays (Dhawan and Sharma, 2010). Nanotoxicological studies require a much more extensive physico-chemical characterization than other chemical compounds, though the lack of standardized methodologies makes difficult to compare the safety/toxicity assessments from different research groups (Nel *et al.*, 2006; Buzea *et al.*, 2007; Dhawan and Sharma, 2010).

2.1 Physico-chemical properties affecting NM toxicity

The physico-chemical properties affecting NM toxicity are mainly attributable to their small size, surface chemistry, dissolution, shape and chemical composition (Nel *et al.*, 2006).

2.1.1 Size

Size is a critical parameter in determining NM properties and toxicological impacts. Many studies report a relationship between toxicity and size in both *in vitro* and *in vivo* systems. In particular, these studies showed higher toxic effects for small NPs than larger ones (Liu *et al.*, 2010; Gliga *et al.*, 2014; Ivask *et al.*, 2014; Zhang *et al.*, 2014). The negative correlation between size and toxicity is mediated by several factors, such as NM ability to cross biological barriers and cellular membranes (Buzea *et al.*, 2007; Freese *et al.*, 2012; Zhang *et al.*, 2014). Given the importance of size in influencing

possible toxic effects of NMs, their stability in biological media needs to be evaluated. Indeed, NMs tend to aggregate or agglomerate in gas or liquid suspensions (Oberdörster *et al.*, 2007). Agglomeration involves the adhesion of particles to each other, mainly due to Van der Waal's forces, while aggregation involves a fusion of particles [Fig. 3; (Stone *et al.*, 2009; Dhawan and Sharma, 2010)]. This means that agglomerates might be easily separated by dispersants or small amount of energy, while dispersion of aggregates is unlikely (Stone et al., 2009).

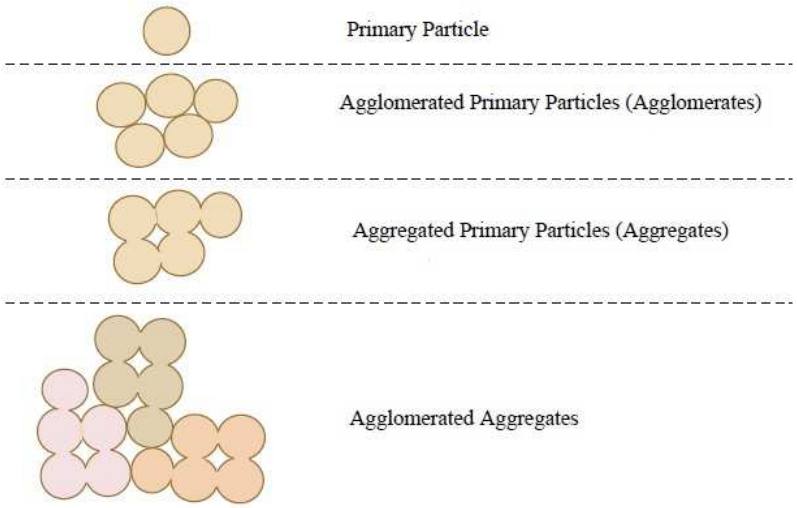

FIGURE 3. Agglomeration and aggregation of nanoparticles. Aggregates can additionally agglomerate (modified from Oberdöster et al., 2007).

Agglomeration depends on concentration, surface chemistry and suspension medium and, in the agglomeration state, NMs may behave as larger particles, depending on the size of agglomerates (Buzea *et al.*, 2007; Oberdörster *et al.*, 2007).

2.1.2 Surface chemistry

NM surface is responsible for the interactions with biological systems (Nel *et al.*, 2009). NM characteristics determining surface properties are chemical composition and surface functionalization (Nel *et al.*, 2009). Uncoated NMs, especially metal ones (MeNMs), undergo surface modifications in biological environments (Auffan *et al.*, 2009; Benetti *et al.*, 2014). The most common modifications are surface passivation, changes in surface charge, protein absorption, interactions with small molecules and ion release (Fig. 4).

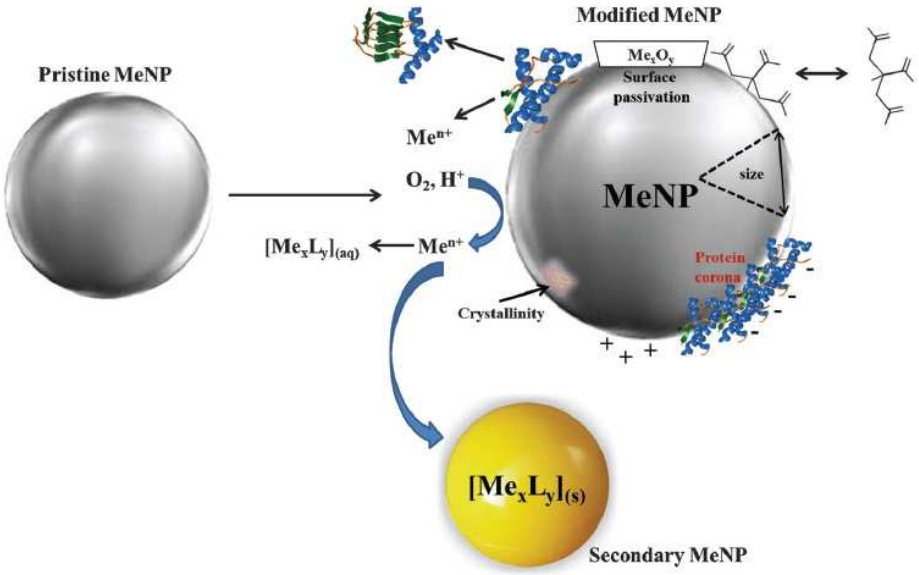

FIGURE 4. Chemical modifications of metal NP (MeNP) in biological environment: oxidative dissolution (Me^{n+}), surface passivation (Me_xO_y), changes in surface charge, protein adsorption and interactions with small molecules. The interaction of released ions with biological components can leads to soluble ($[Me_xL_y]_{aq}$) or insoluble ($[Me_xL_y]_s$) complexes. These latter may lead to the formation of secondary MeNP (from Benetti et al., 2014).

NM surfaces can be functionalized during their synthesis (Christian *et al.*, 2008; Pachón and Rothenberg, 2008). All these modifications can drastically change NM physico-chemical properties, such as agglomeration, magnetic, electric and optical properties, dissolution, chemical reactivity and toxicity (Nel *et al.*, 2006; Buzea *et al.*, 2007). For example, cationic NMs result to be more toxic than negative-charged ones as they have major affinity to the negative phospholipid head groups or protein domains on cell membranes (Sharifi *et al.*, 2012).

2.1.3 Dissolution

NM toxicity can be mediated by ion release in both biological media and intracellular compartments (Misra *et al.*, 2012; Sabbioni *et al.*, 2014). Understanding the role of ion release in NM toxicity is crucial to disclose molecular mechanisms affecting the impact of NM on biological systems. NP dissolution depends on several physico-chemical parameters as shown in Figure 5.

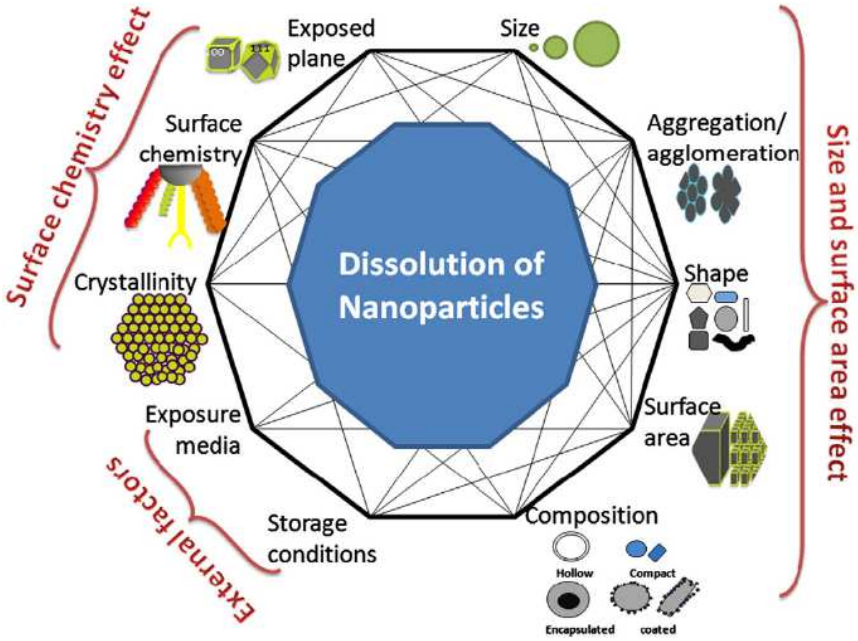

FIGURE 5. Physico-chemical factors affecting dissolution of NPs (from Misra *et al.*, 2012)

Size affects dissolution as showed by the higher ion release from small NPs compared to the larger ones (Zhang *et al.*, 2010; Zhang *et al.*, 2011; Xiu *et al.*, 2012; Wang *et al.*, 2014). Dissolution, indeed, follows the Gibb–Thomson effect, which predicts that MeNP with smaller radius of curvature are energetically unfavorable and subject to dissolution, having a higher equilibrium solubility than macroparticles (Batley and McLaughlin, 2007). Moreover, size affects dissolution by influencing the specific surface area and the number of NMs for the same mass/volume dose (Gliga *et al.*, 2014; Wang *et al.*, 2014). As dissolution involves NM surface, the presence of coatings can alter ion release (Kirchner *et al.*, 2005; Kittler *et al.*, 2010; Zook *et al.*, 2011; Gliga *et al.*, 2014; Wang *et al.*, 2014). Coated NMs are generally more stable in suspension than uncoated ones that agglomerate easily causing a slower dissolution kinetic due to the reduction of NP exposed surface area (Gliga *et al.*, 2014). Furthermore, dissolution can be also influenced by the nature of coatings, for example PVP-stabilized AgNPs show a higher degree of dissolution than citrate-coated ones (Kittler *et al.*, 2010; Zook *et al.*, 2011; Wang *et al.*, 2014). In addition to NM physico-chemical properties, experimental conditions – time, temperature, pH, NM concentration and medium composition – influence ion release (Kittler *et al.*, 2010). Increase in temperature and acidic pH lead to an increased

dissolution degree (Kittler *et al.*, 2010; Studer *et al.*, 2010; Zhang *et al.*, 2010). NM concentration has an effect on dissolution kinetics (Zhang *et al.*, 2011; Zook *et al.*, 2011). In particular, dissolution rate is positively related to concentration, whereas the possible agglomeration process could reduce initial dissolution kinetic (Zhang *et al.*, 2011; Zook *et al.*, 2011). Again, biological media have an important role in dissolution kinetics due to NM modifications (Benetti *et al.*, 2014). For example, fetal bovine serum in cell culture media prevents agglomeration of AgNPs and affects dissolution (Park *et al.*, 2010). Very few studies have focused on environmental transformations of NMs. Regarding AgNPs, the most common modification is the formation of a silver sulfide corrosion layer that is related to surface passivation and a reduction in dissolution (Levard *et al.*, 2011).

Until now, it was analyzed ion release occurring in environmental and biological solutions. Actually, NMs can enter into cells as particle and then dissolve (Benetti *et al.*, 2014; Ortega *et al.*, 2014; Sabbioni *et al.*, 2014). This mechanism, named Trojan Horse, is reported to be an important process leading to NM toxicity when extracellular dissolution cannot fully explain observed toxicity (Park *et al.*, 2010; Studer *et al.*, 2010; Cronholm *et al.*, 2013; Novak *et al.*, 2013; Ortega *et al.*, 2014).

2.1.4 Shape

Particle shape is an additional key factor that determines the toxicity of NMs (Sharifi *et al.*, 2012). Shape influences cellular uptake, organ clearance, agglomeration and aggregation, and ion release (Buzea *et al.*, 2007). Endocytosis of NPs is easier and faster compared to rod-shaped or fiber-like NPs (Sharifi *et al.*, 2012). Moreover, long fiber-like NMs appear to be not effectively cleared from respiratory tract due to the inability of macrophages to phagocytize them, so leading to accumulation and potential chronic toxic effects (Buzea *et al.*, 2007).

2.1.5 Chemical composition

Although size, surface area and shape are important parameters in conferring NM toxicity, chemistry composition has an important role in inducing oxidative stress and cellular machinery alterations (Sharifi *et al.*, 2012). Chemical composition appears to be

relevant when comparing different NMs with similar physical properties (Granchi *et al.*, 1998; Yang *et al.*, 2009; Cho *et al.*, 2012).

2.2 Assessment of NM toxicity

Due to the importance of NM in many application fields, it is very important to test their biological effects. However, the lacking of standard protocols in nanotoxicology makes difficult to compare studies from different laboratories and disclose the real impact on the environment and human health (Dhawan and Sharma, 2010)

2.2.1 NM characterization

To find a correlation between biological effects and NM properties, a comprehensive physico-chemical characterization is needed (Dhawan and Sharma, 2010). The physico-chemical properties commonly evaluated in nanotoxicology field are: size, shape, aggregation or agglomeration states, surface area and dissolution. As reported in Table 2, different methodological approaches can be used for determining these properties (Dhawan and Sharma, 2010; Fadeel and Garcia-Bennett, 2010; Love *et al.*, 2012).

TABLE 2. Nanoparticle properties and common characterization methods.

Physico-chemical properties	Characterization methods [a]
Size	TEM, SEM, AFM, DLS, UV-vis (for plasmonic NMs)
Shape	TEM, AFM
Agglomeration or aggregation state	DLS, UV-vis (for plasmonic NMs)
Surface area	BET
Dissolution	Ultracentrifugation or ultrafiltration coupled with ICP-MS and ion-selective electrode potentiometry

a: Acronyms: TEM, transmission electron microscopy; AFM, atomic force microscopy; DLS, dynamic light scattering;UV-vis, UV-visible spectroscopy; BET, nitrogen adsorption/desorption isotherm; ICP-MS, inductively coupled plasma mass spectrometry

Notably, different methods could provide different information, and sometimes a full physico-chemical characterization is hampered by the intrinsic properties of NMs. For example, TEM analysis provide information about primary size distribution of NMs but, in aggregate samples it is not always possible to recognize particle boundaries (Dhawan and Sharma, 2010; Tomaszewska *et al.*, 2013). Aggregation can also influence DLS analysis in particular for possible sedimentation of aggregates (Teeguarden *et al.*, 2007). Indeed, DLS provides information about the hydrodynamic radius and aggregation of NMs dispersed in solutions in relation to their Brownian motion and, consequently, is strongly affected by sedimentation (Dhawan and Sharma, 2010). Furthermore, it is not suitable to study polydisperse NMs (Dhawan and Sharma, 2010; Tomaszewska *et al.*, 2013). BET technique to study surface area is deeply affected by aggregation as it calculates specific surface area accessible to gases (Dhawan and Sharma, 2010). Finally, different techniques to study dissolution can lead to different information. Ultracentrifugation could overestimate ion release because of the presence of NMs in supernatant, while ultrafiltration measures only free ions or ions bound to small molecules able to pass through the pores, retaining protein-bounded ions. Ion-selective electrode potentiometry is interfered by complex matrices such as biological media (Bregoli *et al.*, 2013).

2.2.2 *In vitro* models

Nanotoxicology, as well as traditional toxicology, can study the effects of NMs using both *in vitro* and *in vivo* systems. The *in vitro* systems have obvious advantages, including the reduction of animal testing, the speed of results and the relatively lower cost compared to *in vivo* studies (Stone *et al.*, 2009; Hartung and Sabbioni, 2011). The ethical considerations about animal testing is taken in particular consideration as NM properties can be easily manipulated generating "new" material to be tested. For evaluating NM biocompatibility, *in vitro* methods are therefore considered useful in nanotoxicology research (Sharifi *et al.*, 2012). *In vitro* testing also permits to change physico-chemical parameters in order to investigate molecular mechanisms underlying NM toxicity (Stone *et al.*, 2009). The main disadvantage is that *in vitro* systems are not able to fully replicate the complex physiological interactions occurring in organisms

(Stone *et al.*, 2009). *In vitro* models can be represented by (i) primary cells, deriving from tissue explants or disaggregate tissues, usually considered the closest models for organs and (ii) cell lines, often derived from transformed or transfected cells which have lost basic proliferation control mechanisms. Cell lines are extensively used in nanotoxicology as they are easy to manage and present low batch-to-batch variability (Bregoli *et al.*, 2013). Usually, *in vitro* models are chosen to reflect a critical component of the exposure route (Love *et al.*, 2012; Bregoli *et al.*, 2013). There are four common exposure routes to NMs: ingestion, dermal contact, inhalation and injection (Sellers *et al.*, 2010; Love *et al.*, 2012). For each exposure route, different *in vitro* cell lines exist and some example are reported in Table 3. Systemic exposure to NMs can be studied using *in vitro* cell models mimicking liver and kidney (Bregoli *et al.*, 2013).

TABLE 3. Cell lines used in nanotoxicology research in relation to NP exposure.

Exposure route	Cell lines	References
Ingestion	Caco-2 (undifferentiated human colon cells)	Love *et al.*, 2012; Piret*et al.*, 2012; Gerloff *et al.*, 2013
Dermal	HaCaT (human keratinocytes), L929 (murine fibroblast), NIH3T3 (mouse embryonic fibroblasts)	Liu*et al.*, 2010; Yildirimer *et al.*, 2011; Love *et al.*, 2012
Inhalation	A549 (human lung epithelial cells), BEAS-2B human bronchial epithelium)	Simon-Deckers *et al.*, 2008; Yildirimer *et al.*, 2011; Love *et al.*, 2012; Wan*et al.*, 2012
Injection and systemic exposure	THP-1 (human monocytes), HepG2 (human hepatocytes), HEK 293 (human embryonic kidney cells)	Cui *et al.*, 2005; Kawata *et al.*, 2009; Su *et al.*, 2010; Yildirimer *et al.*, 2011; Lankoff *et al.,* 2012; Smith *et al.*, 2012;

2.2.3 *In vitro* toxicity assessment

The most commonly *in vitro* techniques used for studying NM toxicity are based on the evaluation of cell viability by analyzing different cellular processes, such as metabolic

activity, DNA synthesis, colony formation and membrane integrity (Marquis *et al.*, 2009). However, the peculiar physico-chemical properties of NMs can alter the results of common assays (Monteiro-Riviere *et al.*, 2009; Han *et al.*, 2011; Kroll *et al.*, 2012; Love *et al.*, 2012). In particular, NMs can interfere at different levels: (i) optically interference with dye or probe; (ii) promoting the conversion of the substrates used in the assays; (iii) and influencing enzymatic activity (Kroll *et al.*, 2012). Generally, the interferences due to the presence of NMs can be overcame by NM removal from the medium before performing *in vitro* assays (Kroll *et al.*, 2012). In some cases, interferences can be mediated by released ions, so resulting to be dependent on NM chemical composition (Han *et al.*, 2011; Kroll *et al.*, 2012). Han *et al.,* (2011) have shown that lactate dehydrogenase (LDH) assay was not suitable for evaluating cytotoxicity of metallic copper NPs (CuNPs). This assay evaluates cellular membrane damages by analyzing the activity of LDH released in cell culture medium from damaged cells. CuNPs were found to release Cu^{2+} ions that inhibit LDH activity (Han *et al.*, 2011). Fluorescence-based assays can be interfered by metallic NMs or their ions, as for cobalt and nickel. These metals quench the fluorescence signal of molecular probes altering *in vitro* assay results (Atherton and Beaumont, 1986; Fabbrizzi *et al.*, 1996). Parallel to viability assays, *in vitro* NM uptake is also important to investigate NM toxicity since it provides a better understanding of NM toxicity mechanisms (Marquis *et al.*, 2009).

2.3 Mechanisms of NM toxicity

The extensive use of NMs in many application fields raises questions about safety. NMs are able to enter into organisms through both physiological and non-physiological routes leading to the internalization of non-essential elements (Benetti *et al.*, 2014). Once internalized, NMs undergo modifications affecting biodistribution, cellular internalization, ion release and toxicity (Benetti *et al.*, 2014).

From a mechanistic perspective, NMs induce different effects on biological systems that can lead to different pathophysiological outcomes (Table 4).

TABLE 4. NM effects and potential toxicological outcomes (from Somwanshi *et al.,* 2013)

Experimental NM effects	Potential pathophysiological outcomes
ROS generation	Protein, DNA and membrane injury, oxidative stress
Oxidative stress	Phase II enzyme induction, inflammation, mitochondrial perturbation
Mitochondrial perturbation	Inner membrane damage, permeability transition pore opening, energy failure, apoptosis, apo-necrosis, cytotoxicity
Inflammation	Tissue infiltration with inflammatory cells, fibrosis, granulomas, atherogenesis, acute phase protein expression (e.g., C-reactive protein)
Uptake by reticulo-endothelial system	Asymptomatic sequestration and storage in liver, spleen, lymphnodes, possible organ enlargement and dysfunction
Protein denaturation, degradation	Loss of enzyme activity, auto-antigenicity
Nuclear uptake	DNA damage, nucleoprotein clumping, autoantigens
Uptake in neuronal tissue	Brain and peripheral nervous system injury
Perturbation of phagocytic function, "particle overload," mediator release	Chronic inflammation, fibrosis, granulomas, interference in clearance of infectious agents
Endothelial dysfunction, effects on blood clotting	Atherogenesis, thrombosis, stroke, myocardial infarction
Generation of neoantigens, breakdown in immune tolerance	Autoimmunity, adjuvant effects
Altered cell cycle regulation	Proliferation, cell cycle arrest, senescence
DNA damage	Mutagenesis, metaplasia, carcinogenesis

Reactive oxygen species (ROS) generation and the consequent oxidative stress is currently the best-developed paradigm for NM toxicity (Nel *et al.*, 2006). In particular, the enhancement of ROS generation by NMs can occur at different levels, including: (i)

the chemical reactivity of both particles and related impurities; (ii) the physical interaction of NMs with cellular structures, such as the plasma membrane, mitochondria and the endoplasmic reticulum; involved in the catalysis of biological reduction-oxidation processes; (iii) and the depletion of antioxidant defenses (Unfried *et al.*, 2007). Furthermore, the release of transition metal ions deriving from NM dissolution or from particle impurities can catalyze Fenton-like reactions (Eq. 1) resulting in hydroxyl radicals, the depletion of antioxidant mechanisms and oxidative stress generation (Stohs and Bagchi, 1995; Nel *et al.*, 2006).

$$M(X) + O_2^{\cdot -} \rightarrow M(X\text{-}1) + O_2$$
$$2O_2^{\cdot -} + 2H^+ \rightarrow H_2O_2 + O_2$$
$$M(X\text{-}1) + H_2O_2 \rightarrow M(X) + {}^{\cdot}OH + OH$$

EQUATION 1. Fenton-like reaction generated by a transition metal (M) leading to the formation of hydroxyl radical (·OH). (from Stohs and Bagchi, 1995)

The induction of ROS can also cause oxidative DNA damage that leads to base pair mutations, deletions or insertions (Unfried *et al.*, 2007). NMs and their released ions can also interact with proteins leading to possible loss of functionality, such as the inhibition of enzyme activities (Somwanshi *et al.*, 2013; Benetti *et al.*, 2014). For example, Cd^{2+}released by CdSe quantum dots leads to cell death by binding to sulfhydryl groups of proteins, especially mitochondrial proteins (Benetti *et al.*, 2014). Moreover, genome integrity can also be affected by the inhibition of DNA repair processes. In particular, this phenomenon could be relevant considering released soluble metals from NMs that interfere with this processes, such as arsenic, iron or copper (Kawanishi *et al.*, 2002; Kessel *et al.*, 2002).

With particular reference to insoluble NMs, they have been usually associated to lower acute toxic effects (Brunner *et al.*, 2006). However, this property can be also associated to accumulation and biopersistence within the biological system and, as a consequence, may provoke a range of late effects (Borm *et al.*, 2006; Brunner *et al.*, 2006).

3 References

Abhilash M. (2010). Potential applications of Nanoparticles. *Int. J. Pharm. Biol. Sci.* 1(1).

Ajayan P. M. and Zhou O. Z. (2001). Applications of carbon nanotubes. *Carbon nanotubes*. Berlin, Springer: 391-425.

Atherton S. J. and Beaumont P. C. (1986). Quenching of the fluorescence of DNA-intercalated ethidium bromide by some transition-metal ions. *J. Phys. Chem.* 90(10): 2252-2259.

Auffan M., Rose J., Wiesner M. R. and Bottero J.-Y. (2009). Chemical stability of metallic nanoparticles: a parameter controlling their potential cellular toxicity in vitro. *Environ. Pollut.* 157(4): 1127-1133.

Batley G. and McLaughlin M. J. (2007). Fate of manufactured nanomaterials in the Australian environment. *CSIRO Niche Manufacturing Flagship Report for the Department of Sustainability, Environment, Water, Population and Communities*.

Benetti F., Bregoli L., Olivato I. and Sabbioni E. (2014). Effects of metal (loid)-based nanomaterials on essential element homeostasis: The central role of nanometallomics for nanotoxicology. *Metallomics* 6(4): 729-747.

Borm P., Klaessig F. C., Landry T. D., Moudgil B., Pauluhn J., Thomas K., Trottier R. and Wood S. (2006). Research strategies for safety evaluation of nanomaterials, part V: role of dissolution in biological fate and effects of nanoscale particles. *Toxicol. Sci.* 90(1): 23-32.

Bregoli L., Benetti F., Venturini M. and Sabbioni E. (2013). ECSIN's methodological approach for hazard evaluation of engineered nanomaterials. *J. Phys.Conf. Ser.*, IOP Publishing.

Brunner T. J., Wick P., Manser P., Spohn P., Grass R. N., Limbach L. K., Bruinink A. and Stark W. J. (2006). In vitro cytotoxicity of oxide nanoparticles: comparison to

asbestos, silica, and the effect of particle solubility. *Environ. Sci. Technol.* 40(14): 4374-4381.

Buzea C., Pacheco I. I. and Robbie K. (2007). Nanomaterials and nanoparticles: sources and toxicity. *Biointerphases* 2(4): MR17-MR71.

Cho W.-S., Duffin R., Thielbeer F., Bradley M., Megson I. L., MacNee W., Poland C. A., Tran C. L. and Donaldson K. (2012). Zeta potential and solubility to toxic ions as mechanisms of lung inflammation caused by metal/metal-oxide nanoparticles. *Toxicol. Sci.*: kfs006.

Christian P., Von der Kammer F., Baalousha M. and Hofmann T. (2008). Nanoparticles: structure, properties, preparation and behaviour in environmental media. *Ecotoxicology* 17(5): 326-343.

Cronholm P., Karlsson H. L., Hedberg J., Lowe T. A., Winnberg L., Elihn K., Wallinder I. O. and Moller L. (2013). Intracellular uptake and toxicity of Ag and CuO nanoparticles: a comparison between nanoparticles and their corresponding metal ions. *Small* 9(7): 970-982.

Cui D., Tian F., Ozkan C. S., Wang M. and Gao H. (2005). Effect of single wall carbon nanotubes on human HEK293 cells. *Toxicol. Lett.* 155(1): 73-85.

Dhawan A. and Sharma V. (2010). Toxicity assessment of nanomaterials: methods and challenges. *Anal. Bioanal. Chem.* 398(2): 589-605.

Donaldson K., Stone V., Tran C., Kreyling W. and Borm P. J. (2004). Nanotoxicology. *Occup. Environm.* Med. 61(9): 727-728.

Dothager R. S. and Piwnica-Worms D. (2011). Nano in Cancer: Linking Chemistry, Biology, and Clinical Applications In Vivo. *Cancer Res.* 71(17): 5611-5615.

European Commission. Commission Recommendation of 18 October 2011 on the definition of nanomaterial. .*Secondary Commission Recommendation of 18 October 2011 on the definition of nanomaterial.* L 275: 38-40.

Fabbrizzi L., Licchelli M., Pallavicini P., Sacchi D. and Taglietti A. (1996). Sensing of transition metals through fluorescence quenching or enhancement. A review. *Analyst* 121(12): 1763-1768.

Fadeel B. and Garcia-Bennett A. E. (2010). Better safe than sorry: understanding the toxicological properties of inorganic nanoparticles manufactured for biomedical applications. *Adv. Drug Deliver. Rev.* 62(3): 362-374.

Freese C., Gibson M. I., Klok H.-A., Unger R. E. and Kirkpatrick C. J. (2012). Size-and coating-dependent uptake of polymer-coated gold nanoparticles in primary human dermal microvascular endothelial cells. *Biomacromolecules* 13(5): 1533-1543.

Garnett M. C. and Kallinteri P. (2006). Nanomedicines and nanotoxicology: some physiological principles. *Occ. Med.* 56(5): 307-311.

Gerloff K., Pereira D. I., Faria N., Boots A. W., Kolling J., Förster I., Albrecht C., Powell J. J. and Schins R. P. (2013). Influence of simulated gastrointestinal conditions on particle-induced cytotoxicity and interleukin-8 regulation in differentiated and undifferentiated Caco-2 cells. *Nanotoxicology* 7(4): 353-366.

Gliga A. R., Skoglund S., Wallinder I. O., Fadeel B. and Karlsson H. L. (2014). Size-dependent cytotoxicity of silver nanoparticles in human lung cells: the role of cellular uptake, agglomeration and Ag release. *Part. Fibre Toxicol.* 11(1): 11.

Granchi D., Cenni E., Ciapetti G., Savarino L., Stea S., Gamberini S., Gori A. and Pizzoferrato A. (1998). Cell death induced by metal ions: necrosis or apoptosis? *J. Mater. Sci. Mater. Med.* 9(1): 31-37.

Han X., Gelein R., Corson N., Wade-Mercer P., Jiang J., Biswas P., Finkelstein J. N., Elder A. and Oberdorster G. (2011). Validation of an LDH assay for assessing nanoparticle toxicity. *Toxicology* 287(1-3): 99-104.

Hartung T. and Sabbioni E. (2011). Alternative in vitro assays in nanomaterial toxicology. *Wiley Interdiscip. Rev. Nanomed. Nanobiotechnol.*

Ivask A., Kurvet I., Kasemets K., Blinova I., Aruoja V., Suppi S., Vija H., Käkinen A., Titma T. and Heinlaan M. (2014). Size-Dependent Toxicity of Silver Nanoparticles to Bacteria, Yeast, Algae, Crustaceans and Mammalian Cells In Vitro. *PloS one* 9(7): e102108.

Jain K. (2008). Nanomedicine: application of nanobiotechnology in medical practice. *Med. Prin. Pract.* 17(2): 89-101.

Jones C. F. and Grainger D. W. (2009). In vitro assessments of nanomaterial toxicity. *Adv. Drug Deliver. Rev.* 61(6): 438-456.

Kawanishi S., Hiraku Y., Murata M. and Oikawa S. (2002). The role of metals in site-specific DNA damage with reference to carcinogenesis. *Free Radic. Biol. Med.* 32(9): 822-832.

Kawata K., Osawa M. and Okabe S. (2009). In vitro toxicity of silver nanoparticles at noncytotoxic doses to HepG2 human hepatoma cells. *Environ. Sci. Technol.* 43(15): 6046-6051.

Kessel M., Liu S. X., Xu A., Santella R. and Hei T. K. (2002). Arsenic induces oxidative DNA damage in mammalian cells. *Mol. Cell. Biochem.* 234-235(1-2): 301-308.

Kirchner C., Liedl T., Kudera S., Pellegrino T., Munoz Javier A., Gaub H. E., Stolzle S., Fertig N. and Parak W. J. (2005). Cytotoxicity of colloidal CdSe and CdSe/ZnS nanoparticles. *Nano Lett.* 5(2): 331-338.

Kittler S., Greulich C., Diendorf J., Koller M. and Epple M. (2010). Toxicity of silver nanoparticles increases during storage because of slow dissolution under release of silver ions. *Chem. Mater.* 22(16): 4548-4554.

Kroll A., Pillukat M. H., Hahn D. and Schnekenburger J. (2012). Interference of engineered nanoparticles with in vitro toxicity assays. *Arch. Toxicol.* 86(7): 1123-1136.

Lankoff A., Sandberg W. J., Wegierek-Ciuk A., Lisowska H., Refsnes M., Sartowska B., Schwarze P. E., Meczynska-Wielgosz S., Wojewodzka M. and Kruszewski M.

(2012). The effect of agglomeration state of silver and titanium dioxide nanoparticles on cellular response of HepG2, A549 and THP-1 cells. *Toxicol. Let.* 208(3): 197-213.

Levard C., Reinsch B. C., Michel F. M., Oumahi C., Lowry G. V. and Brown G. E. (2011). Sulfidation processes of PVP-coated silver nanoparticles in aqueous solution: impact on dissolution rate. *Environ. Sci. Technol.* 45(12): 5260-5266.

Link S. and El-Sayed M. A. (1999). Size and temperature dependence of the plasmon absorption of colloidal gold nanoparticles. *J. Phys. Chem. B* 103(21): 4212-4217.

Liu W., Wu Y., Wang C., Li H. C., Wang T., Liao C. Y., Cui L., Zhou Q. F., Yan B. and Jiang G. B. (2010). Impact of silver nanoparticles on human cells: effect of particle size. *Nanotoxicology* 4(3): 319-330.

Love S. A., Maurer-Jones M. A., Thompson J. W., Lin Y.-S. and Haynes C. L. (2012). Assessing nanoparticle toxicity. *Annu. Rev. Anal. Chem.* 5: 181-205.

Marquis B. J., Love S. A., Braun K. L. and Haynes C. L. (2009). Analytical methods to assess nanoparticle toxicity. *Analyst* 134(3): 425-439.

Michalet X., Pinaud F. F., Bentolila L. A., Tsay J. M., Doose S., Li J. J., Sundaresan G., Wu A. M., Gambhir S. S. and Weiss S. (2005). Quantum dots for live cells, in vivo imaging, and diagnostics. *Science* 307(5709): 538-544.

Misra S. K., Dybowska A., Berhanu D., Luoma S. N. and Valsami-Jones E. (2012). The complexity of nanoparticle dissolution and its importance in nanotoxicological studies. *Sci. Total Environ.* 438: 225-232.

Monteiro-Riviere N. A., Inman A. O. and Zhang L. W. (2009). Limitations and relative utility of screening assays to assess engineered nanoparticle toxicity in a human cell line. *Toxicol. Appl. Pharmacol.* 234(2): 222-235.

Nel A., Xia T., Mädler L. and Li N. (2006). Toxic potential of materials at the nanolevel. *Science* 311(5761): 622-627.

Nel A. E., Madler L., Velegol D., Xia T., Hoek E. M., Somasundaran P., Klaessig F., Castranova V. and Thompson M. (2009). Understanding biophysico-chemical interactions at the nano-bio interface. *Nat. Mater.* 8(7): 543-557.

Novak S., Drobne D., Golobic M., Zupanc J., Romih T., Gianoncelli A., Kiskinova M., Kaulich B., Pelicon P., Vavpetic P., Jeromel L., Ogrinc N. and Makovec D. (2013). Cellular internalization of dissolved cobalt ions from ingested CoFe2O4 nanoparticles: in vivo experimental evidence. *Environ. Sci. Technol.* 47(10): 5400-5408.

Oberdörster G., Stone V. and Donaldson K. (2007). Toxicology of nanoparticles: a historical perspective. *Nanotoxicology* 1(1): 2-25.

Ortega R., Bresson C., Darolles C., Gautier C., Roudeau S., Perrin L., Janin M., Floriani M., Aloin V. and Carmona A. (2014). Low-solubility particles and a Trojan-horse type mechanism of toxicity: the case of cobalt oxide on human lung cells. *Part. Fibre Toxicol.* 11(1): 14.

Pachón L. D. and Rothenberg G. (2008). Transition-metal nanoparticles: synthesis, stability and the leaching issue. *Appl. Organomet. Chem.* 22(6): 288-299.

Park E. J., Yi J., Kim Y., Choi K. and Park K. (2010). Silver nanoparticles induce cytotoxicity by a Trojan-horse type mechanism. *Toxicol. In Vitro* 24(3): 872-878.

Piret J.-P., Vankoningsloo S., Mejia J., Noël F., Boilan E., Lambinon F., Zouboulis C. C., Masereel B., Lucas S. and Saout C. (2012). Differential toxicity of copper (II) oxide nanoparticles of similar hydrodynamic diameter on human differentiated intestinal Caco-2 cell monolayers is correlated in part to copper release and shape. *Nanotoxicology* 6(7): 789-803.

Sabbioni E., Fortaner S., Farina M., Del Torchio R., Petrarca C., Bernardini G., Mariani-Costantini R., Perconti S., Di Giampaolo L., Gornati R. and Di Gioacchino M. (2014). Interaction with culture medium components, cellular uptake and intracellular distribution of cobalt nanoparticles, microparticles and ions in Balb/3T3 mouse fibroblasts. *Nanotoxicology* 8(1): 88-99.

Schrand A. M., Rahman M. F., Hussain S. M., Schlager J. J., Smith D. A. and Syed A. F. (2010). Metal-based nanoparticles and their toxicity assessment. *Wiley Interdiscip Rev Nanomed Nanobiotechnol* 2(5): 544-568.

Sellers K., Mackay C., Bergeson L. L., Clough S. R., Hoyt M., Chen J., Henry K. and Hamblen J. (2010). Nanotechnology and the Environment. *CRC Press*, pp.281.

Sharifi S., Behzadi S., Laurent S., Forrest M. L., Stroeve P. and Mahmoudi M. (2012). Toxicity of nanomaterials. *Chem. Soc. Rev* 41(6): 2323-2343.

Simon-Deckers A., Gouget B., Mayne-L'Hermite M., Herlin-Boime N., Reynaud C. and Carriere M. (2008). In vitro investigation of oxide nanoparticle and carbon nanotube toxicity and intracellular accumulation in A549 human pneumocytes. *Toxicology* 253(1): 137-146.

Smith W. E., Brownell J., White C. C., Afsharinejad Z., Tsai J., Hu X., Polyak S. J., Gao X., Kavanagh T. J. and Eaton D. L. (2012). In vitro toxicity assessment of amphiphillic polymer-coated CdSe/ZnS quantum dots in two human liver cell models. *ACS Nano* 6(11): 9475-9484.

Somwanshi S., Dolas R., Siddheshwar S., Merekar A., Godge R. and Pattan S. (2013). Nanomedicine Drug Delivery System. *Asian J. Biomed. Phar. Sci.* 3(22): 9-15.

Stohs S. and Bagchi D. (1995). Oxidative mechanisms in the toxicity of metal ions. *Free Radic. Biol. Med.* 18(2): 321-336.

Stone V., Johnston H. and Schins R. P. (2009). Development of in vitro systems for nanotoxicology: methodological considerations. *Crit. Rev. Toxicol.* 39(7): 613-626.

Stone V., Nowack B., Baun A., van den Brink N., von der Kammer F., Dusinska M., Handy R., Hankin S., Hassellöv M. and Joner E. (2010). Nanomaterials for environmental studies: Classification, reference material issues, and strategies for physico-chemical characterisation. *Sci. Total Enviro.* 408(7): 1745-1754.

Studer A. M., Limbach L. K., Van Duc L., Krumeich F., Athanassiou E. K., Gerber L. C., Moch H. and Stark W. J. (2010). Nanoparticle cytotoxicity depends on intracellular solubility: comparison of stabilized copper metal and degradable copper oxide nanoparticles. *Toxicol. Lett.* 197(3): 169-174.

Su Y., Hu M., Fan C., He Y., Li Q., Li W., Wang L.-h., Shen P. and Huang Q. (2010). The cytotoxicity of CdTe quantum dots and the relative contributions from released cadmium ions and nanoparticle properties. *Biomaterials* 31(18): 4829-4834.

Teeguarden J. G., Hinderliter P. M., Orr G., Thrall B. D. and Pounds J. G. (2007). Particokinetics in vitro: dosimetry considerations for in vitro nanoparticle toxicity assessments. *Toxicol. Sci.* 95(2): 300-312.

Tomaszewska E., Soliwoda K., Kadziola K., Tkacz-Szczesna B., Celichowski G., Cichomski M., Szmaja W. and Grobelny J. (2013). Detection limits of DLS and UV-Vis spectroscopy in characterization of polydisperse nanoparticles colloids. *J. Nanomater.* 2013: 60.

Unfried K., Albrecht C., Klotz L.-O., Von Mikecz A., Grether-Beck S. and Schins R. P. (2007). Cellular responses to nanoparticles: target structures and mechanisms. *Nanotoxicology* 1(1): 52-71.

Wan R., Mo Y., Feng L., Chien S., Tollerud D. J. and Zhang Q. (2012). DNA damage caused by metal nanoparticles: involvement of oxidative stress and activation of ATM. *Chem. Res. Toxicol.* 25(7): 1402-1411.

Wang X., Ji Z., Chang C. H., Zhang H., Wang M., Liao Y. P., Lin S., Meng H., Li R. and Sun B. (2014). Use of coated silver nanoparticles to understand the relationship of particle dissolution and bioavailability to cell and lung toxicological potential. *Small* 10(2): 385-398.

Xiu Z.-m., Zhang Q.-b., Puppala H. L., Colvin V. L. and Alvarez P. J. (2012). Negligible particle-specific antibacterial activity of silver nanoparticles. *Nano Lett.* 12(8): 4271-4275.

Yang H., Liu C., Yang D., Zhang H. and Xi Z. (2009). Comparative study of cytotoxicity, oxidative stress and genotoxicity induced by four typical nanomaterials: the role of particle size, shape and composition. *J. Appl. Toxicol.* 29(1): 69-78.

Yildirimer L., Thanh N. T., Loizidou M. and Seifalian A. M. (2011). Toxicology and clinical potential of nanoparticles. *Nano Today* 6(6): 585-607.

Zhang H., Chen B. and Banfield J. F. (2010). Particle size and pH effects on nanoparticle dissolution. *J. Phys. Chem.* C 114(35): 14876-14884.

Zhang T., Wang L., Chen Q. and Chen C. (2014). Cytotoxic potential of silver nanoparticles. *Yonsei Med. J.* 55(2): 283-291.

Zhang W., Yao Y., Sullivan N. and Chen Y. (2011). Modeling the primary size effects of citrate-coated silver nanoparticles on their ion release kinetics. *Environ. Sci. Technol.* 45(10): 4422-4428.

Zook J. M., Long S. E., Cleveland D., Geronimo C. L. and MacCuspie R. I. (2011). Measuring silver nanoparticle dissolution in complex biological and environmental matrices using UV-visible absorbance. *Anal. Bioanal. Chem.* 401(6): 1993-2002.

AIM OF WORK

Since the biological behavior of NPs depends on parameters such as size, shape, surface area and aggregation state, the safety evaluation of NMs cannot rely on the toxicological profile of the bulk material that has been historically determined. This has also led to conclude that the biological evaluation of NMs should be performed on a case by case basis, making more complicated the risk assessment process for NMs. However, no experimental study has been dedicated to the possible anticipation of toxicological properties of NPs on the basis of certain affinity of their chemical nature. This study intends to be a contribution to fill this gap. We consider the case of zerovalent NPs derived from three transition metals such as Fe, Co, Ni, that are elements belonging to the main transition group or *d- block* and sharing ferromagnetic properties. Despite their chemical similarities, these elements have a different physiological role in living systems. Iron plays important role for many biological processes (e.g. oxygen transport in vertebrates; catalysis in enzymatic reactions involved in cellular respiration and oxidation/reduction processes). Cobalt physiological function is confined to vitamin B_{12}, which is involved in different reaction as a coenzyme (i.e. reduction of ribose to deoxyribose; the rearrangement of diols and similar molecules; the rearrangement of malonyl to succynil; and the transfer of methyl group). In mammals, no essential role of nickel has been described yet. However, this metal is involved in some dihydrogen reactions in symbiotic anaerobic bacteria and in keeping ammonia balance in some plants and animals where it is present in the active site of urease. As nanomaterials, Fe, Co and Ni rise great interest for a wide range of applications, such as magnetic fluids, catalysis, biomedicine (such as contrast agents in magnetic resonance imaging, theranostics agents in tumor therapy and site-specific drug delivery agents), magnetic energy storage, information storage and environmental remediation to treat toxic contaminants. In relation to their potential nanotechnological applications and to the consequent increase in human and environmental exposure, studies dealing with their toxicological effect are needed.

Objectives

The present research is focused on the comprehension of the toxicity of a specific category of inorganic engineered nanoparticles (NPs): zerovalent FeNPs, CoNPs and NiNPs. Three biological systems mimicking inhalation, dermal contact and systemic exposure (A549, L929 and HepG2 cell lines) were selected as *in vitro* models to assess the potential toxicity of the NPs and to identify some factors determining the toxicological response. The general objective of this work is related to a better understanding of the toxic effects induced in different *in vitro* cell culture models by Fe-, Co- and NiNPs and their potential released ionic forms, focusing the attention on some factors affecting the biological response. In order to fulfill this purpose the following specific aims were pursued:

I. Physico-chemical characterization of FeNPs, CoNPs, NiNPs.

The aim is to determine critical parameters (size, shape, agglomeration state) that are related to NP behavior and toxicity and are important to allow interlaboratory reproducibility. In addition, chemical and biological contaminations were also investigated to avoid artifacts.

II. Dissolution of NPs in culture media.

The aim is to assess the role of potentially released metal ions in the induction of toxicological responses.

III. *In vitro* toxicity induced by the NPs on the three cell models.

The aim is to establish the ranking of toxicity of the individual type of NPs and to compare their effects in different cell models. The toxicological analyses were performed evaluating cell viability by two assays (ATP and MTS) and establishing dose-response curves.

IV. Cellular uptake of NPs and their corresponding ions.

The aim is to correlate the toxic effects induced by the NP s and their ions released with the degree of cellular internalization.

As listed below, results will be presented in different chapter reflecting the individual chemical element constituent of the NP considered:

Chapter 1: Zerovalent iron nanoparticle toxicity
Chapter 2: The essential role of cobalt ions in mediating cobalt nanoparticle toxicity
Chapter 3: Nickel nanoparticles: the dual toxicity mechanism

CHAPTER 1

Zerovalent iron nanoparticle toxicity

1 Abstract

In this study, the toxic effects of zerovalent iron particles (FeNPs) and their relative ions (Fe^{2+} and Fe^{3+}) were investigated in three different *in vitro* models: carcinomic human alveolar basal epithelial cell line (A549) and murine aneuploid fibrosarcoma cell line (L929) as in vitro models for inhalation and dermal contact, and human hepatocellular liver carcinoma cell line (HepG2) as a liver model. Toxicity results were related to NP dissolution and iron internalization. In all the three cell models, FeNPs showed lower toxic effects compared to Fe^{2+} and Fe^{3+} probably in relation to the absence of free iron ions. Furthermore, hepatocytes (HepG2 cells) resulted less susceptible than the other two cellular models in agreement with the metal handling by liver and the physiological role of iron. Overall, FeNP low toxicity appear in relation to a low dissolution rate and to the physiological role of iron.

2 Introduction

Iron (Fe) is the second most abundant metal on Earth crust, after aluminum, and belongs to *d block* of transition metals (Cotton and Wilkinson, 1972). It is an essential element common to all living organisms, as it is involved in oxidation-reduction catalysis and bioenergetics (Da Silva and Williams, 2001). Due to the iron ability to catalyze redox reactions and generate oxygen and nitrogen radical species, its homeostasis in biological systems is strictly maintained (Emerit *et al.*, 2001; Hentze *et al.*, 2004; Andrews and Schmidt, 2007). Fe-based NPs display higher reactivity and magnetism with respect to bulk materials and are largely explored to potential applications in many fields, including biomedicine, catalysis, data storage and environmental remediation (Laurent *et al.*, 2008; Sellers *et al.*, 2010; Yuan and Tasciuc, 2011). Zerovalent iron nanoparticles (FeNPs) are characterized by a great reactivity, also compared to other Fe-based NPs (such as Fe_2O_3- and Fe_3O_4-NPs), and they are proposed as innovative materials in environmental remediation to treat toxic contaminants, such as chlorinated

hydrocarbons and chromium, trichloroethylene (TCE), arsenic and certain metals and, in the presence of oxygen phenols in groundwater (Zhu *et al.*, 2009; Dickinson and Scott, 2010; Sellers *et al.*, 2010). The high FeNP reactivity may induce toxicological effects (Auffan *et al.*, 2008; Lee *et al.*, 2008; Keenan *et al.*, 2009; Li *et al.*, 2010). Different investigations have found an oxidative stress-related toxicity of iron-based NPs occurring both in extracellular media and inside cells (Lee *et al.*, 2008; Keenan *et al.*, 2009; Malvindi *et al.*, 2014). Oxidative stress induced by FeNPs is related to the oxidation of Fe^0 to $Fe^{2+}$and the subsequent conversion to Fe^{3+}, leading to the formation of free radical species, membrane damage, protein carbonylation, and DNA damage (Dean and Nicholson, 1994; Winterbourn, 1995; Emerit *et al.*, 2001; Nunez *et al.*, 2001; Crichton *et al.*, 2002). Despite the potential FeNP toxicity, cells present well-defined homeostatic mechanisms that manage iron in physiological conditions (Crichton *et al.*, 2002; Andrews and Schmidt, 2007; Dunn *et al.*, 2007). These mechanisms can participate in reducing FeNP toxicity. Indeed, it has been observed that astrocytes exposed to iron oxide NPs showed no damages probably because of the iron storage protein ferritin upregulation (Hohnholt *et al.*, 2013).

In this work, we investigated the potential toxic effect of FeNPs by using two viability assays (MTS and ATP assay) in three different *in vitro* models: A549 (epithelial cells from human lung carcinoma) as *in vitro* model for inhalation exposure; L929 (fibroblast cells from murine subcutaneous connective tissue) as model of dermal contact exposure; and HepG2 (epithelial cells from human hepatocellular carcinoma) as liver model. To better understand the role of ion release in mediating cell damage, we tested Fe^{2+} and Fe^{3+} toxicity in the same cell models, and evaluated FeNP dissolution kinetics in the experimental conditions.

3 Materials and Methods

3.1 Chemicals and reagents

Metallic zerovalent FeNPs (Product Code:FE-M-03M-NP.025N) were purchased in dry form from American Elements® (Merelex Corporation, Los Angeles, CA, USA). They had

the following properties as indicated by the supplier: average diameter of 25 nm (with size range from 20 to 40 nm), specific area of 30-50 m^2/g and spherical shape. Acid solution of HNO_3 (67-69% SpA) and HCl (33-36% UpA) were purchased from Romil (Cambridge, UK). Reagents for biological characterization were: Tryptic Soy Agar (TSA; Biolife Italiana S.r.l.; Milan, IT); Venor®GeM Mycoplasma detection kit (Minerva Biolabs, Berlin, De), GoTaq® DNA polymerase, 5X Colorless GoTaq® Reaction Buffer, Blue/Orange 6X loading dye, 100bp DNA ladder (Promega; Madison, WI, USA); all reagents for the detection of endotoxins were purchased from Charles River Laboratories International, Inc (Charleston, SC, USA). $FeSO_4 \cdot 7H_2O$ (Product Code: F8633), $FeCl_3 \cdot 6H_2O$ (Product Code: 31232), Triton X-100, and agarose were purchased from Sigma–Aldrich (Gillingham, UK). Sodium Dodecyl Sulphate (SDS), staurosporine (STS), Trizma® base primary standard and buffer, ethylenediaminetetraacetic acid disodium salt dehydrate (EDTA), acetic acid (puriss., 99-100%), ethidium bromide solution (10 mg/mL in H_2O) and Phosphate Buffer Saline (PBS)were purchased from Sigma-Aldrich (St. Louis, MO, USA). Cytotoxicity was tested with CellTiter 96 AQueous Non-Radioactive Cell Proliferation Assay kit Promega (Madison, WI, USA) and ATPlite (Perkin Elmer, Waltham, MA, USA). Human lung carcinoma epithelial cells (A549), murine subcutaneous connective tissue fibroblast cells (L929) and human hepatocellular carcinoma epithelial cells (HepG2) were obtained from American Type Culture Collection (Manassas, VA, USA). Solutions for cell culture were: Ham's F-12K and Eagle Minimum Essential Medium (EMEM), fetal bovine serum (FBS), penicillin-streptomycin solution, L-glutamine, phosphate buffered saline (PBS), Dulbecco's phosphate buffered saline with calcium and magnesium (DPBS), Trypsin-EDTA, all purchased from Lonza (Basel, CH). Protein quantification was conducted by using MicroBCA™ Protein Assay Kit (Thermo Scientific; Rockford, IL, USA).

3.2 FeNP characterization

FeNPs were characterized for chemical and biological contaminations and morphological properties.

3.2.1 Chemical characterization

To detect FeNP chemical impurities a semi-quantitative analysis (ranging from 6 to 240 amu) by inductively coupled plasma mass spectrometry (ICP-MS; NexION 300D, Perkin Elmer Inc.; Waltham, MA, USA) was conducted. In particular, dry FeNPs were solubilized with a microwave assisted acid digestion. NPs were weighted in specific Teflon vessels and suspended with 75% HNO_3 (67-69% SpA) and 25% HCl (33-36% UpA). Blank samples were added to the analysis to detect possible environmental contaminations. Microwave digestion was performed by using a Mars V microwave(CEM Corporation; Matthews, NC, USA)and the program used has foreseen two different steps: i) increase of temperature until 175°C in 5.5 minutes and ii) maintaining of 175°C for 4.5 minutes to complete digestion. After this acid digestion, solutions were diluted with ultrapure water (18,3 $M\Omega \cdot cm^{-1}$) and analyzed by ICP-MS with a semi-quantitative method. The most concentrated elements detected were quantified by using an external calibration curve. To limit signal drift, a rhodium solution (10 µg/L) as internal standard was added online to each standard and sample solutions.

3.2.2 Biological contaminations

In order to assess microbiological contaminations and endotoxins, FeNPs were suspended at the concentration of 1 mg/mL in sterile water and ultrasonicated for 4 minutes at 50% of amplitude, corresponding to 28000 J (Misonix S-4000 Ultrasonic Liquid Processors, Qsonica LLC.; Newtown, CT, USA). To detect possible generic fungal and bacterial contaminations, 100 µL of the suspensions were plated in TSA plates and incubated at 37°C for 72 h. After the incubation, the presence of colonies on the plates was verified. In addition, mycoplasma contaminations were specifically tested using the Venor®GeM Mycoplasma detection kit according to manufacturer's instructions. Briefly, the possible mycoplasma contamination was detected by amplifying the highly conserved 16S rRNA coding region that generate an amplicon of approximately 267 bp. Internal DNA control of 191 bp was present in each sample, in order to confirm a successfully performed polymerase chain reaction (PCR). After PCR (Mastercycler; Eppendorf s.r.l.; Milan, IT), a 1.5% agarose gel in a Tris/acetic/ EDTA buffer (40 mMTris,

20 mM acetic acid and 1 mM EDTA) including ethidium bromide, as DNA staining, was cast and 10 µL of each PCR reaction, mixed with 2µL of Blue/Orange 6X loading dye were loaded for electrophoresis (Peqlab Biotechnologie GmbH; Erlangen, DE); a 100bp DNA ladder was used. At the end of the electrophoresis, gel were observed by a UV transilluminator (UVITEC; Cambridge, UK) and photographed.

The presence of endotoxin on suspension supernatants was tested by using the Limulus Amebocyte Lysate (LAL) Kinetic-turbidimetric method (Charles River Endosafe; Charleston, SC, USA). This analysis was conducted in a 96-well plate and consisted in optical density (λ = 340 nm) measurements over time with the microplate reader (Synergy4, Bio-Tek Instruments Inc.; Winooski, VT, USA). The assay included a standard curve of *Escherichia coli* endotoxin (from 5 to 0.005 EU/mL) and different dilutions of supernatants with and without standard in order to evaluate possible interferences. In particular, the onset time, which means the time required for the absorbance to increase significantly over the background (0.05 OD units), was calculated and a linear relation between standard endotoxin concentrations and onset time was established in order to calculate sample endotoxin concentrations.

3.2.3 Morphological characterization

Morphological analyses were performed with two different techniques. In particular, FeNPs were suspended in sterile water at the concentration of 1 mg/mL, ultrasonicated (Misonix S-4000 Ultrasonic Liquid Processors, Qsonica LLC.; Newtown, CT, USA) for 4 minutes at 50% of amplitude (corresponding to 28000J). This suspension was diluted in water at the concentration of 100 µg/mL to be examined by Transmission Electron Microscopy (TEM; FEI Tecnai 12 G2 electron microscope, FEI Co.; Eindhoven, NL) with Twin lens configuration after deposition on carbon coated, mesh 400 copper grids and left to dry. Micrographs were recorded on a side-mounted Morada CCD (Olympus Soft imaging Solutions GmbH, Münster, Germany) at magnifications ranging from 42000× to 265000×. To evaluate the aggregation state of NPs in suspension, dilution at the concentration of 10 µg/mL in cell culture complete media and water were done to be analyzed with the ZetasizerNano ZS Dynamic Light Scattering (DLS; Malvern Instruments; Malvern, UK). A blank (only cell culture media) sample were analyzed too.

For the DLS analysis, suspensions were equilibrated at 25°C for 3 minutes and five measurements for each sample were performed.

3.3 FeNP dissolution

FeNP suspensions in cell culture media were analyzed for ion release under our experimental conditions. Different suspensions (0, 10, 100 and 1000 µg/mL) of FeNPs in cell culture media were prepared from a stock suspension (10 mg/mL) that was ultrasonicated for 4 minutes at 50% of amplitude (corresponding to 28000 J). Each suspension was incubated at 37°C, 5% CO_2 and 90% of humidity for 0, 6, 24 and 48 h in 24-well plates (1mL for each well). At the end of incubation NPs were removed from suspensions by collecting samples in 2 mL tubes, centrifuging twice at 16000 g for 10 minutes and finally ultracentrifuging (Optima™ L-100XP Ultracentrifuge; Beckman Coulter; Urbana, IL, USA) for 2 hours at 300000 g at 4°C. Ultracentrifugation was conducted in polycarbonate tubes (Beckman Coulter; Urbana, IL, USA) with the rotor type 70.1.Ti (Beckman Coulter). Supernatants were collected and diluted with a 2% HNO_3 solution prior to being analyzed for iron quantification with ICP-MS (NexION 300D, Perkin Elmer; Waltham, MA, USA).Simultaneously, 100 µg/mL solutions of Fe^{2+} and Fe^{3+} in cell culture media and ddH_2O were analyzed to monitor the ion behavior during the experiment. In addition, not ultracentrifuged NP suspensions and ion solutions were quantitatively analyzed by ICP-MS. In particular, ion solutions were simply diluted in 2% HNO_3 solution in the calibration curve concentration range, whereas, NP suspensions were solubilized by microwave acid digestion (Mars V,CEM). 500 µL of each suspension were transferred in specific Teflon vessels and 10 mL of HNO_3(67-69% SpA) were added. Blank samples were included to the analysis to detect possible environmental contaminations. Microwave digestion program has foreseen two different steps: i) increase of temperature until 175°C in 7 minutes and ii) maintaining of 175°C for 3 minutes to complete digestion. After this acid digestion, solutions were diluted with ultrapure water (18,3 $M\Omega \cdot cm^{-1}$) and analyzed by ICP-MS (NexION 300D, Perkin Elmer; Waltham, MA, USA). ICP-MS quantitative analyses of ionic release and NP and ion solution were performed using an external calibration

curve. To limit signal drift, a rhodium solution (10 µg/L) as internal standard was added online to each standard and sample solutions.

3.4 Cell viability analyses

3.4.1 Cell culture and sub-culturing procedure

A549, L929 and HepG2 cells were maintained following ATCC indications. A549 cells were cultured in Ham's F12K medium with the addition of 10 % FBS, 100 units/mL streptomycin and 100 µg/mL penicillin. HepG2 and L929 cells were cultured in EMEM with the addition of 10%FBS, 100 units/mL streptomycin and 100 µg/mL penicillin and 2mM L-glutamine. All the three cell lines were kept at 37°C, 5% CO_2 and 90% of humidity for maintenance and for experiments.

3.4.2 FeNP, Fe^{2+} and Fe^{3+}toxicity

In order to evaluate the cytotoxic effects of FeNPs, Fe^{2+} and Fe^{3+}, cells were seeded in 96-well microplate and, 24h after seeding, treated with different concentrations of NP and ions for 6, 24 and 48 h. The seeding densities of cells were those at which cells proliferated overtime: 5000 cell/well for A549 and L929 cells, and 15000 cell/well for HepG2 cells. Treatment solutions or suspensions were freshly prepared before each test. In particular, NPs were suspended in sterile water and ultrasonicated for 4 minutes at 50% of amplitude (corresponding at 28000 J) in order to make a stock suspension that was diluted in the proper cell culture media without exceeding the 10% of the total volume of the treatment. Ion stock solutions were prepared in ddH_2O, filtered with 0.22 µm pore size filter and diluted in cell culture media as NP stock suspensions. Experiments were performed in triplicate. Viability was assessed after the removal of cell culture media and washing of cells with DPBS in order to eliminate possible NP interferences (Kroll *et al.*, 2012). The two assays used were: MTS assay and ATP assay were performed according to manufacturer's instructions. The MTS assay analyzes the conversion of a tetraziolium salt 3-(4,5-dimethylthiazol-2-yl)-5-(3-carboxymethoxyphenyl)-2-(4-sulfophenyl)-2H] (MTS) into its reduced and soluble formazan form by mitochondrial enzyme of metabolically active cells and was

evaluated by recording absorbance at 490 nm. ATP assay is based on light production caused by the reaction of ATP with added luciferase and D-luciferin and quantify the ATP content. Both absorbance and luminescence were recorded with the Synergy4 microplate reader (Bio-Tek Instruments).

3.4.3 Late effects

Possible late effects induced by of FeNPs, Fe^{2+} and Fe^{3+} exposure were analyzed by incubating cells with each iron compound for 6 h, removing treatments and replacing with fresh culture media, after washing cells twice with DPBS, and finally analyzing ATP content at 24 and 48 h post treatment.

3.4.4 Cellular uptake

Cellular uptake of FeNPs, $Fe^{2+}$and $Fe^{3+}$was quantitatively analyzed by ICP-MS (NexION 300D, Perkin Elmer). Cells were seeded in 24-well plate at densities 10 times higher compared to those used in 96-well plate experiments. After 24h the seeding, cells were treated with 10 µg/mL of FeNP or ions for 24 h from stock suspensions prepared similarly to cytotoxicity tests. At the end of the exposure, cells were washed three-times with PBS to remove NPs and ions not internalized. Cells were then detached with 200 µL of Trypsin-EDTA and collected with 800 µL of PBS to be analyzed for protein quantification and uptake. Samples dedicated to protein quantification were centrifuged at 16000 g for 5 minutes. Then, supernatants were discarded and cell pellets were lysed with a lysis solution containing PBS 1X, 1% Triton X-100 and 1% SDS. Protein quantification was conducted using the microBCA assay. Bovine Serum Albumin (BSA) provided by the kit was diluted to prepare different standards in the linear concentration range of 10-40 µg/mL and manufacturer's instructions were followed. To analyze uptake, samples were centrifuged at 400 g for 15 minutes. Once supernatants were discarded pellets were digested by adding 1 mL of aqua regia (fresh mixture of concentrated nitric acid and hydrochloric acid in the volume ratio 1 : 3).After an overnight incubation at room temperature, samples were incubated 12 h at 70°C in Thermoblock (FALC Instruments; Treviglio, IT) and finally diluted in ultrapure H_2O (18,3 $M\Omega \cdot cm^{-1}$). The obtained solutions were quantitatively analyzed by ICP-MS

(NexION 300D, Perkin Elmer; Waltham, MA, USA) by using the Dynamic Reaction Cell (DRC) method with a standard calibration curve and a rhodium solution as internal standard.

3.5 Statistical analyses

Statistical analyses were performed using Origin Pro 8.0 software (OriginLab; Northampton, MA, USA). Cytotoxicity results were fitted by sigmoid functions and EC50 values were calculated. Where bimodal dose-response curves appeared more appropriate, F-tests were performed to compare unimodal and bimodal models. Statistical significances were determined by ANOVA analysis (P value < 0.05).

4 Results

4.1 FeNP characterization

The analysis of chemical purity of FeNPs showed the presence of two main metal contaminants: cobalt (Co) and manganese (Mn) (Table 1). On the contrary, microbiological contaminations were absent and endotoxin levels were below 0.01 EU/mL (corresponding to levels detected for sterile water).

TABLE 1. Elemental FeNP contaminations.

	Concentration	
Element	µg/g [a] ± SD	% [b] ± SD
Co	196 ± 1	0.0196 ± 0.0001
Mn	61.7 ± 0.8	0.0062 ± 0.0001

a: dry weight
b: % expressed as w/w (dry weight)
SD: standard deviation (mean of three determinations).

An accurate primary size distribution was hampered because of particle aggregation, as observed from TEM images in which FeNPs appeared polydispersed in size, in a crystalline form and spheroidal in shape (Fig. 1). Aggregation and polydispersion were confirmed by DLS analysis (Fig. 2).

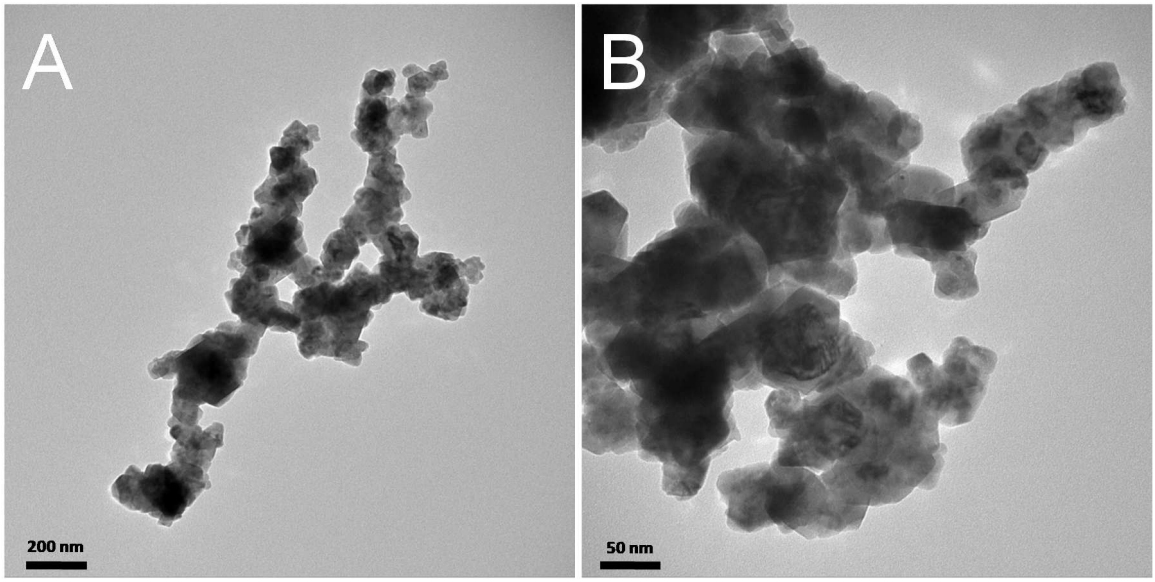

FIGURE 1. TEM images of FeNPs at different instrumental magnifications: A) 97000 ×; B) 195000 ×

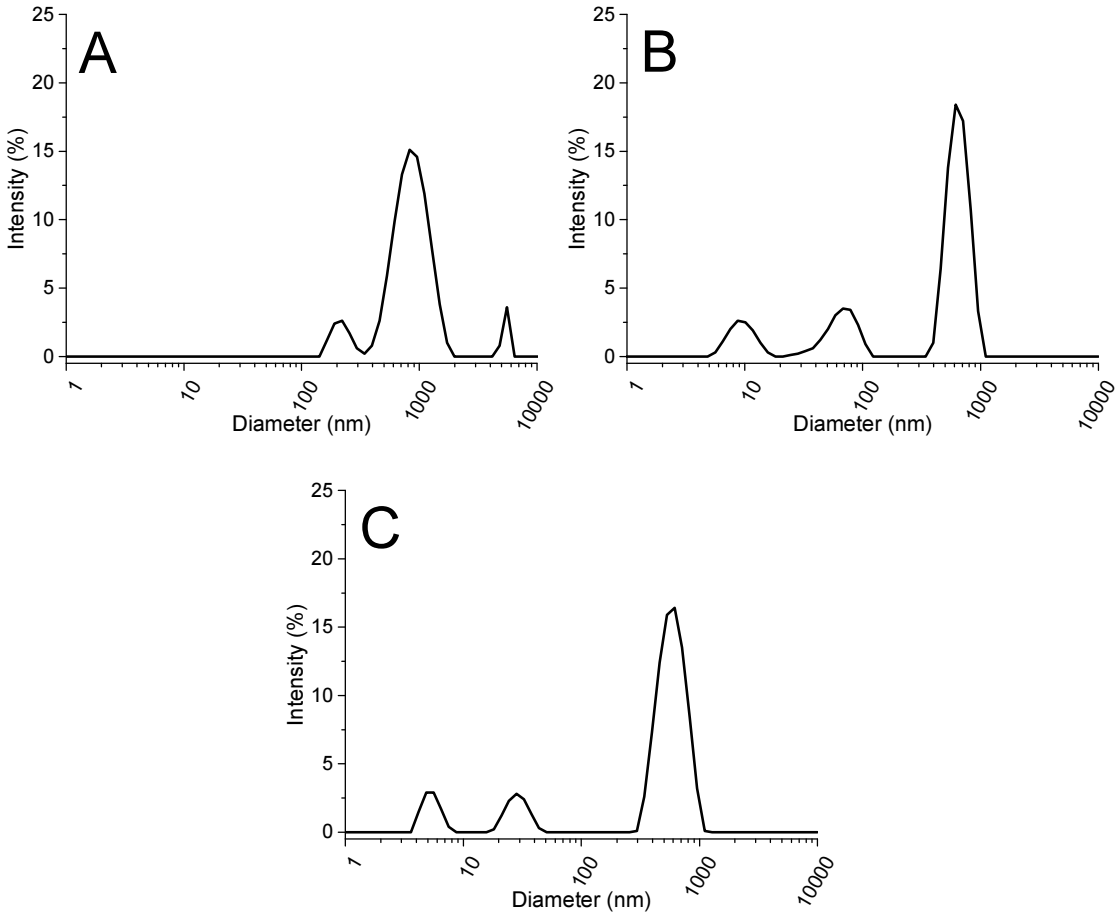

FIGURE 2. DLS size distribution performed in A) water (PdI = 0.543); B) Ham's F-12K medium (PdI = 0.678)and C) EMEM medium (PdI = 0.698).

4.2 FeNP dissolution

Before evaluating dissolution of FeNPs in water and cell culture media, the effect of ultracentrifugation on both Fe^{2+} and Fe^{3+} was investigated. While in aqueous solution ultracentrifugation did not affect ion solubility, in the presence of cell culture media iron concentration in solution was drastically reduced (Fig. 3).

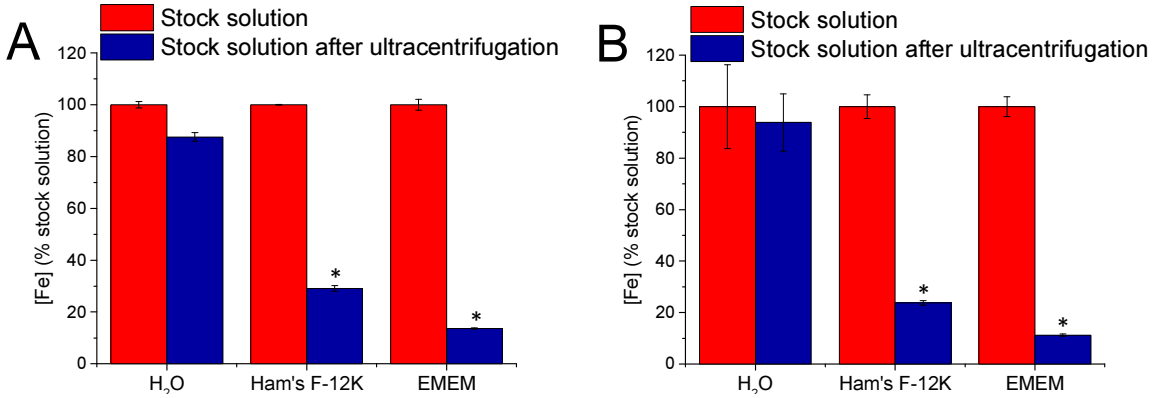

FIGURE 3. Analysis of concentrations Fe^{2+} (A) and Fe^{3+} (B) before and after ultracentrifugation in water and cell culture media. Data are expressed as mean of three different measurements, each of them expressed as % of stock solution concentrations. Error bars represent standard deviations of three different measurements. * Significant different from stock solution (P value < 0.05)

Furthermore, ion precipitation occurred during the first 6 h ($P < 0.05$), while no differences were noted for longer incubation times (Fig. 4). However, Fe^{2+} in water did not undergo precipitation (Fig. 4A)

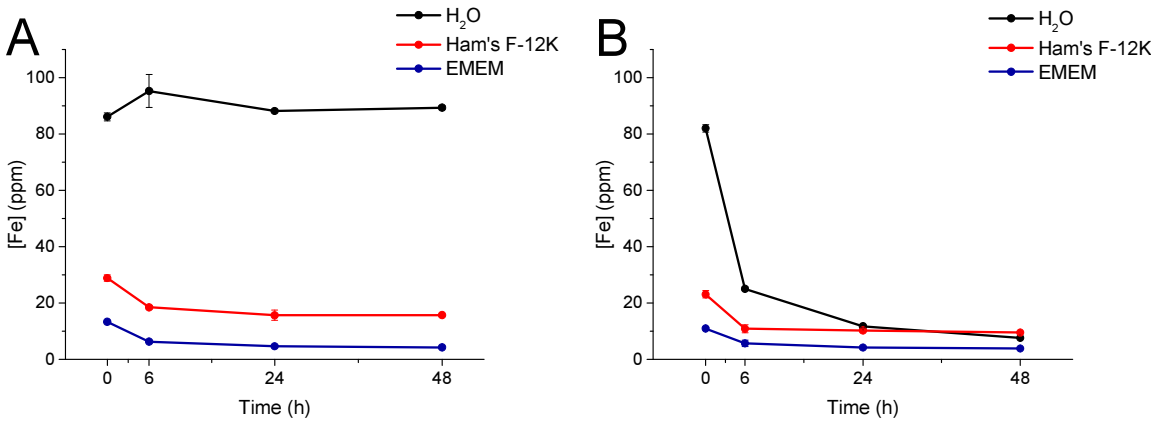

FIGURE 4. Ions in solutions over time in water and cell culture media (Ham's F-12K and EMEM). A) Fe^{2+}; B) Fe^{3+}. Data are expressed as means of three measurements and error bars represents standard deviations.

EMEM cell culture medium induced iron precipitation more than Ham's F-12K (Fig. 3, 4). Despite precipitation phenomena, probably due to the formation of iron hydroxides, FeNP dissolution kinetics were studied. After ultracentrifugation, the level of iron in the soluble fraction did not change significantly compared to iron in cell culture media (Fig. 5).

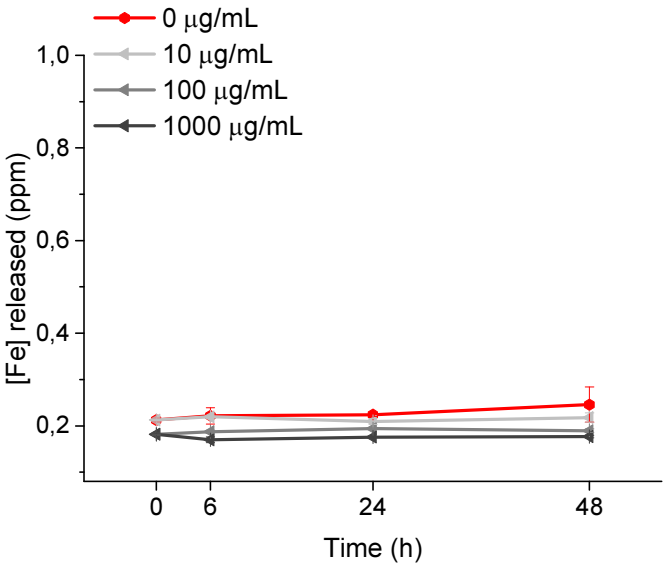

FIGURE 5. Ions released by FeNPs in Ham's F-12K medium over time. Data are expressed as means of three measurements and error bars represents standard deviations.

4.3 FeNP, Fe^{2+} and Fe^{3+} toxicity

Cell viability after exposure to FeNP, Fe^{2+} and Fe^{3+} was performed by using two different viability assays. Where possible, dose-response curves were fitted (Fig. 6, 7, 8) and EC50 was calculated (Table 2). ATP and MTS assays showed similar dose- and time-dependent effects of FeNPs, $Fe^{2+}$and Fe^{3+} in the three *in vitro* models (Fig. 6, 7, 8). In particular, FeNPs did not induce a complete reduction of metabolic activity or ATP content, while the two ionic forms caused a total reduction of viability from 24 h of exposure. However, FeNP effect occurred at lower concentration with respect to $Fe^{2+}$and Fe^{3+} ions. The main difference between the two assays was related to FeNP toxicity on HepG2 cells. In HepG2 cells, the reduction of ATP content was not confirmed by a reduction in metabolic activity (Fig.8). Considering both the maximum effects and EC50 values,

HepG2 cells resulted to be the less susceptible *in vitro* model, while A549 showed high sensitivity to the treatments (Fig.6, 7, 8; Table 2).

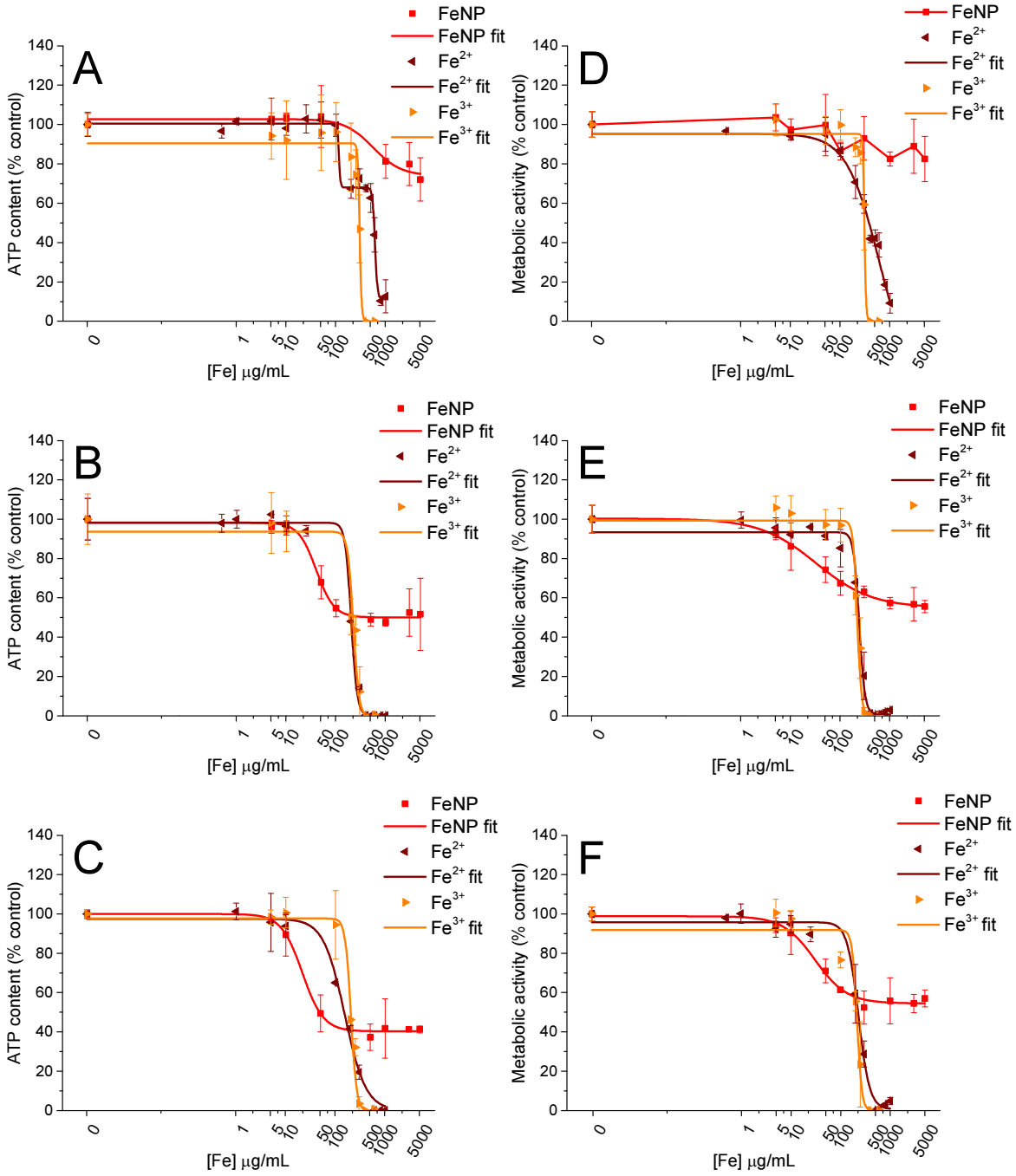

FIGURE 6. Dose-response curves obtained by treating A549 cells with FeNPs, Fe^{2+} and Fe^{3+} for 6 (A, D), 24 (B, E) and 48h (C, F). Panels A, B, C refer to ATP assay, while panels D, E, F refer to MTS assay. Data are expressed as mean of three independent experiments and error bars represent standard deviations.

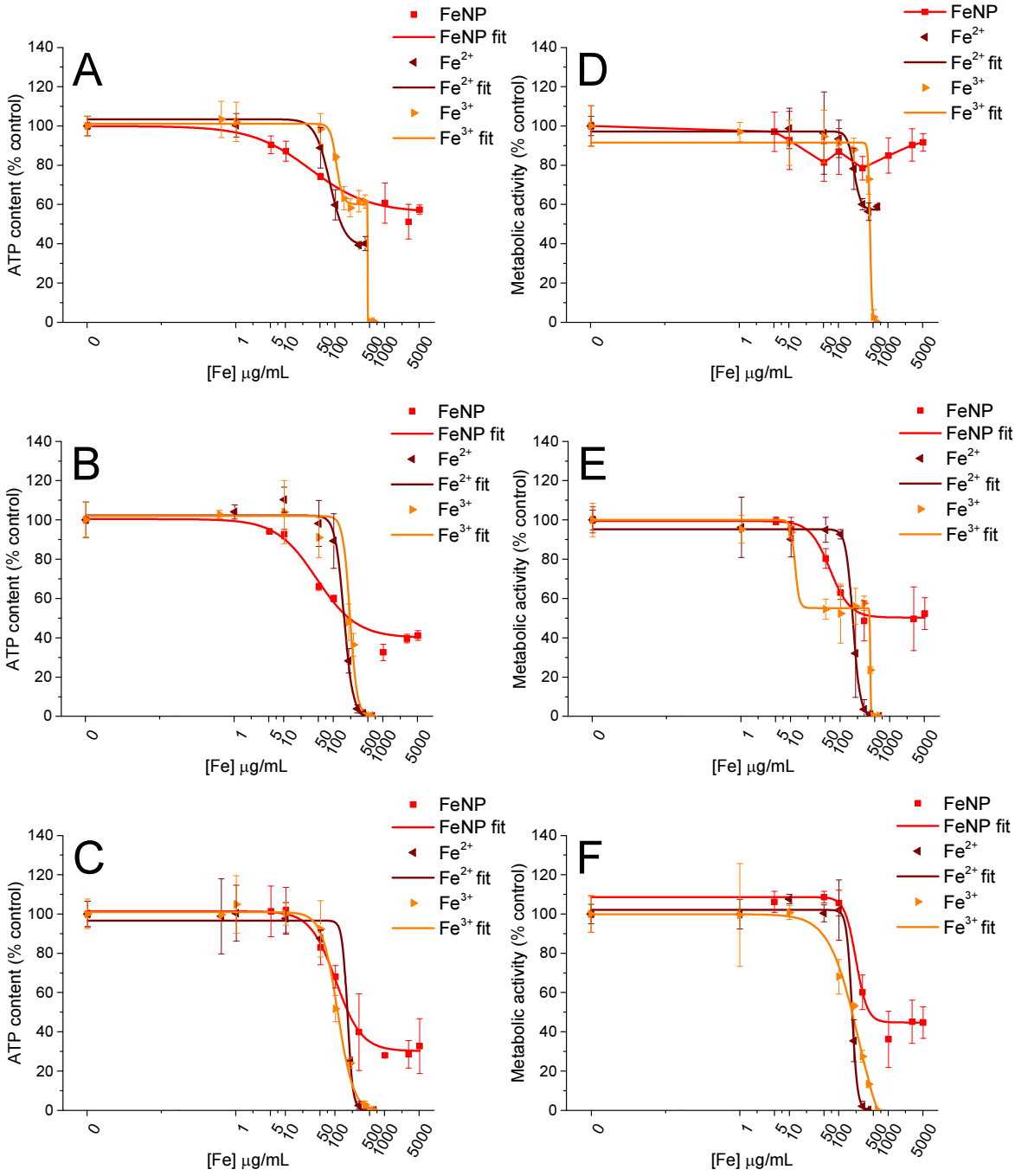

FIGURE 7. Dose-response curves obtained by treating L929 cells with FeNPs, Fe^{2+} and Fe^{3+} for 6 (A, D), 24 (B, E) and 48 h (C, F). Panels A, B, C refer to ATP assay, while panels D, E, F refer to MTS assay. Data are expressed as mean of three independent experiments and error bars represent standard deviations.

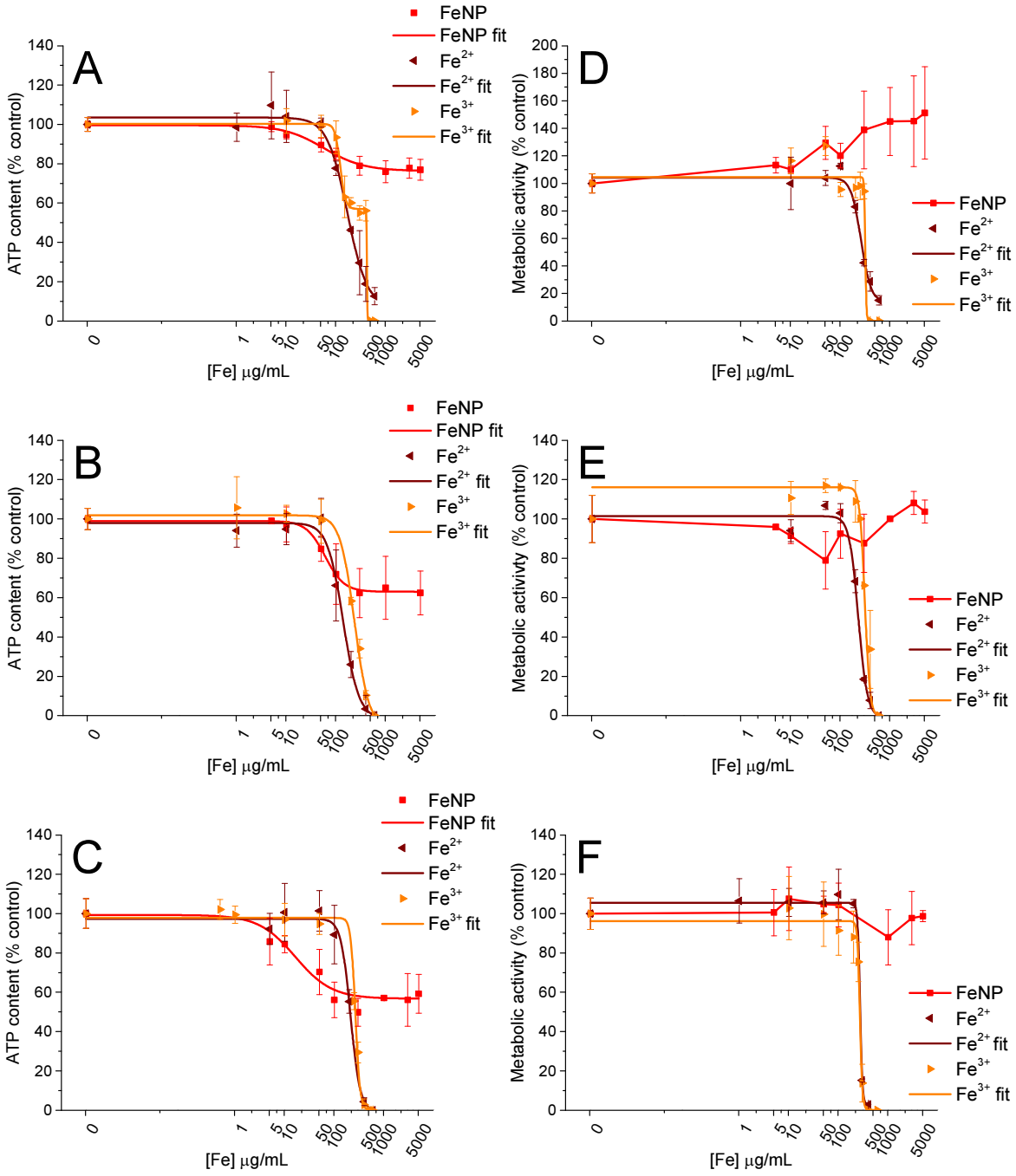

FIGURE 8. Dose-response curves obtained by treating HepG2 cells with FeNPs, Fe^{2+} and Fe^{3+} for 6 (A, D), 24 (B, E) and 48h (C, F). Panels A, B, C refer to ATP assay, while panels D, E, F refer to MTS assay. Data are expressed as mean of three independent experiments and error bars represent standard deviations.

TABLE 2. EC50 values of FeNPs, Fe^{2+} and Fe^{3+} in the three cell models at 6, 24 and 48 h.

	EC50 (µg/mL)								
	A549			L929			HepG2		
Compound	6 h	24 h	48 h	6 h	24 h	48 h	6 h	24 h	48 h
	ATP assay								
FeNP	557.4	40.1	21.5	31.3	52.3	102.4	57	60.4	16.4
Fe^{2+}	114/609*	201.8	153.7	77.3	161.1	176	169.2	139.2	212
Fe^{3+}	300.4	224	205.2	105/449*	213.2	111.6	122/420*	235.7	266.3
	MTS assay								
FeNP	N.E	32.3	30.8	N.E.	61.1	221.6	N.E.	N.E.	N.E.
Fe^{2+}	604.6	238.7	229.2	202.1	179.7	184.7	259.4	229	269.8
Fe^{3+}	305.5	218	215.5	425.9	12.5/398*	249.2	317.3	310.3	269.6

N.E.: no effect.

* Double EC50 values calculated from bimodal dose-response curves.

4.4 Late effects

In order to better understand the intracellular behavior of FeNPs, we treated cells for 6 h and then, after 24 h and 48 h of recovery, we observed their effects on ATP content. Late effects following short incubation times showed that FeNP toxicity lost its time-dependency, considering maximum effect that corresponded to that observed after 6 h treatment (Fig. 9A, 9B, 10A, 10B). Considering Fe^{2+} and Fe^{3+}, they induced a reduced toxicity but still time-dependent always considering maximum effects, as in some cases dose-response curves could not be obtained (Fig. 9C, 9D, 9E, 9F, 10C, 10D, 10E, 10F; Table 3).

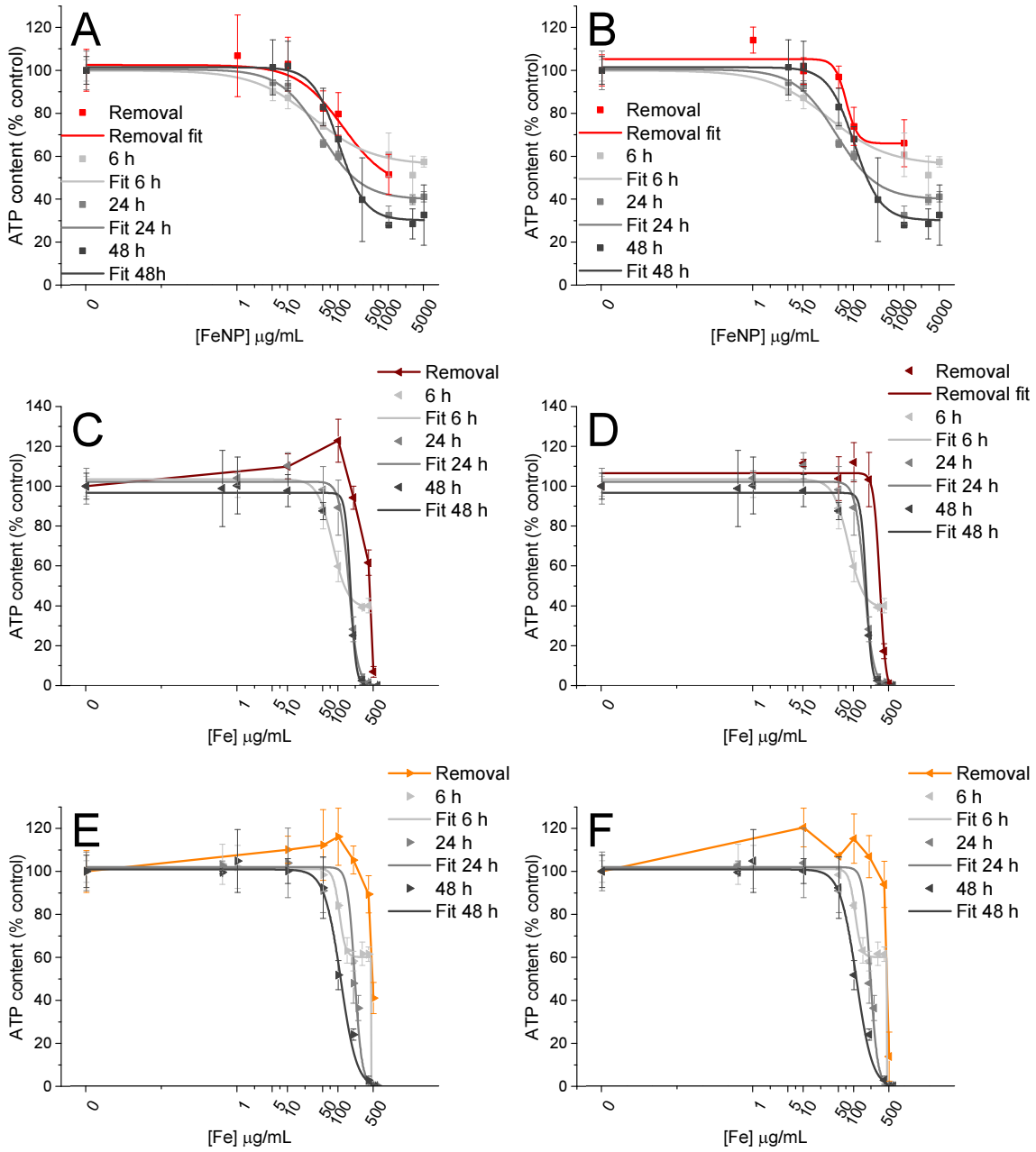

FIGURE 9. FeNP (A, B), Fe^{2+} (C, D) and Fe^{3+} (E, F) toxicity on L929 cells measured by ATP assays after the removal of treatments (6 h post treatments). ATP assay were performed after 24 h (A, C) and 48 h (B, D) from treatment. Dose-response curves obtained by treating cells with FeNPs, Fe^{2+} and Fe^{3+} for 6, 24 and 48 h were also reported. Data are expressed as mean of three independent experiments and error bars represent standard deviations.

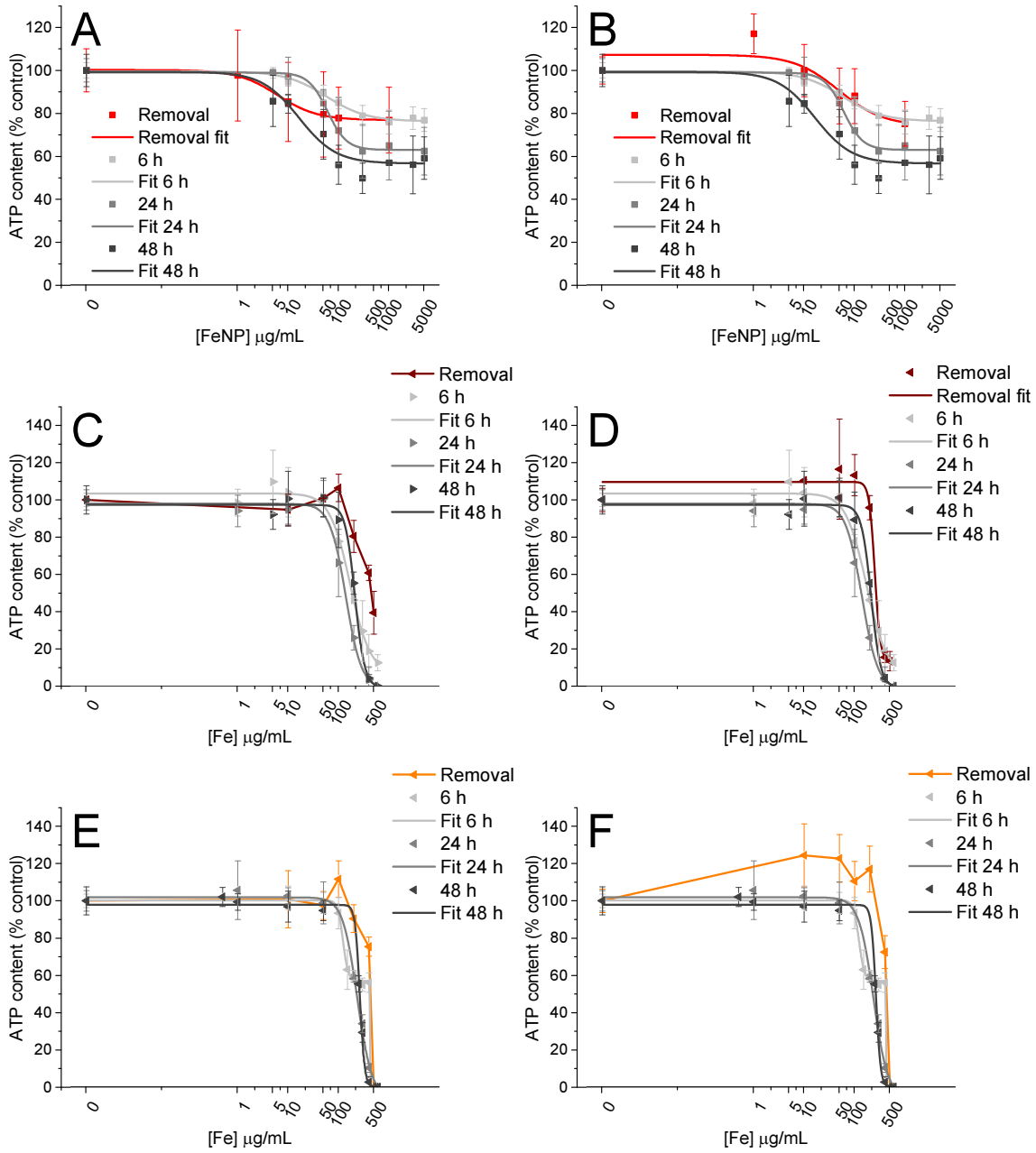

FIGURE 10. FeNP (A, B), Fe^{2+} (C, D) and Fe^{3+} (E, F) toxicity on HepG2 cells measured by ATP assays after the removal of treatments (6 h post treatments). ATP assay were performed after 24 h (A, C) and 48 h (B, D) from treatment. Dose-response curves obtained by treating cells with FeNPs, Fe^{2+} and $Fe^{3+}$for 6, 24 and 48 h were also reported. Data are expressed as mean of three independent experiments and error bars represent standard deviations.

TABLE 3. Maximum effect and EC50 values of L929 and HepG2 cells after 6 h of exposure with Co compound and 24 and 48 h of recovery.

	L929		HepG2	
Compound	**24 h**	**48 h**	**24 h**	**48 h**
	Max effect (% control)			
FeNP	45	66	76.9	74.2
Fe^{2+}	6.9	0	39.4	13
Fe^{3+}	41	13.3	0	0
	EC50 (μg/mL)			
FeNP	123	70.2	6.1	48.4
Fe^{2+}	N.D.	327	N.D.	251
Fe^{3+}	N.D.	N.D.	N.D.	N.D.

N.D: not determined

4.5 Cellular uptake

As different toxicities were observed among cell lines, the intracellular concentration of iron was quantified, as a higher cell susceptibility could be related to the higher uptake. With this respect, iron uptake was quantified by ICP-MS and the resulting concentrations normalized for protein concentration. As shown in Fig. 9, cell treated with FeNPs internalized iron more efficiently than cells treated with $Fe^{2+}$and Fe^{3+}in all the three cell models. In addition, the extent of internalization was different among in the three cell models. In particular, FeNPs were significantly less internalized by HepG2 cells compared to A549 and L929 cells, which rather showed a similar uptake (Fig.9).

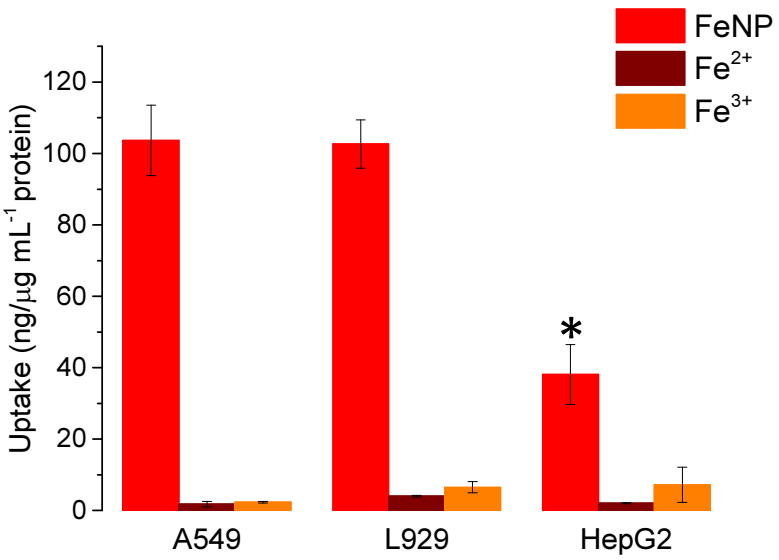

FIGURE 11. Uptake of FeNPs, Fe^{2+} and Fe^{3+}in A549, L929 and HepG2 cells. Data are expressed as ng of Fe for µg/mL of proteins and error bars are standard deviations. *Significant difference among cell models ($P < 0.05$).

5 Discussion

FeNPs aggregates in both water and cell culture media, as already reported for bare metallic NPs (Oberdörster *et al.*, 2007; Teeguarden *et al.*, 2007). This process hampered NP characterization, such as particle size distribution and specific surface area. Aggregation can also modify size-related NP properties as aggregated NPs act as bigger particles (Borm *et al.*, 2006; Buzea *et al.*, 2007; Oberdörster *et al.*, 2007). In particular, aggregation reduces NP dissolution decreasing specific surface area, and affects the cellular dose as bigger particles settle more rapidly and, as a consequence, they can easily interact with cells (Teeguarden *et al.*, 2007; Dhawan and Sharma, 2010; Fadeel and Garcia-Bennett, 2010; Misra *et al.*, 2012). Dissolution is a fundamental property in determining metal NP toxicity. Therefore, ion release under experimental conditions was evaluated. In this work, we have chosen one of most common methodological approach for assessing dissolution. Soluble iron was separated from FeNPs by ultracentrifugation and then quantified them by ICP-MS (Zook *et al.*, 2011; Misra *et al.*, 2012; Bregoli *et al.*, 2013). Ultracentrifugation appears to increase $Fe^{2+}$and Fe^{3+} precipitation, in particular in cell culture media. However, Fe ions precipitation occurs spontaneously in the presence of dioxygen at pH 7 because of iron hydroxide formation

(Da Silva and Williams, 2001). This process could interfere with the detection of ions release by NPs; accordingly, the failure to detect Fe ions in solution could be due to the precipitation of the ions themselves instead of the lack of dissolution processes.

Administration of FeNPs induces lower toxic effects than Fe^{2+} and Fe^{3+} ions on the three *in vitro* models, probably due to the low ability of NPs to release ions. The low dissolution of FeNPs can also explain the time-independency of late effects observed after short exposure with FeNPs (6 h). This suggests that FeNP toxicity could be independent from ion release and depend on other mechanisms such as oxidative stress though the oxidation of NP surface (Auffan *et al.*, 2009; Studer *et al.*, 2010). As a consequence, time-dependency of FeNP toxicity could be related to the increase of NP internalization rather than ion release. Furthermore, hepatocytes (HepG2 cells) result less susceptible than the other two cellular models. HepG2 cells have been used as liver model. Hepatocytes are specialized cells involved in maintaining systemic metal homeostasis via well-defined molecular mechanisms and possess an efficient antioxidant mechanisms (Crichton *et al.*, 2002; Andrews and Schmidt, 2007). Therefore, HepG2 cells are able to manage iron, both as FeNPs and ions, more promptly than A549 and L929 cells. Although Fe ions induced higher effects than FeNPs, the latter have an impact on cell viability at lower concentrations. This could be due to the ability of these cells to respond to low concentrations of Fe^{2+} and Fe^{3+} by activating homeostatic pathways, and to FeNP toxic mechanisms probably independent from ion release.

In conclusion, FeNPs induce low toxicity in all three cell models. This *in vitro* moderate effect could be related to the very low NP dissolution occurring both in cell culture media and inside cells and to the presence of an homeostatic mechanisms that can decrease the effects of the released ions, as described in Fig. 12. On the other hand, the observed low *in vitro* FeNP toxicity may not reflect the *in vivo* condition due to possible relation of low dissolution with biopersistance, high accumulation, low clearance and chronic effects (Borm *et al.*, 2006).

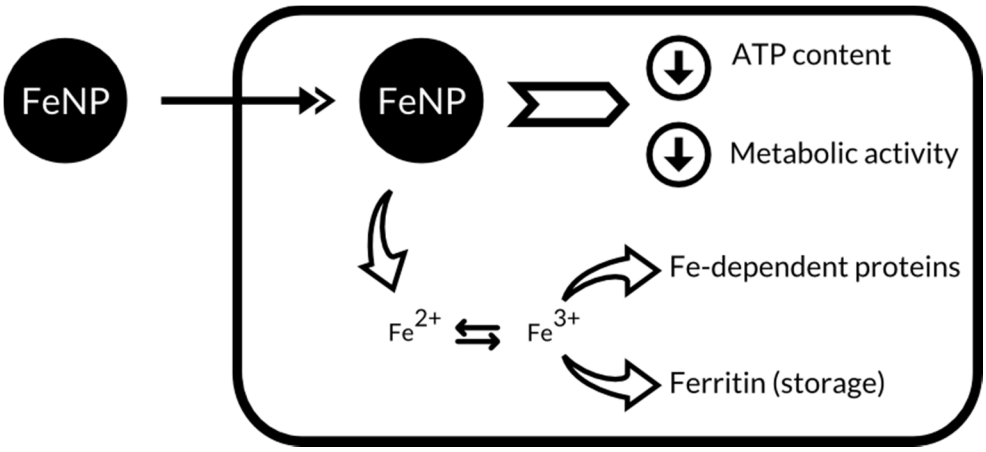

FIGURE 12. Possible mechanism for FeNP toxicity. When cells are exposed to FeNPs, they can internalize them. Once FeNPs are internalized inside cells, they can release Fe^{2+} that can be used for the incorporation in iron-dependent proteins or stored in ferritin, reducing the toxic effects of released ions. The effects on cell viability (i.e. the reduction of ATP content and metabolic activity) seem to be related to processes due to the presence of NPs inside cells and probably occurring at their surface.

6 References

Andrews N. C. and Schmidt P. J. (2007). Iron homeostasis. *Annu. Rev. Physiol.* 69: 69-85.

Auffan M., Achouak W., Rose J., Roncato M. A., Chaneac C., Waite D. T., Masion A., Woicik J. C., Wiesner M. R. and Bottero J. Y. (2008). Relation between the redox state of iron-based nanoparticles and their cytotoxicity toward Escherichia coli. *Environ. Sci. Technol.* 42(17): 6730-6735.

Auffan M., Rose J., Wiesner M. R. and Bottero J.-Y. (2009). Chemical stability of metallic nanoparticles: a parameter controlling their potential cellular toxicity in vitro. *Environ. Pollut.* 157(4): 1127-1133.

Borm P., Klaessig F. C., Landry T. D., Moudgil B., Pauluhn J., Thomas K., Trottier R. and Wood S. (2006). Research strategies for safety evaluation of nanomaterials, part V: role of dissolution in biological fate and effects of nanoscale particles. *Toxicol. Sci.* 90(1): 23-32.

Bregoli L., Benetti F., Venturini M. and Sabbioni E. (2013). ECSIN's methodological approach for hazard evaluation of engineered nanomaterials. *J. Phys.Conf. Ser.*, IOP Publishing.

Buzea C., Pacheco I. I. and Robbie K. (2007). Nanomaterials and nanoparticles: sources and toxicity. *Biointerphases* 2(4): MR17-MR71.

Cotton F. A. and Wilkinson G. (1972). Advanced inorganic chemistry. A comprehensive text. *John Wiley & Sons, Inc.*, New York. pp.1145.

Crichton R. R., Wilmet S., Legssyer R. and Ward R. J. (2002). Molecular and cellular mechanisms of iron homeostasis and toxicity in mammalian cells. *J. Inorg. Biochem.* 91(1): 9-18.

Da Silva J. F. and Williams R. (2001). The biological chemistry of the elements: the inorganic chemistry of life. *Oxford University Press*, Oxford. pp.561.

Dean R. T. and Nicholson P. (1994). The action of nine chelators on iron-dependent radical damage. *Free Radic. Res.* 20(2): 83-101.

Dhawan A. and Sharma V. (2010). Toxicity assessment of nanomaterials: methods and challenges. *Anal. Bioanal. Chem.* 398(2): 589-605.

Dickinson M. and Scott T. B. (2010). The application of zero-valent iron nanoparticles for the remediation of a uranium-contaminated waste effluent. *J. Hazard. Mater.* 178(1-3): 171-179.

Dunn L. L., Suryo Rahmanto Y. and Richardson D. R. (2007). Iron uptake and metabolism in the new millennium. *Trends Cell Biol.* 17(2): 93-100.

Emerit J., Beaumont C. and Trivin F. (2001). Iron metabolism, free radicals, and oxidative injury. *Biomed. Pharmacother.* 55(6): 333-339.

Fadeel B. and Garcia-Bennett A. E. (2010). Better safe than sorry: understanding the toxicological properties of inorganic nanoparticles manufactured for biomedical applications. *Adv. Drug Deliver. Rev.* 62(3): 362-374.

Hentze M. W., Muckenthaler M. U. and Andrews N. C. (2004). Balancing acts: molecular control of mammalian iron metabolism. *Cell* 117(3): 285-297.

Hohnholt M. C., Geppert M., Luther E. M., Petters C., Bulcke F. and Dringen R. (2013). Handling of iron oxide and silver nanoparticles by astrocytes. *Neurochem. Res.* 38(2): 227-239.

Keenan C. R., Goth-Goldstein R., Lucas D. and Sedlak D. L. (2009). Oxidative stress induced by zero-valent iron nanoparticles and Fe(II) in human bronchial epithelial cells. *Environ. Sci. Technol.* 43(12): 4555-4560.

Kroll A., Pillukat M. H., Hahn D. and Schnekenburger J. (2012). Interference of engineered nanoparticles with in vitro toxicity assays. *Arch. Toxicol.* 86(7): 1123-1136.

Laurent S., Forge D., Port M., Roch A., Robic C., Vander Elst L. and Muller R. N. (2008). Magnetic iron oxide nanoparticles: synthesis, stabilization, vectorization, physico-chemical characterizations, and biological applications. *Chem. Rev.* 108(6): 2064-2110.

Lee C., Kim J. Y., Lee W. I., Nelson K. L., Yoon J. and Sedlak D. L. (2008). Bactericidal effect of zero-valent iron nanoparticles on Escherichia coli. *Environ. Sci. Technol.* 42(13): 4927-4933.

Li Z., Greden K., Alvarez P. J., Gregory K. B. and Lowry G. V. (2010). Adsorbed polymer and NOM limits adhesion and toxicity of nano scale zerovalent iron to E. coli. *Environ. Sci. Technol.* 44(9): 3462-3467.

Malvindi M. A., De Matteis V., Galeone A., Brunetti V., Anyfantis G. C., Athanassiou A., Cingolani R. and Pompa P. P. (2014). Toxicity assessment of silica coated iron oxide nanoparticles and biocompatibility improvement by surface engineering. *PloS one* 9(1): e85835.

Misra S. K., Dybowska A., Berhanu D., Luoma S. N. and Valsami-Jones E. (2012). The complexity of nanoparticle dissolution and its importance in nanotoxicological studies. *Sci.Total Environ.* 438: 225-232.

Nunez M. T., Tapia V., Toyokuni S. and Okada S. (2001). Iron-induced oxidative damage in colon carcinoma (Caco-2) cells. *Free Radic. Res.* 34(1): 57-68.

Oberdörster G., Stone V. and Donaldson K. (2007). Toxicology of nanoparticles: a historical perspective. *Nanotoxicology* 1(1): 2-25.

Sellers K., Mackay C., Bergeson L. L., Clough S. R., Hoyt M., Chen J., Henry K. and Hamblen J. (2010). Nanotechnology and the Environment. *CRC Press, Taylor & Francis Group* New York. pp.281.

Studer A. M., Limbach L. K., Van Duc L., Krumeich F., Athanassiou E. K., Gerber L. C., Moch H. and Stark W. J. (2010). Nanoparticle cytotoxicity depends on

intracellular solubility: comparison of stabilized copper metal and degradable copper oxide nanoparticles. *Toxicol. Lett.* 197(3): 169-174.

Teeguarden J. G., Hinderliter P. M., Orr G., Thrall B. D. and Pounds J. G. (2007). Particokinetics in vitro: dosimetry considerations for in vitro nanoparticle toxicity assessments. *Toxicol. Sci.* 95(2): 300-312.

Winterbourn C. C. (1995). Toxicity of iron and hydrogen peroxide: the Fenton reaction. *Toxicol. Lett.* 82-83: 969-974.

Yuan Y. and Tasciuc D.-A. B. (2011). Comparison between experimental and predicted specific absorption rate of functionalized iron oxide nanoparticle suspensions. *J. Magn. Magn. Mater.* 323(20): 2463-2469.

Zhu H., Jia Y., Wu X. and Wang H. (2009). Removal of arsenic from water by supported nano zero-valent iron on activated carbon. *J. Hazard. Mater.* 172(2): 1591-1596.

Zook J. M., Long S. E., Cleveland D., Geronimo C. L. and MacCuspie R. I. (2011). Measuring silver nanoparticle dissolution in complex biological and environmental matrices using UV-visible absorbance. *Anal. Bioanal. Chem.* 401(6): 1993-2002.

CHAPTER 2

The essential role of cobalt ions in mediating cobalt nanoparticle toxicity

1 Abstract

In this study, we analyzed the toxic effects of cobalt nanoparticles (CoNPs) and its relative ion (Co^{2+}). In particular, toxicity was evaluated in three different *in vitro* models: carcinomic human alveolar basal epithelial cell line (A549) and murine aneuploid fibrosarcoma cell line (L929) as in vitro models for inhalation and dermal contact, and human hepatocellular liver carcinoma cell line (HepG2) as a liver model. Furthermore, dissolution kinetics and cellular uptake were analyzed. CoNPs and Co^{2+} showed similar dose-response curves. This similarity can be related to high Co released by NPs. Differences in cell susceptibility were found (A549 > L929 > HepG2), but did not result to be related to differences in intracellular Co concentrations. Overall, our findings suggest that CoNP toxicity is closely related to NP dissolution process.

2 Introduction

Cobalt (Co) is a transition element of the *d block* (Cotton and Wilkinson, 1972; Da Silva and Williams, 2001). From a physiological point of view, the role of cobalt in biological systems is mediated by vitamin B_{12} or cobalamin, which is involved as a coenzyme in different biochemical reactions, such as the reduction of ribose to deoxyribose; the rearrangement of diols and similar molecules; the rearrangement if malonyl to succynil; and the transfer of methyl group (Roth *et al.*, 1996; Da Silva and Williams, 2001). As nanoparticle, cobalt (CoNP) has high magnetism and can find application in different fields, such as industrial (as information storage, magnetic fluids and catalysts) and biomedical applications (in particular as highly sensitive magnetic resonance imaging contrast agents) (Colognato *et al.*, 2008; Horev-Azaria *et al.*, 2011). Several studies reported a dose- and time-dependent toxicity of CoNPs on different cellular models (Peters *et al.*, 2004; Mo *et al.*, 2008; Wan *et al.*, 2008; Kwon *et al.*, 2009; Ponti *et al.*, 2009; Horev-Azaria *et al.*, 2011; Jiang *et al.*, 2012; Wan *et al.*, 2012; Sabbioni *et al.*, 2014a). From

a mechanistic point of view, CoNPs toxicity and genotoxicity are due to ROS production and inhibition of antioxidant defenses (Wan *et al.*, 2008; Jiang *et al.*, 2012; Vales *et al.*, 2013; Wan *et al.*, 2012; Sabbioni *et al.*, 2014a). Since cobalt ions are known to be toxic, (Simonsen *et al.*, 2012), the release of Co^{2+} from CoNPs is usually considered a predominant factor in inducing toxicity (Kwon *et al.*, 2009; Ponti *et al.*, 2009; Jiang *et al.*, 2012).

The aim of this work was to better understand the factors that affect CoNP toxicity. To achieve this goal, we compared CoNP and Co^{2+} dose-response curves obtained with two viability assays (MTS and ATP assay) in three different cell models: A549 (epithelial cells from human lung carcinoma) as *in vitro* model for inhalation exposure; L929 (fibroblast cells from murine subcutaneous connective tissue) as model of dermal contact exposure; and HepG2 (epithelial cells from human hepatocellular carcinoma) as liver model. Then, late effects induced in the three model have been evaluated. These results were explained in light of ion release kinetics and cellular uptake.

3 Materials and Methods

3.1 Chemicals and reagents

Metallic zerovalent CoNPs (Product Code:CO-M-0251M-NP.030N) were purchased in dry form from American Elements® (Merelex Corporation, Los Angeles, CA, USA). They had the following properties, as indicated by the supplier: average diameter of 28 nm (with size range from 2 to 60 nm), specific area of 40-60 m^2/g and spherical shape. Acid solution of HNO_3 (67-69% SpA) and HCl (33-36% UpA) were purchased from Romil (Cambridge, UK). Reagents for biological characterization were: Tryptic Soy Agar (TSA; Biolife Italiana S.r.l.; Milan, IT); Venor®GeM Mycoplasma detection kit (Minerva Biolabs, Berlin, De), GoTaq® DNA polymerase, 5X Colorless GoTaq® Reaction Buffer, Blue/Orange 6X loading dye, 100bp DNA ladder (Promega; Madison, WI, USA); all reagents for the detection of endotoxin were purchased from Charles River Laboratories International, Inc (Charleston, SC, USA). $CoCl_2$ (Product Code: 60818), vitamin B_{12} (Product Code:V6629) Triton X-100 and agarose were purchased from Sigma–Aldrich

(Gillingham, UK). Sodium Dodecyl Sulphate (SDS), staurosporine (STS), Trizma® base primary standard and buffer, ethylenediaminetetraacetic acid disodium salt dehydrate (EDTA), acetic acid (puriss., 99-100%), ethidium bromide solution (10 mg/mL in H_2O) and Phosphate Buffer Saline (PBS)were purchased from Sigma-Aldrich (St. Louis, MO, USA). Cytotoxicity was tested with CellTiter 96 AQueous Non-Radioactive Cell Proliferation Assay kit Promega (Madison, WI, USA) and ATPlite (Perkin Elmer, Waltham, MA, USA). Human lung carcinoma epithelial cells (A549), murine subcutaneous connective tissue fibroblast cells (L929) and human hepatocellular carcinoma epithelial cells (HepG2) were obtained from American Type Culture Collection (Manassas, VA, USA). Solutions for cell culture were: Ham's F-12K and Eagle Minimum Essential Medium (EMEM), fetal bovine serum (FBS), penicillin-streptomycin solution, L-glutamine, phosphate buffered saline (PBS), Dulbecco's phosphate buffered saline with calcium and magnesium (DPBS), Trypsin-EDTA, all purchased from Lonza (Basel, CH). Protein quantification was conducted by using MicroBCA™ Protein Assay Kit (Thermo Scientific; Rockford, IL, USA).

3.2 CoNP characterization

CoNPs were characterized for chemical and biological contaminations and morphological properties.

3.2.1 Chemical characterization

To detect CoNP chemical impurities a semi-quantitative analysis (ranging from 6 to 240 amu) by inductively coupled plasma mass spectrometry (ICP-MS; NexION 300D, Perkin Elmer Inc.; Waltham, MA, USA) was conducted. In particular, dry NPs were solubilized with a microwave assisted acid digestion. NPs were weighted in specific Teflon vessels and suspended with 75% HNO_3 (67-69% SpA) and 25% HCl (33-36% UpA). Blank samples were added to the analysis to detect possible environmental contaminations. Microwave digestion was performed by using a Mars V microwave (CEM Corporation; Matthews, NC, USA) and the program used has foreseen two different steps: i) increase of temperature until 175°C in 5.5 minutes and ii) maintaining of 175°C for 4.5 minutes to complete digestion. After this acid digestion, solutions were diluted with ultrapure

water (18,3 MΩ·cm^{-1}) and analyzed by ICP-MS with a semi-quantitative method. The most concentrated elements detected were quantified by using an external calibration curve. To limit signal drift, a rhodium solution (10 µg/L) as internal standard was added online to each standard and sample solutions.

3.2.2 Biological contaminations

In order to avoid microbiological contaminations that could influence cellular responses during experiments, microbiological contaminations and endotoxin presence were tested on CoNPs suspensions. In particular, NPs were suspended at the concentration of 1 mg/mL in sterile water and ultrasonicated for 4 minutes at 50% of amplitude, corresponding to 28000 J (Misonix S-4000 Ultrasonic Liquid Processors, Qsonica LLC.; Newtown, CT, USA). To detect possible generic fungal and bacterial contaminations, 100 µL of the suspensions were plated in TSA plates and incubated at 37°C for 72 h. After the incubation, the presence of colonies on the plates was verified. In addition, mycoplasma contaminations were specifically tested using the Venor®GeM Mycoplasma detection kit according to manufacturer's instructions. Briefly, the possible mycoplasma contamination was detected by amplifying the highly conserved 16S rRNA coding region that generate an amplicon of approximately 267 bp. Internal DNA control of 191 bp was present in each sample, in order to confirm a successfully performed polymerase chain reaction (PCR). After PCR (Mastercycler; Eppendorf s.r.l.; Milan, IT), a 1.5% agarose gel in a Tris/acetic/ EDTA buffer (40 mMTris, 20 mM acetic acid and 1 mM EDTA) including ethidium bromide, as DNA staining, was cast and 10 µL of each PCR reaction, mixed with 2 µL of Blue/Orange 6X loading dye were loaded for electrophoresis (Peqlab Biotechnologie GmbH; Erlangen, DE); a 100 bp DNA ladder was used. At the end of the electrophoresis, gel were observed by a UV transilluminator (UVITEC; Cambridge, UK) and photographed.

The presence of endotoxins on suspension supernatants was tested by using the Limulus Amebocyte Lysate (LAL) Kinetic-turbidimetric method (Charles River Endosafe; Charleston, SC, USA). This analysis was conducted in a 96-well plate and consisted in optical density (λ = 340 nm) measurements over time with the microplate reader (Synergy4, Bio-Tek Instruments Inc.; Winooski, VT, USA). The assay included a

standard curve of *Escherichia coli* endotoxin (from 5 to 0.005 EU/mL) and different dilutions of supernatants with and without standard in order to evaluate possible interferences. In particular, the onset time, which means the time required for the absorbance to increase significantly over the background (0.05 OD units), was calculated and a linear relation between standard endotoxin concentrations and onset time was established in order to calculate sample endotoxin concentrations.

3.2.3 Morphological characterization

Morphological analyses were performed with two different techniques. In particular, CoNPs were suspended in sterile water at the concentration of 1 mg/mL, ultrasonicated (Misonix S-4000 Ultrasonic Liquid Processors, Qsonica LLC.; Newtown, CT, USA) for 4 minutes at 50% of amplitude (corresponding to 28000 J). This suspension was diluted in water at the concentration of 100 µg/mL to be examined by Transmission Electron Microscopy (TEM; FEI Tecnai 12 G2 electron microscope, FEI Co.; Eindhoven, NL) with Twin lens configuration after deposition on carbon coated, mesh 400 copper grids and left to dry. Micrographs were recorded on a side-mounted Morada CCD (Olympus Soft imaging Solutions GmbH, Münster, Germany) at magnifications ranging from 42000× to 265000×. To evaluate the aggregation state of NPs in suspension, dilution at the concentration of 10 µg/mL in cell culture complete media and water were done to be analyzed with the ZetasizerNano ZS Dynamic Light Scattering (DLS; Malvern Instruments; Malvern, UK). A blank (only cell culture media) sample were analyzed too. For the DLS analysis, suspensions were equilibrate at 25°C for 3 minutes and five measurements for sample were performed.

3.2.4 CoNP dissolution

CoNP suspensions in cell culture media were analyzed for ion release under our experimental conditions. In particular, different suspensions of CoNPs in cell culture media (0, 10, 100 and 1000 µg/mL) were prepared as in all the other analyses) were prepared from a stock suspension (10 mg/mL) that was ultrasonicated for 4 minutes at 50% of amplitude (corresponding to 28000 J). Each suspension was incubated at 37°C, 5% CO_2 and 90% of humidity for 0, 6, 24 and 48 h in 24-well plates (1 mL for each well).

At the end of incubation NPs were removed from suspensions by collecting samples in 2 mL tubes, centrifuging twice at 16000 g for 10 minutes and finally ultracentrifunging (Optima^{TM} L-100XP Ultracentrifuge; Beckman Coulter; Urbana, IL, USA) for 2 hours at 300000 g at 4°C. Ultracentrifugation was conducted in polycarbonate tubes (Beckman Coulter; Urbana, IL, USA) with the rotor type 70.1.Ti (Beckman Coulter). Supernatants were collected and diluted with a 2% HNO_3 solution prior to being analyzed for ion quantification with ICP-MS (NexION 300D, Perkin Elmer; Waltham, MA, USA).Simultaneously, 100 µg/mL solutions of Co^{2+}in cell culture media and ddH_2O were analyzed to monitor the ion behavior during the experiment. In addition, not ultracentrifuged NP suspensions and ion solutions were quantitatively analyzed by ICP-MS. In particular, ion solutions were simply diluted in 2% HNO_3 solution in the calibration curve concentration range, whereas, NP suspensions were solubilized by microwave acid digestion (Mars V,CEM). 500 µL of each suspension were transferred in specific Teflon vessels and 10 mL of HNO_3(67-69% SpA) were added. Blank samples were included to the analysis to detect possible environmental contaminations. Microwave digestion program has foreseen two different steps: 1) increase of temperature until 175°C in 7 minutes and 2) maintaining of 175°C for 3 minutes to complete digestion. After this acid digestion, solutions were diluted with ultrapure water (18,3 MΩ·cm^{-1}) and analyzed by ICP-MS (NexION 300D, Perkin Elmer; Waltham, MA, USA). ICP-MS quantitative analyses of ionic release and NP and ion solution were performed using an external calibration curve. To limit signal drift, a rhodium solution (10 µg/L) as internal standard was added online to each standard and sample solutions.

Furthermore, the effect of sonication on ion release was investigated. In particular, two stock suspensions of CoNPs were prepared in sterile H_2O at the concentration of 10 mg/mL. The first stock was ultrasonicated, while the second vortexed for 1 minute. Two different analysis were performed by ICP-MS (as described above): i) total Co concentration after digestion; ii) Co quantification after removal of NPs from stock suspension by ultracentrifugation; iii) soluble Co concentration after dilution of aqueous suspension in EMEM (1 mg/mL) and removal of NPs by ultracentrifugation.

3.3 Cell viability analyses

3.3.1 Cell culture and sub-culturing procedure

A549, L929 and HepG2 cells were maintained following ATCC indications. A549 cells were cultured in Ham's F12K medium with the addition of 10 % FBS, 100 units/mL streptomycin and 100 µg/mL penicillin. HepG2 and L929 cells were cultured in EMEM with the addition of 10%FBS, 100 units/mL streptomycin and 100 µg/mL penicillin and 2mM L-glutamine. All the three cell lines were kept at 37°C, 5% CO_2 and 90% of humidity for maintenance and for experiments.

3.3.2 CoNP and Co^{2+} toxicity

In order to evaluate the cytotoxic effects of CoNPs and Co^{2+}, cells were seeded in 96-well microplate and, 24 h after seeding, treated with different concentrations of NP and ions for 6, 24 and 48 h. The seeding densities of cells were those at which cells proliferated overtime: 5000 cell/well for A549 and L929 cells, and 15000 cell/well for HepG2 cells. Treatment solutions or suspensions were freshly prepared before each test. In particular, NPs were suspended in sterile water and ultrasonicated for 4 minutes at 50% of amplitude (corresponding to 28000 J) in order to make a stock suspension that was diluted in the proper cell culture media without exceeding the 10% of the total volume of the treatment. Ion stock solutions were prepared in ddH_2O, filtered with 0.22 µm pore size filter and diluted in cell culture media as NP stock suspensions. Experiments were performed in triplicate. Viability was assessed after the removal of cell culture media and washing of cells with DPBS in order to eliminate possible NP interferences (Kroll *et al.*, 2012). The two assays used were: MTS assay and ATP assay were performed according to manufacturer's instructions. The MTS assay analyzes the conversion of a tetraziolium salt 3-(4,5-dimethylthiazol-2-yl)-5-(3-carboxymethoxyphenyl)-2-(4-sulfophenyl)-2H] (MTS) into its reduced and soluble formazan form by mitochondrial enzyme of metabolically active cells and was evaluated by recording absorbance at 490 nm. ATP assay is based on light production caused by the reaction of ATP with added luciferase and D-luciferin and quantify the ATP content. Both absorbance and

luminescence were recorded with the Synergy4 microplate reader (Bio-Tek Instruments).

3.3.3 Vitamin B_{12} toxicity

Vitamin B_{12} (Vit B_{12}) was tested on all the three cell models with the ATP assay (following the same experimental procedure used for CoNPs and Co^{2+}). Briefly, cells were treated with different concentration of Vit B_{12} for 6, 24 and 48 h. At the end of treatment, cells were washed twice with DPBS and ATP assay was performed following manufacturer's instructions.

3.3.4 Late effects

Possible late effects induced by of CoNPs and Co^{2+} exposure were analyzed by incubating cells with each cobalt compound for 6 h, removing treatments and replacing with fresh culture media, after washing cells twice with DPBS, and finally analyzing ATP content at 24 and 48 h post treatment.

3.4 Cellular uptake

Cellular uptake of CoNPs and Co^{2+} was quantitatively analyzed by ICP-MS (NexION 300D, Perkin Elmer). Cells were seeded in 24-well plate at densities 10 times higher compared to those used in 96-well plate experiments. After 24 h from seeding, cells were treated with 10 µg/mL of CoNPs or Co^{2+} for 24 h from stock suspensions prepared similarly to cytotoxicity tests. At the end of exposure time, cells were washed three-times with PBS to remove NPs and ions not internalized. Cells were then detached with 200 µL of Trypsin-EDTA and collected with 800 µL of PBS to be analyzed for protein quantification and uptake. Samples dedicated to protein quantification were centrifuged at 16000 g for 5 minutes. Then, supernatants were discarded and cell pellets were lysed with a lysis solution containing PBS 1X, 1% Triton X-100 and 1% SDS. Protein quantification was conducted using the microBCA assay. Bovine Serum Albumin (BSA) provided by the kit was diluted to prepare different standards in the linear concentration range of 10-40 µg/mL and manufacturer's instructions were followed. To analyze uptake, samples were centrifuged at 400 g for 15 minutes. Once supernatants

were discarded pellets were digested with 1mL of HNO_3. After an overnight incubation at room temperature, samples were incubated 12 h at 70°C in Thermoblock (FALC Instruments; Treviglio, IT) and finally diluted in ultrapure H_2O (18,3 $M\Omega \cdot cm^{-1}$). The obtained solutions were quantitatively analyzed by ICP-MS (NexION 300D, Perkin Elmer; Waltham, MA, USA) by using Dynamic Reaction Cell (DRC) method with a standard calibration curve and a rhodium solution as internal standard.

3.5 Statistical analyses

Statistical analyses were performed using Origin Pro 8.0 software (OriginLab; Northampton, MA, USA). Considering fitting curve analyses, cytotoxicity results were fitted by sigmoid functions and EC50 values were calculated. Statistical significances were determined by ANOVA analysis (P value < 0.05).

4 Results

4.1 CoNP characterization

CoNPs showed three main elemental contaminants: aluminum (Al), arsenic (As) and boron (B) (Table 1). With respect to biological contaminations, no microbiological contaminations were found, and the endotoxin levels were below 0.01 EU/mL (corresponding to levels found in sterile water).

TABLE 1. Elemental contaminations of CoNPs.

	Concentration	
Element	µg/g [a] ± SD	% [b] ± SD
Al	1258 ± 493	0.13 ± 0.05
As	171 ± 18	0.02 ± 0.002
B	423 ± 91	0.042 ± 0.009

a: dry weight
b: % expressed as w/w (dry weight)
SD: standard deviation (mean of three determinations).

From TEM images, CoNPs appeared heterogeneous in size, spheroidal in shape and with a crystalline structure (Fig. 1). A strong aggregation state hampered an accurate size determination, even with manual particle selection methods. The presence of aggregates was confirmed by analyzing CoNP suspensions with DLS, as indicated by the high polidispersity index and the presence of very large objects. In the presence of cell culture media, smaller aggregates compared to water suspensions were observed (Fig. 2).

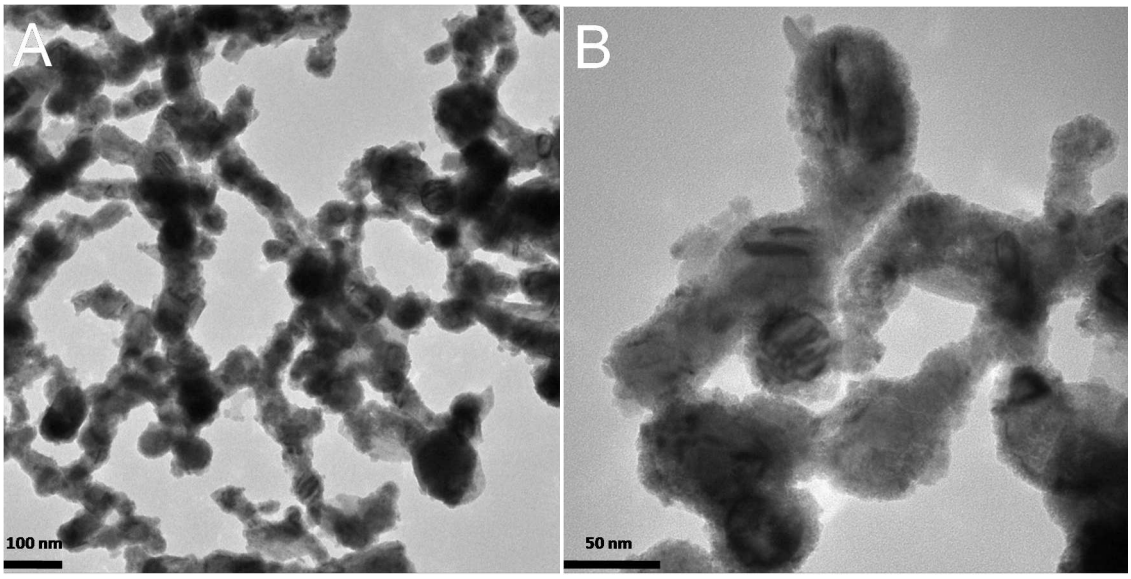

FIGURE 1. TEM images of CoNPs at different instrumental magnification: A) 97000 ×; B) 310000 ×.

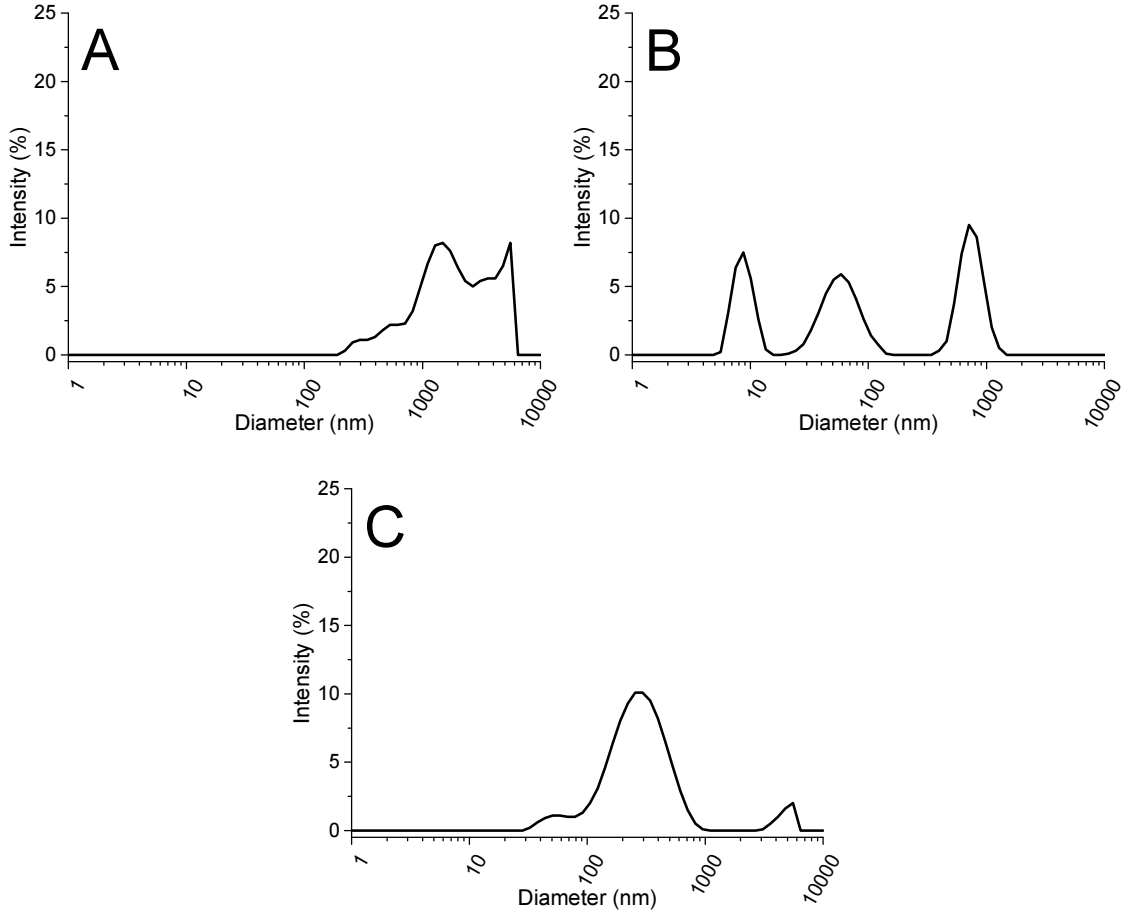

FIGURE 2. DLS size distribution performed in A) water (PdI = 0.472); B) Ham's F-12K medium (PdI = 0.563) and C) EMEM (PdI = 0.448).

4.2 CoNP dissolution

Before performing dissolution studies of CoNPs by ultracentrifugation, the behavior of Co^{2+} in water and in EMEM and Ham's F-12K culture media was studied. After ultracentrifugation, a significant reduction of Co^{2+} content was found in both cell culture media, while no differences were detected in aqueous solutions (Fig.3). However, no changes in Co^{2+} content after ultracentrifugation were observed over time, suggesting that no precipitation occurred under our experimental conditions (Fig. 4). Dissolution experiments of CoNPs showed that Co^{2+} is released in a dose- and time-dependent manner (Fig. 5). Although the total amount of released Co increases as a function of CoNP concentration (Fig. 5A, 5B), the relative amount of soluble Co is higher

at low NP concentrations (Fig. 5C, 5D). No significant differences in CoNP behavior between the two media were observed.

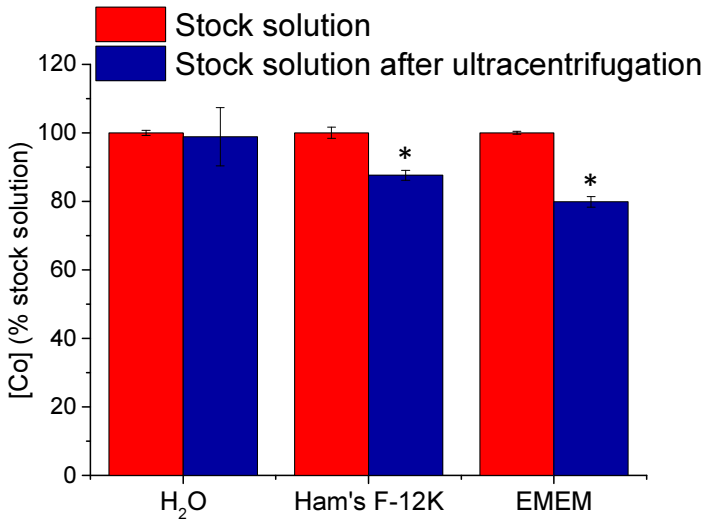

FIGURE 3. Analysis of concentrations of Co^{2+} before and after ultracentrifugation in water and cell culture media (Ham's F-12K and EMEM). Data are expressed as mean of three different measurements, each of them expressed as % of stock solution concentrations. Error bars represent standard deviations of three different measurements. *Significant different from stock solution (P value < 0.05)

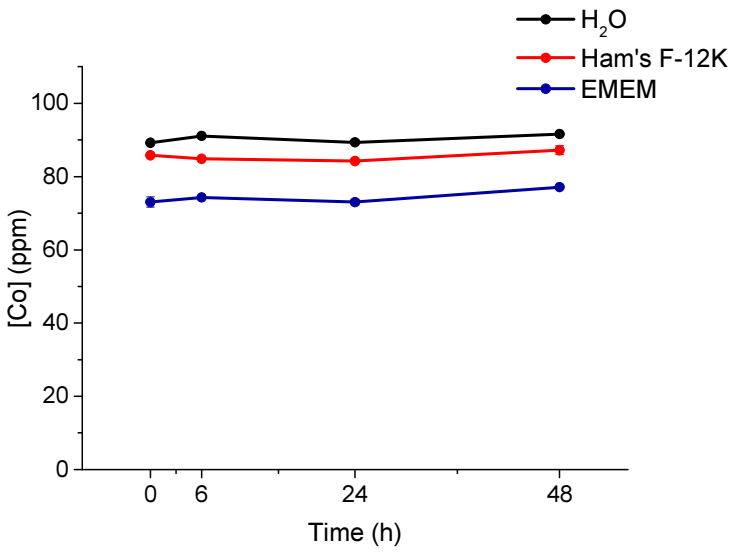

FIGURE 4. Co^{2+} in solutions in water and cell culture media (Ham's F-12K and EMEM) over time. Data are expressed as means of three measurements and error bars represents standard deviations.

Interestingly, high ionic concentration was found at the starting time (0 h). To verify the role of sonication in inducing CoNP dissolution, Co content in both sonicated and no-

sonicated NP stock suspensions was determined. No significant differences in ion release with or without sonication were found. Indeed, by analyzing the supernatant of the 10 mg/mL CoNP aqueous suspension, 1.4 ppm of Co^{2+} in the no-sonicated sample and 1.2 ppm in the sonicated one were measured, suggesting that in our experimental conditions sonication does not affect dissolution. Interestingly, the analysis of Co soluble fraction in cell culture media (obtained by dilution of the two stock suspensions) revealed higher amount (about 10%) compared to those obtained in aqueous stock suspensions (about 0.1%).

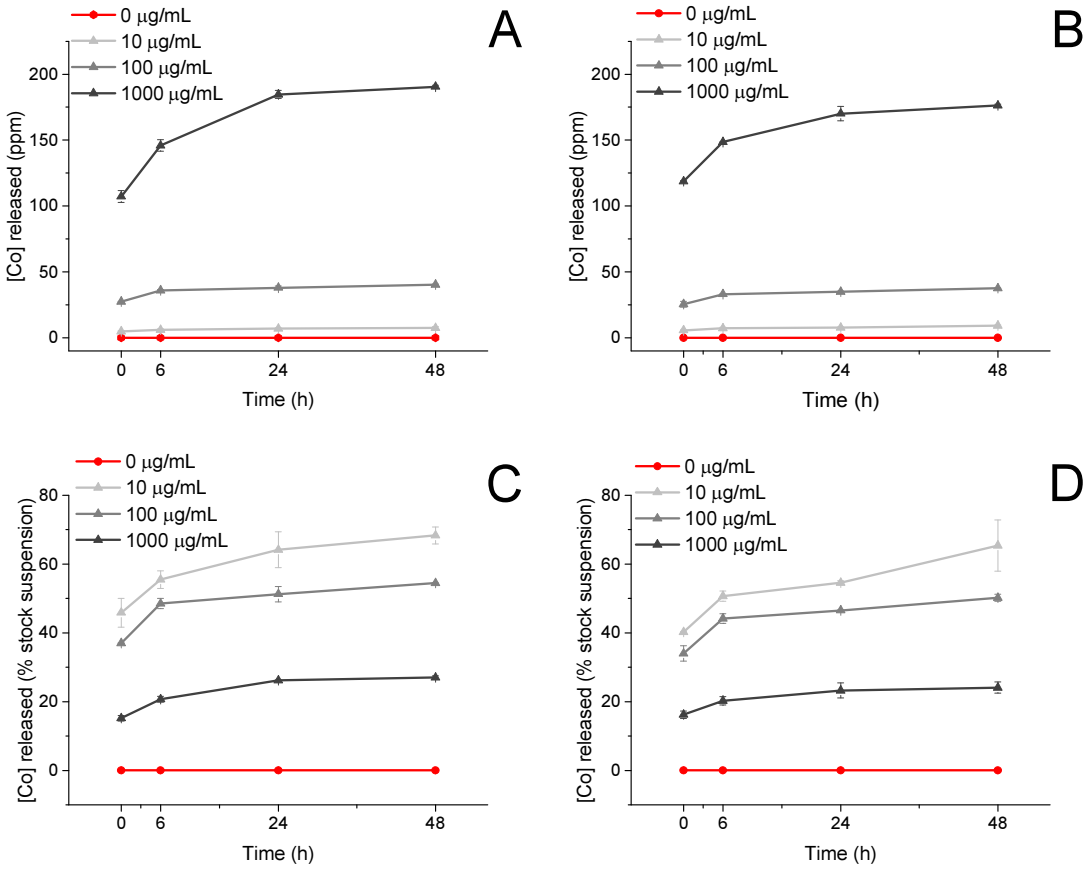

FIGURE 5. Ions released by CoNPs in Ham's F-12K (A, C) and EMEM (B, D) media overtime. Ion concentrations are reported as ppm (A, B) and % of stock suspension (C, D). Data are expressed as means of three measurements and error bars represents standard deviations.

4.3 CoNP and Co^{2+} toxicity

Cell viability after treatment with CoNPs and Co^{2+} for 6, 24 and 48 h was evaluated by performing two different assays (ATP and MTS). For each exposure time, dose-response curves were fitted (Fig. 6, 7, 8) and EC50 values calculated (Table 2). ATP and MTS assays showed a dose-dependent effects of CoNPs and Co^{2+} in all the three *in vitro* models (Fig. 6, 7, 8). Moreover, EC50 values obtained from dose-response curve showed also a time dependency of toxicity (Table 2). Although the impact on cell viability of CoNPs and Co^{2+} ions depended on the *in vitro* model used, dose-response

curves and the relative EC50 values indicated a similar toxic effect for both CoNPs and Co^{2+} ions for each cell model. Major differences were observed at 6 h exposure time, while for longer exposure (24 and 48 h) the effects on cell viability were comparable between NPs and ions.

The *in vitro* cell models showed different susceptibility to both CoNP and Co^{2+} ions with the following ranking: A549 > L929 > HepG2 (Table 2).

TABLE 2. EC50 values of CoNPs and Co^{2+} in the three cell models at 6, 24 and 48 h.

	EC50 (μg/mL)								
	A549			L929			HepG2		
Compound	6 h	24 h	48 h	6 h	24 h	48 h	6 h	24 h	48 h
	ATP assay								
CoNP	81.8	27.6	3.4	181.8	39.4	12.9	202.2	70.7	6.9
Co^{2+}	19.3	17.8	11.3	183	28.1	12.2	220.9	43	12.3
	MTS assay								
CoNP	237.3	26.6	19.6	113.3	34.5	13.3	169.8	75	40.8
Co^{2+}	133.8	49.6	21.6	81.7	34.2	11.3	291.3	64.9	25.1

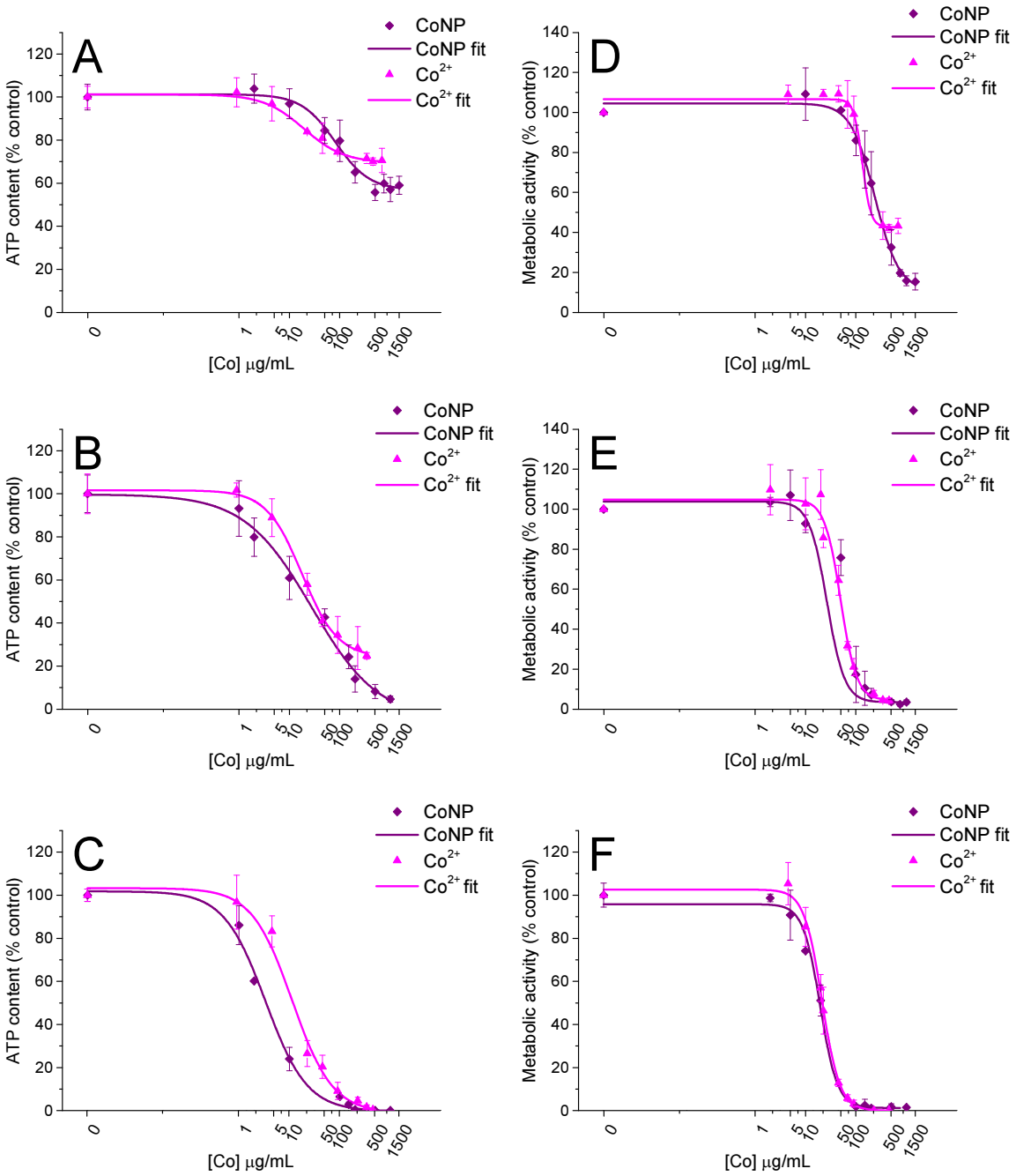

FIGURE 6. Dose-response curves obtained by treating A549 cells with CoNPs and Co^{2+} for 6 (A, D), 24 (B, E) and 48h (C, F). Panels A, B, C refer to ATP assay, while panels D, E, F refer to MTS assay. Data are expressed as mean of three independent experiments and error bars represent standard deviations.

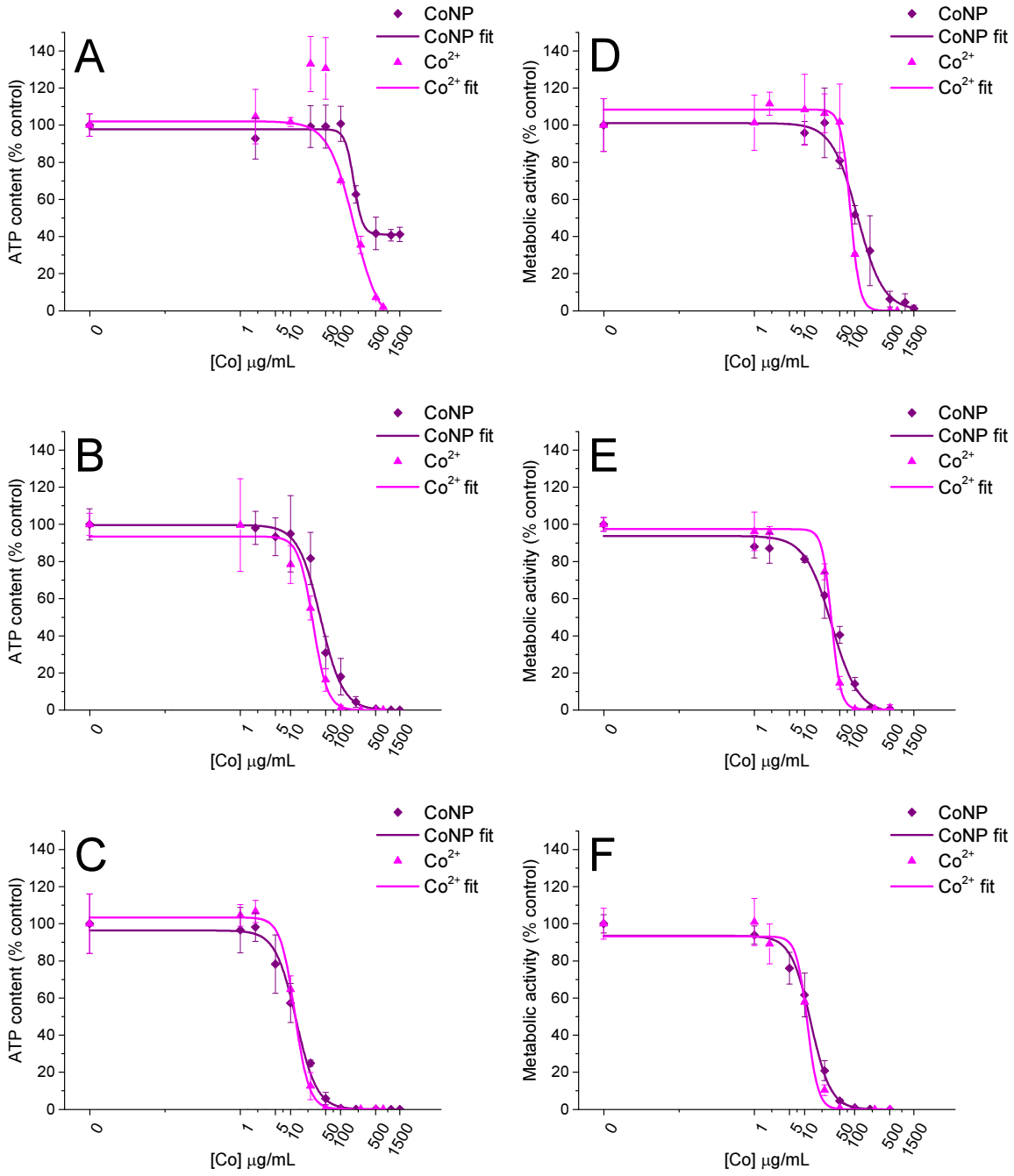

FIGURE 7. Dose-response curves obtained by treating L929 cells with CoNPs and Co^{2+} for 6 (A, D), 24 (B, E) and 48h (C, F). Panels A, B, C refer to ATP assay, while panels D, E, F refer to MTS assay. Data are expressed as mean of three independent experiments and error bars represent standard deviations.

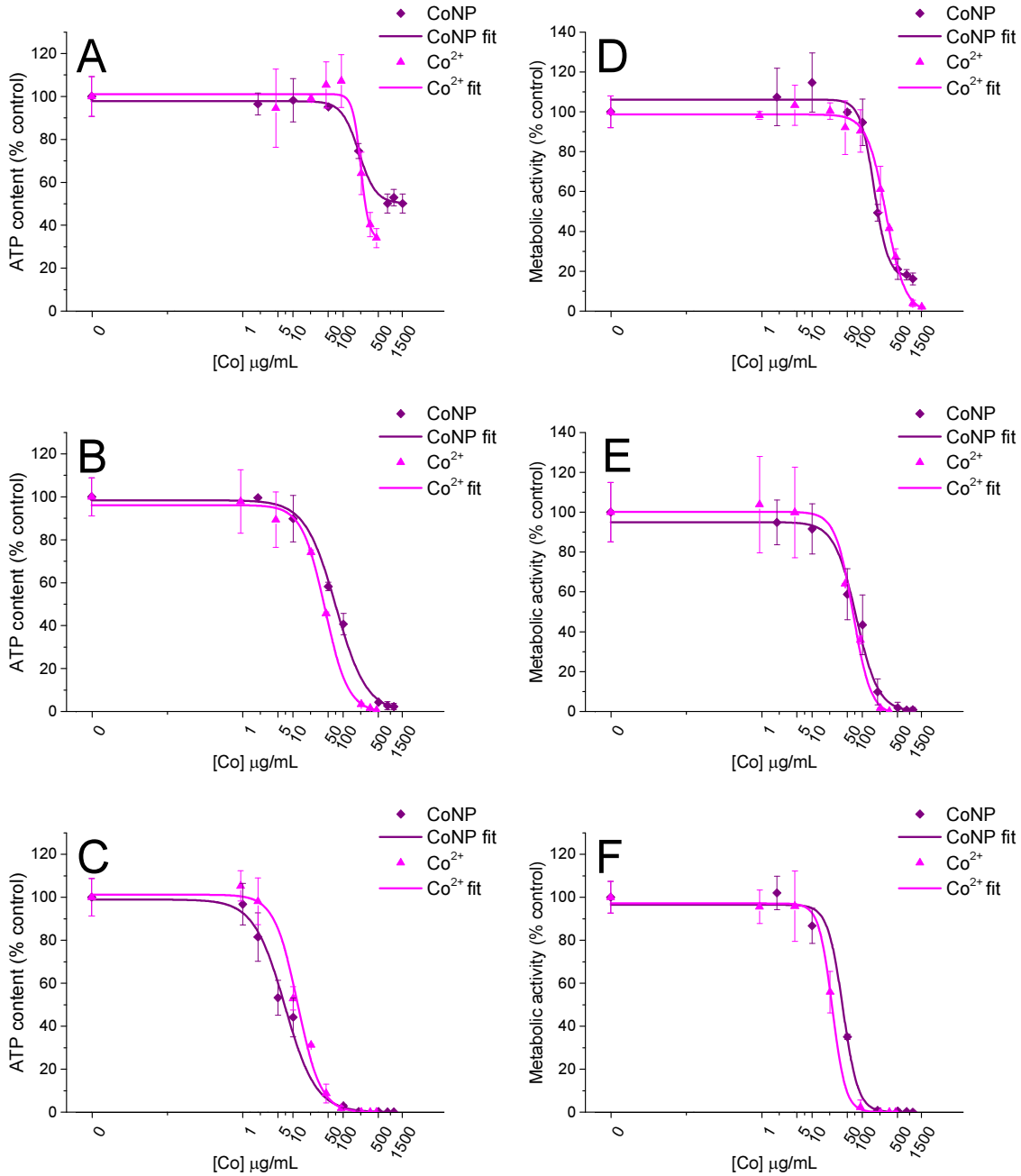

FIGURE 8. Dose-response curves obtained by treating HepG2 cells with CoNPs and Co^{2+} for 6 (A, D), 24 (B, E) and 48h (C, F). Panels A, B, C refer to ATP assay, while panels D, E, F refer to MTS assay. Data are expressed as mean of three independent experiments and error bars represent standard deviations.

4.4 Vitamin B_{12} toxicity

Vit B_{12} is the only physiological form for cobalt. Therefore, its impact of physiological cobalt on cell viability in the same concentration range used for CoNP and Co^{2+} was also studied. As shown in Fig. 9, Vit B_{12} does not affect cell viability. Since Vit B_{12} is the well-known physiological form of cobalt, our findings confirmed that biological systems are able to use essential elements only in their physiological forms.

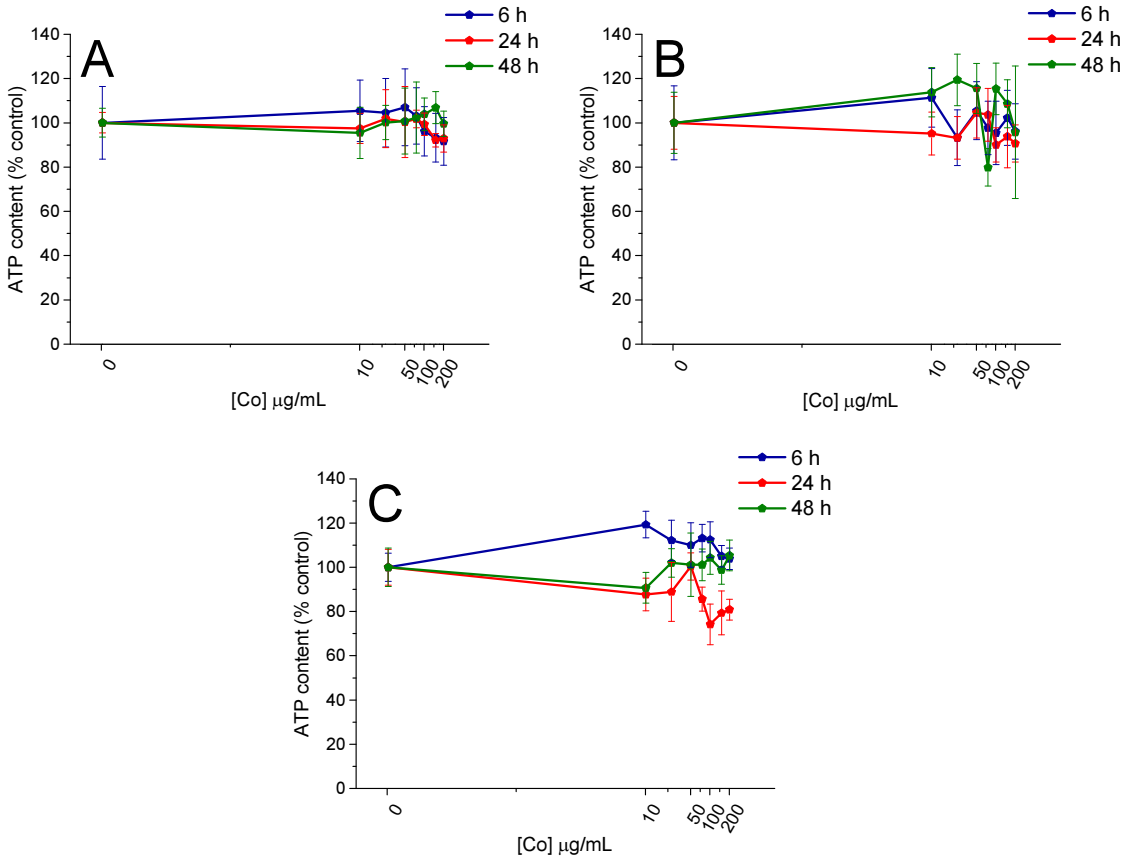

FIGURE 9. Vitamin B_{12} toxicity on A549 (A), L929 (B) and HepG2 (C) cells at different exposure time (6, 24, 48 h) evaluated by ATP assay. Data are expressed as mean of three independent experiments and error bars represent standard deviations.

4.5 Late effects

Late effects on cell viability after short-time exposure to CoNP and Co^{2+} ions were evaluated. Cells were treated with CoNP and Co^{2+} for 6 h, and their viability measured after 24 and 48 h after the removal of treatments. Dose-response curves for Co^{2+} and

CoNPs were time-dependent and showed a reduced toxicity than those obtained after long incubation times (Fig. 10, 11). Furthermore, CoNP toxicity resulted time-dependent if maximum effects were considered, whereas EC50 values did not change between 24 and 48 h (Table 3). On the other hand, Co^{2+} time-dependent toxicity can be observed by considering both maximum effects and EC50 values (Table 3).

TABLE 3. Maximum effect and EC50 values of L929 and HepG2 cells after 6 h of exposure with Co compound and 24 and 48 h of recovery.

	L929		HepG2	
Compound	**24 h**	**48 h**	**24 h**	**48 h**
	Max effect (% control)			
CoNP	15.4	5.7	71.9	25.8
Co^{2+}	0	0	11.9	0
	EC50 (μg/mL)			
CoNP	20.7	26.9	11.3	14.8
Co^{2+}	101.6	75.5	N.D.	72.2

N.D: not determined

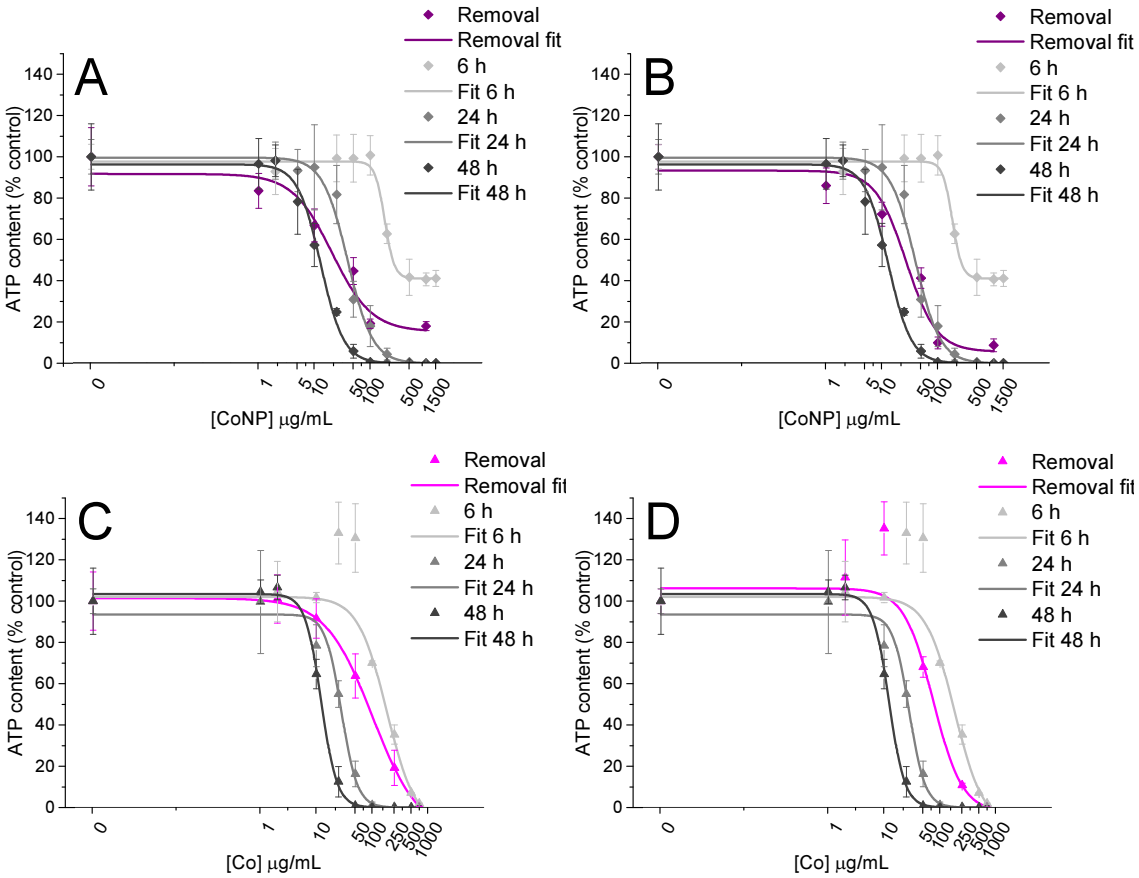

FIGURE 10. CoNP (A, B) and Co^{2+} (C, D) toxicity on L929 cells measured by ATP assays after the removal of treatments (6 h post treatments). ATP assay were performed after 24 h (A, C) and 48 h (B, D) from treatment. Dose-response curves obtained by treating cells with CoNP and Co^{2+} for 6, 24 and 48 h were also reported. Data are expressed as mean of three independent experiments and error bars represent standard deviations.

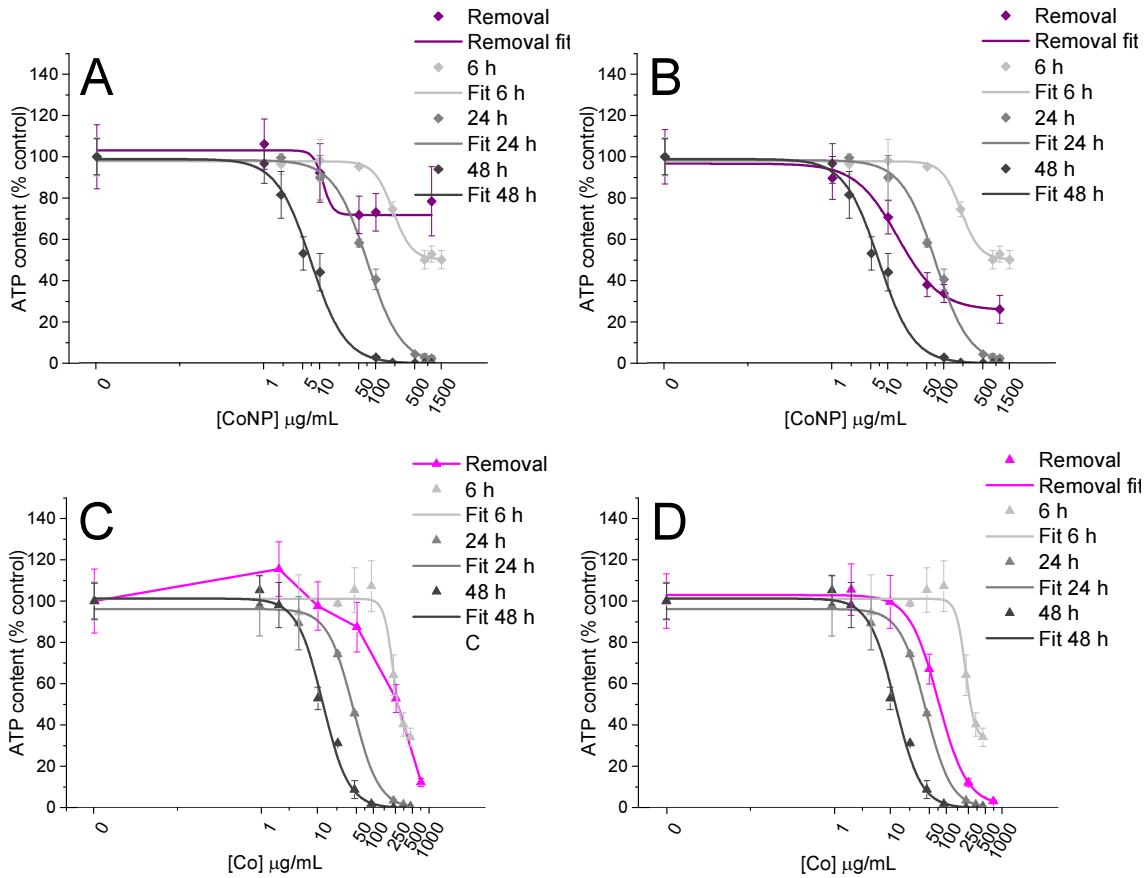

FIGURE 11. CoNP (A, B) and Co^{2+} (C, D) toxicity on HepG2 cells measured by ATP assays after the removal of treatments (6 h post treatments). ATP assays were performed after 24 h (A, C) and 48 h (B, D) from treatment. Dose-response curves obtained by treating cells with CoNP and Co^{2+} for 6, 24 and 48 h were also reported. Data are expressed as means of three independent experiments and error bars represent standard deviation.

4.6 Cellular uptake

Uptake experiments, concerning exposure of cells for 24 h with CoNPs and Co^{2+} ions, showed intracellular concentration of cobalt significantly higher with NP exposure compared to ionic treatments (Fig. 12). This suggest a more efficiently internalization of the cobalt in the form of particles than its ionic form (Fig. 12). In addition, intracellular cobalt concentrations were significantly different in the three *in vitro* models, with L929 cells showing higher cobalt content that A549 and HepG2 cells ($P < 0.05$).

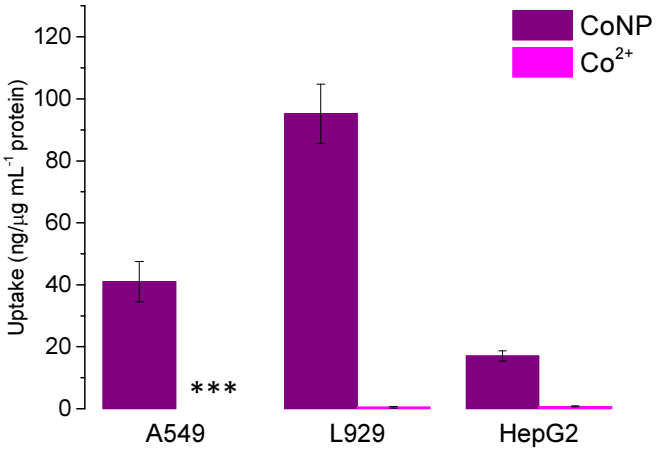

FIGURE 12. Uptake of CoNPs and Co^{2+}in A549, L929 and HepG2 cells. Data are expressed as ng of Co for µg/mL of proteins and error bars are standard deviations. ***Under detection limit (0.47µg/mL).

5 Discussion

Uncoated CoNPs appear strongly aggregated, though in cell culture media aggregates are smaller than in aqueous suspension. This is probably due to the interaction of NP with serum proteins as already observed with other metallic NPs (Murdock *et al.*, 2008). CoNPs release ions in a time- and concentration-dependent fashion, as observed in other studies (Ponti *et al.*, 2009; Jiang *et al.*, 2012; Sabbioni *et al.*, 2014b). Moreover, we confirmed a higher dissolution rate at lower CoNP concentrations (Sabbioni *et al.*, 2014). This could be due to the presence of larger aggregates and lower surface-to-volume ratios at high CoNP concentrations (Misra *et al.*, 2012; Gliga *et al.*, 2014). Cell culture media favors ion release from CoNP surface because of the presence of Co sequestering agents, such as albumin and histidine, that shift the equilibrium toward free ions (Sabbioni *et al.*, 2014b).

CoNPs and Co^{2+} induce a time- and dose-dependent toxicity in all the three *in vitro* models. After 6 h exposure, CoNP are less toxic than Co^{2+} ions, while after 24 and 48 h incubation CoNP and Co^{2+} ions show similar effects on cell viability, in agreement with their time-dependent dissolution. Their similar toxicity has been reported in the literature, though these studies carried out in other *in vitro* models showed a higher toxicity of CoNPs compared to Co^{2+} for shorter exposure time, in apparent contrast with

our findings (Ponti *et al.*, 2009; Jiang *et al.*, 2012; Sabbioni *et al.*, 2014a). The removal of treatment after 6 h, and the evaluation of cell viability after 24 and 48 h recovery, shows that CoNP and Co^{2+} toxicity is reduced but maintains time-dependency. With particular reference to CoNPs, we can speculate that their toxicity is closely related to dissolution occurring in cell culture media or inside cells. Indeed, the removal of NPs after 6 h, so limiting extracellular ions, causes a time-dependent toxicity at 24 and 48 h in agreement with their intracellular time-dependent dissolution. It has been also analyzed the toxicity of the only physiological form of cobalt, Vit B_{12}. Despite the high concentration (considering that human nutritional requirement is 4 μg for adults), Vit B_{12} does not induce any adverse effect, in agreement with its physiological role (Seetharam and Alpers, 1982). This finding confirmed the crucial role of the chemical form in relation to the biological effects of elements in biological systems, as they can use and manage trace elements, including cobalt, only in defined chemical form, being other chemical species able to induce toxic effects (Bresson *et al.*, 2013).

Cell uptake studies showed the presence of significant amount of cobalt in cells exposed to CoNP compared to cells exposed to ions. However, in the present study, the cobalt internalization was determined as total cobalt and we could not establish whether its chemical form inside cells, such as particle, ion or both. In any case, our results agree with previous observation on another cell model (fibroblasts Balb/3T3 cells), in which considerable cobalt concentration were reached in cell organelles after CoNP exposure (Sabbioni *et al.*, 2014b). Interestingly, we have found differences in the extent of cobalt internalization in the three *in vitro* cell models. The murine fibroblast L929 cells show higher CoNP internalization than A549 (lung epithelial cells) and HepG2 (hepatocytes) cells. However, the different cell susceptibility seems not related to differences in internalized Co concentration. Indeed, despite their similar uptake, A549 are the most susceptible cell models, while HepG2 cells result to be less affected by Co.

To conclude, CoNPs toxicity is closely related to NP dissolution process occurring in cell culture medium and/or inside cells, as represented by Fig.13.

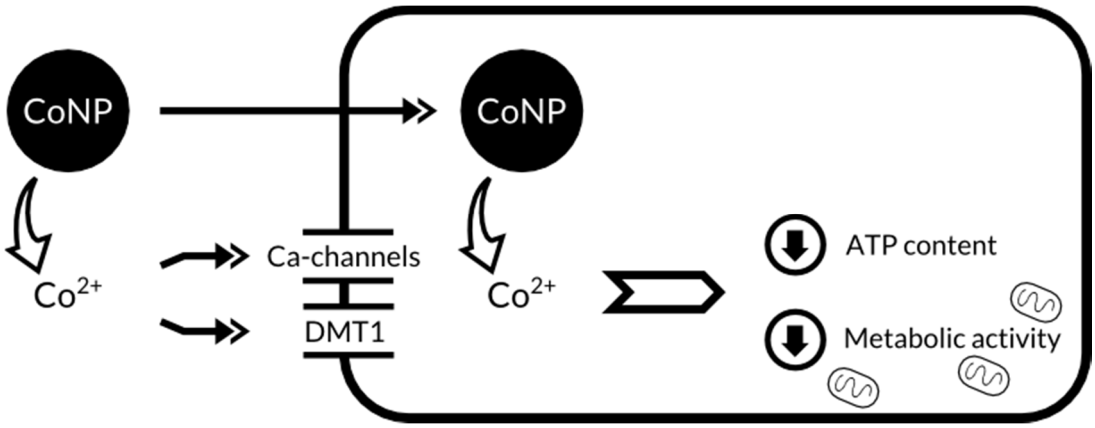

FIGURE 13. Possible mechanism of CoNP toxicity. Cell exposed to CoNPs can internalize CoNPs that release Co^{2+} inside cells. On the other hand, the release of Co^{2+} can also occur in culture medium and free ions can be internalized through divalent metal transporter (DMT1) and calcium channel. Once inside cells, Co^{2+} leads to a decrease in cell viability ATP content and in mitochondrial metabolic activity.

6 References

Bresson C., Darolles C., Carmona A., Gautier C., Sage N., Roudeau S., Ortega R., Ansoborlo E. and Malard V. (2013). Cobalt chloride speciation, mechanisms of cytotoxicity on human pulmonary cells, and synergistic toxicity with zinc. *Metallomics* 5(2): 133-144.

Colognato R., Bonelli A., Ponti J., Farina M., Bergamaschi E., Sabbioni E. and Migliore L. (2008). Comparative genotoxicity of cobalt nanoparticles and ions on human peripheral leukocytes in vitro. *Mutagenesis* 23(5): 377-382.

Cotton F. A. and Wilkinson G. (1972). Advanced inorganic chemistry. A comprehensive text. *John Wiley & Sons, Inc.*, New York. pp.1145.

Da Silva J. F. and Williams R. (2001). The biological chemistry of the elements: the inorganic chemistry of life. *Oxford University Press*, Oxford. pp.561.

Gliga A. R., Skoglund S., Wallinder I. O., Fadeel B. and Karlsson H. L. (2014). Size-dependent cytotoxicity of silver nanoparticles in human lung cells: the role of cellular uptake, agglomeration and Ag release. *Part. Fibre Toxicol.* 11(1): 11.

Horev-Azaria L., Kirkpatrick C. J., Korenstein R., Marche P. N., Maimon O., Ponti J., Romano R., Rossi F., Golla-Schindler U., Sommer D., Uboldi C., Unger R. E. and Villiers C. (2011). Predictive toxicology of cobalt nanoparticles and ions: comparative in vitro study of different cellular models using methods of knowledge discovery from data. *Toxicol. Sci.* 122(2): 489-501.

Jiang H., Liu F., Yang H. and Li Y. (2012). Effects of cobalt nanoparticles on human T cells in vitro. *Biol. Trace Elem. Res.* 146(1): 23-29.

Kroll A., Pillukat M. H., Hahn D. and Schnekenburger J. (2012). Interference of engineered nanoparticles with in vitro toxicity assays. *Arch. Toxicol.* 86(7): 1123-1136.

Kwon Y. M., Xia Z., Glyn-Jones S., Beard D., Gill H. S. and Murray D. W. (2009). Dose-dependent cytotoxicity of clinically relevant cobalt nanoparticles and ions on macrophages in vitro. *Biomed. Mater.* 4(2): 025018.

Misra S. K., Dybowska A., Berhanu D., Luoma S. N. and Valsami-Jones E. (2012). The complexity of nanoparticle dissolution and its importance in nanotoxicological studies. *Sci.Total Environ.* 438: 225-232.

Mo Y., Zhu X., Hu X., Tollerud D. J. and Zhang Q. (2008). Cytokine and NO release from peripheral blood neutrophils after exposure to metal nanoparticles: in vitro and ex vivo studies. *Nanotoxicology* 2(2): 79-87.

Murdock R. C., Braydich-Stolle L., Schrand A. M., Schlager J. J. and Hussain S. M. (2008). Characterization of nanomaterial dispersion in solution prior to in vitro exposure using dynamic light scattering technique. *Toxicol. Sci.* 101(2): 239-253.

Peters K., Unger R. E., Kirkpatrick C. J., Gatti A. M. and Monari E. (2004). Effects of nano-scaled particles on endothelial cell function in vitro: studies on viability, proliferation and inflammation. *J. Mater. Sci. Mater. Med.* 15(4): 321-325.

Ponti J., Sabbioni E., Munaro B., Broggi F., Marmorato P., Franchini F., Colognato R. and Rossi F. (2009). Genotoxicity and morphological transformation induced by cobalt nanoparticles and cobalt chloride: an in vitro study in Balb/3T3 mouse fibroblasts. *Mutagenesis* 24(5): 439-445.

Roth J. R., Lawrence J. G. and Bobik T. A. (1996). Cobalamin (coenzyme B12): synthesis and biological significance. *Annu. Rev. Microbiol.* 50: 137-181.

Sabbioni E., Fortaner S., Farina M., Del Torchio R., Olivato I., Petrarca C., Bernardini G., Mariani-Costantini R., Perconti S., Di Giampaolo L., Gornati R. and Di Gioacchino M. (2014a). Cytotoxicity and morphological transforming potential of cobalt nanoparticles, microparticles and ions in Balb/3T3 mouse fibroblasts: an in vitro model. *Nanotoxicology* 8(4): 455-464.

Sabbioni E., Fortaner S., Farina M., Del Torchio R., Petrarca C., Bernardini G., Mariani-Costantini R., Perconti S., Di Giampaolo L., Gornati R. and Di Gioacchino M. (2014b). Interaction with culture medium components, cellular uptake and intracellular distribution of cobalt nanoparticles, microparticles and ions in Balb/3T3 mouse fibroblasts. *Nanotoxicology* 8(1): 88-99.

Seetharam B. and Alpers D. H. (1982). Absorption and transport of cobalamin (vitamin B12). *Annu. Rev. Nutr.* 2: 343-369.

Simonsen L. O., Harbak H. and Bennekou P. (2012). Cobalt metabolism and toxicology--a brief update. *Sci. Total Environ.* 432: 210-215.

Vales G., Demir E., Kaya B., Creus A. and Marcos R. (2013). Genotoxicity of cobalt nanoparticles and ions in Drosophila. *Nanotoxicology* 7(4): 462-468.

Wan R., Mo Y., Feng L., Chien S., Tollerud D. J. and Zhang Q. (2012). DNA damage caused by metal nanoparticles: involvement of oxidative stress and activation of ATM. *Chem. Res. Toxicol.* 25(7): 1402-1411.

Wan R., Mo Y., Zhang X., Chien S., Tollerud D. J. and Zhang Q. (2008). Matrix metalloproteinase-2 and -9 are induced differently by metal nanoparticles in human monocytes: The role of oxidative stress and protein tyrosine kinase activation. *Toxicol. Appl. Pharmacol.* 233(2): 276-285.

CHAPTER 3

Nickel nanoparticles: the dual toxicity mechanism

1 Abstract

In this study, the toxic effects of nickel nanoparticles (NiNPs) and their relative ions (Ni^{2+}) were evaluated. Toxicity was analyzed in three different *in vitro* models: carcinomic human alveolar basal epithelial cell line (A549) and murine aneuploid fibrosarcoma cell line (L929) as in vitro models for inhalation and dermal contact, and human hepatocellular liver carcinoma cell line (HepG2) as a liver model. In addition, we studied NiNPs dissolution kinetics and nickel intracellular content after cell exposure. NiNPs resulted less toxic than Ni^{2+}. NiNP dose-response relationship was characterized by a bimodal trend. In relation to the time- and dose-dependent NP dissolution, we hypothesized that he first transition was probably due to the NP itself and the second one to the released ions. In order to disclose these effects, NiNP cytotoxicity was evaluated in the presence of two different Ni^{2+} chelators: L-cysteine and L-histidine that show a strong affinity for this ion at the physiological pH range. In their presence, NiNP showed a unimodal dose-response curve with the maximum effect corresponding to the first transition obtained in the absence of nickel chelators. This finding confirms the role of dissolution and released ions in inducing the second transition. Finally, Ni internalization could partially explain differences in cell susceptibility, as A549 cells internalized more efficiently NiNPs than L929 and HepG2 cells and resulted more sensitive to the treatment. Overall, this study shows that NiNP toxicity is mediated by NPs themselves and nickel released ions in an independent manner.

2 Introduction

Nickel (Ni) is a transition metal of the *d block* (Cotton and Wilkinson, 1972). Its biological functions are very limited and confined to some dihydrogen reactions in symbiotic anaerobic bacteria and to urease in some plants and animals where Ni acts to keep ammonia balance (Da Silva and Williams, 2001). Ni in nanoparticulate form can find multiple industrial applications, including catalysts, sensors and energy storage device

in relation to their unique properties, which include high level of surface energy, high magnetism, low melting and burning points and high surface area (Ahamed, 2011; Pietruska *et al.*, 2011; Magaye and Zhao, 2012). Ni-containing NPs were found to be more toxic than fine particles (Zhao *et al.*, 2009). As for metal-based NPs, oxidative stress is involved in nickel NPs (Kang *et al.*, 2003; Ahamed, 2011; Magaye and Zhao, 2012). Independently from the chemical form, such as metallic (NiNP), NiO or Ni_3Si_2, many studies suggest that Ni-containing NPs elicit their effects by means of Ni^{2+} (Griffitt *et al.*, 2008; Pietruska *et al.*, 2011; Muñoz and Costa, 2012). For example, Pietruska *et al.* (2011) have found that both NiNPs and NiONPs caused the activation of HIF-1α signaling pathway in human epithelial cells, just as Ni^{2+}. However, ion released from Ni-based NPs generally cannot fully explain the induced toxicity (Griffitt *et al.*, 2008; Ispas *et al.*, 2009).

This research was conducted to better understand NiNP toxicity. In particular, NiNP and Ni^{2+} toxicity were compared by performing two common viability assays (MTS and ATP assays) in three *in vitro* models: A549 (epithelial cells from human lung carcinoma) as *in vitro* model for inhalation exposure; L929 (fibroblast cells from murine subcutaneous connective tissue) as model of dermal contact exposure; and HepG2 (epithelial cells from human hepatocellular carcinoma) as liver model. In addition, the late effects following a short-time exposure with NiNP and Ni^{2+} were evaluated. The contribution of ion release in NiNP toxicity was studied by analyzing dissolution kinetics in cell culture media, and using two Ni^{2+} chelators during NiNP cell treatment. Toxicological data were related to internalized Ni^{2+} and NiNP for explaining observed differences in toxicity among cell lines.

3 Materials and Methods

3.1 Chemicals and reagents

Metallic NiNPs (Product Code:NI-M-03M-NP.020N) were purchased in dry form from American Elements® (Merelex Corporation, Los Angeles, CA, USA). They had the following properties as indicated by the supplier: average diameter of 20 nm (with size

range from 2 to 50 nm), specific area of 40-60 m^2/g and spherical shape. Acid solution of HNO_3 (67-69% SpA) and HCl (33-36% UpA) were purchased from Romil (Cambridge, UK). Reagents for biological characterization were: Tryptic Soy Agar (TSA; Biolife Italiana S.r.l.; Milan, IT); Venor®GeM Mycoplasma detection kit (Minerva Biolabs, Berlin, De), GoTaq® DNA polymerase, 5X Colorless GoTaq® Reaction Buffer, Blue/Orange 6X loading dye, 100 bp DNA ladder (Promega; Madison, WI, USA); all reagents for the detection of endotoxin were purchased from Charles River Laboratories International, Inc (Charleston, SC, USA). $NiCl_2 \cdot 6H_2O$ (Product Code: N6136), L-cysteine (Product Code:W326305), L-histidine (Product Code: 53319), Triton X-100 and agarose were purchased from Sigma–Aldrich (Gillingham, UK). Sodium Dodecyl Sulphate (SDS), staurosporine (STS), Trizma® base primary standard and buffer, ethylenediaminetetraacetic acid disodium salt dehydrate (EDTA), acetic acid (puriss., 99-100%), ethidium bromide solution (10 mg/mL in H_2O) and Phosphate Buffer Saline (PBS) were purchased from Sigma-Aldrich (St. Louis, MO, USA). Cytotoxicity was tested with CellTiter 96 AQueous Non-Radioactive Cell Proliferation Assay kit Promega (Madison, WI, USA) and ATPlite (Perkin Elmer, Waltham, MA, USA). Human lung carcinoma epithelial cells (A549), murine subcutaneous connective tissue fibroblast cells (L929) and human hepatocellular carcinoma epithelial cells (HepG2) were obtained from American Type Culture Collection (Manassas, VA, USA). Solution for cell culture were: Ham's F-12K and Eagle Minimum Essential Medium (EMEM), fetal bovine serum (FBS), penicillin-streptomycin solution, L-glutamine, phosphate buffered saline (PBS), Dulbecco's phosphate buffered saline with calcium and magnesium (DPBS), Trypsin-EDTA, all purchased from Lonza (Basel, CH). Protein quantification was conducted by using MicroBCA™ Protein Assay Kit (Thermo Scientific; Rockford, IL, USA).

3.2 NiNP characterization

NiNPs were characterized for chemical and biological contaminations, and morphological properties.

3.2.1 Chemical characterization

To detect chemical impurities in NiNPs, a semi-quantitative analysis (ranging from 6 to 240 amu) by inductively coupled plasma mass spectrometry (ICP-MS; NexION 300D, Perkin Elmer Inc.; Waltham, MA, USA) was conducted. In particular, dry NPs were solubilized with a microwave assisted acid digestion. Briefly, NPs were weighted in specific Teflon vessels and suspended with 75% HNO_3 (67-69% SpA) and 25% HCl (33-36% UpA). In order to detect possible environmental contaminations blank samples were included in the analysis. Microwave digestion was performed by using a Mars V microwave (CEM Corporation; Matthews, NC, USA) and the program used has foreseen two different steps: i) increase of temperature until 175°C in 5.5 minutes and ii) maintaining of 175°C for 4.5 minutes to complete digestion. After this acid digestion, solutions were diluted with ultrapure water (18,3 $M\Omega \cdot cm^{-1}$) and analyzed by means of ICP-MS with a semi-quantitative method. The most concentrated elements detected were quantified by using an external calibration curve. To limit signal drift, a rhodium solution (10 µg/L) as internal standard was added online to each standard and sample solutions.

3.2.2 Biological contaminations

In order to avoid microbiological contaminations that could influence cellular responses during experiments, microbiological contaminations and endotoxin presence were tested on CoNPs suspensions. In particular, NPs were suspended at the concentration of 1 mg/mL in sterile water and ultrasonicated for 4 minutes at 50% of amplitude, corresponding to 28000 J (Misonix S-4000 Ultrasonic Liquid Processors, Qsonica LLC.; Newtown, CT, USA). To detect possible generic fungal and bacterial contaminations, 100 µL of the suspensions were plated in TSA plates and incubated at 37°C for 72 h. After the incubation, the presence of colonies on the plates was verified. In addition, mycoplasma contaminations were specifically tested using the Venor®GeM Mycoplasma detection kit according to manufacturer's instructions. Briefly, the possible mycoplasma contamination was detected by amplifying the highly conserved 16S rRNA coding region that generate an amplicon of approximately 267 bp. Internal DNA control of 191 bp was present in each sample, in order to confirm a successfully

performed polymerase chain reaction (PCR). After PCR (Mastercycler; Eppendorf s.r.l.; Milan, IT), a 1.5% agarose gel in a Tris/acetic/ EDTA buffer (4 µmMTris, 20 mM acetic acid and 1 mM EDTA) including ethidium bromide, as DNA staining, was cast and 10 µL of each PCR reaction, mixed with 2µL of Blue/Orange 6X loading dye were loaded for electrophoresis (Peqlab Biotechnologie GmbH; Erlangen, DE); a 100 bp DNA ladder was used. At the end of the electrophoresis, gel were observed by a UV transilluminator (UVITEC; Cambridge, UK) and photographed.

The presence of endotoxins on suspension supernatants was tested by using the Limulus Amebocyte Lysate (LAL) Kinetic-turbidimetric method (Charles River Endosafe; Charleston, SC, USA). This analysis was conducted in a 96-well plate and consisted in optical density (λ = 34µnm) measurements over time with the microplate reader (Synergy4, Bio-Tek Instruments Inc.; Winooski, VT, USA). The assay included a standard curve of *Escherichia coli* endotoxin (from 5 to 0.005 EU/mL) and different dilutions of supernatants with and without standard in order to evaluate possible interferences. In particular, the onset time, which means the time required for the absorbance to increase significantly over the background (0.05 OD units), was calculated and a linear relation between standard endotoxin concentrations and onset time was established in order to calculate sample endotoxin concentrations.

3.2.3 Morphological characterization

Morphological analyses were performed with two different techniques. In particular, CoNPs were suspended in sterile water at the concentration of 1 mg/mL, ultrasonicated (Misonix S-4000 Ultrasonic Liquid Processors, Qsonica LLC.; Newtown, CT, USA) for 4 minutes at 50% of amplitude (corresponding to 28000J). This suspension was diluted in water at the concentration of 100 µg/mL to be examined by Transmission Electron Microscopy (TEM; FEI Tecnai 12 G2 electron microscope, FEI Co.; Eindhoven, NL) with Twin lens configuration after deposition on carbon coated, mesh 400 copper grids and left to dry. Micrographs were recorded on a side-mounted Morada CCD (Olympus Soft imaging Solutions GmbH, Münster, Germany) at magnifications ranging from 42000× to 265000×. To evaluate the aggregation state of NPs in suspension, dilution at the concentration of 10 µg/mL in cell culture complete media and water were done to be

analyzed with the ZetasizerNano ZS Dynamic Light Scattering (DLS; Malvern Instruments; Malvern, UK). A blank (only cell culture media) sample were analyzed too. For the DLS analysis, suspensions were equilibrate at 25°C for 3 minutes and five measurements for sample were performed.

3.3 NiNP dissolution

NiNP suspensions in cell culture media were analyzed for ion release during experimental conditions. In particular, different concentrations (0, 50, 500 and 5000 μg/mL) prepared as in all the other analyses) of NiNPs in cell culture media were prepared from a stock suspension (10 mg/mL) ultrasonicated for 4 minutes at 50% of amplitude (corresponding to 28000 J). Each suspension was incubated at 37°C, 5% $CO_2$and 90% of humidity for 0, 6, 24 and 48 h in 24-well plates (1 mL for each well). At the end of incubation NPs were removed from suspensions by collecting samples in 2 mL tubes, centrifuging twice at 16000 g for 10 minutes and finally ultracentrifuging (Optima™ L-100XP Ultracentrifuge; Beckman Coulter; Urbana, IL, USA) for 2 hours at 300000 g at 4°C. Ultracentrifugation was conducted in polycarbonate tubes (Beckman Coulter; Urbana, IL, USA) with the rotor type 70.1.Ti (Beckman Coulter). Supernatants were collected and diluted with a 2% HNO_3 solution prior to being analyzed for ion quantification with ICP-MS (NexION 300D, Perkin Elmer; Waltham, MA, USA).Simultaneously, 100 μg/mL solutions of Ni^{2+}in cell culture media and ddH_2O were analyzed to monitor the ion behavior during the experiment. In addition, not ultracentrifuged NP suspensions and ion solutions were quantitatively analyzed by ICP-MS. In particular, ion solutions were simply diluted in 2% HNO_3 solution in the calibration curve concentration range, whereas, NP suspensions were solubilized by microwave acid digestion (Mars V,CEM). 500 μL of each suspension were transferred in specific Teflon vessels and 10 mL of HNO_3(67-69% SpA) were added. Blank samples were included to the analysis to detect possible environmental contaminations. Microwave digestion program has foreseen two different steps: 1) increase of temperature until 175°C in 7 minutes and 2) maintaining of 175°C for 3 minutes to complete digestion. After this acid digestion, solutions were diluted with ultrapure water (18,3 $M\Omega \cdot cm^{-1}$) and analyzed by ICP-MS (NexION 300D, Perkin Elmer; Waltham, MA, USA). ICP-MS

quantitative analyses of ionic release and NP and ion solution were performed using an external calibration curve. To limit signal drift, a rhodium solution (10 µg/L) as internal standard was added online to each standard and sample solutions.

3.4 Cell viability analyses

3.4.1 Cell culture and sub-culturing procedure

A549, L929 and HepG2 cells were maintained following ATCC indications. A549 cells were cultured in Ham's F12K medium with the addition of 10 % FBS, 100 units/mL streptomycin and 100 µg/mL penicillin. HepG2 and L929 cells were cultured in EMEM with the addition of 10%FBS, 100 units/mL streptomycin and 100 µg/mL penicillin and 2mM L-glutamine. All the three cell lines were kept at 37°C, 5% CO_2 and 90% of humidity for maintenance and for experiments.

3.4.2 NiNP and Ni^{2+} toxicity

In order to evaluate the cytotoxic effects of NiNPs and Ni^{2+}, cells were seeded in 96-well microplate and, 24h after seeding, treated with different concentrations of NPs and ions for 6, 24 and 48 h. The seeding densities of cells were those at which cells proliferated overtime: 5000 cell/well for A549 and L929 cells, and 15000 cell/well for HepG2 cells. Treatment solutions or suspensions were freshly prepared before each test. In particular, NPs were suspended in sterile water and ultrasonicated for 4 minutes at 50% of amplitude (corresponding at 28000 J) in order to make a stock suspension that was diluted in the proper cell culture media without exceeding the 10% of the total volume of the treatment. Ion stock solutions were prepared in ddH_2O, filtered with 0.22 µm pore size filter and diluted in cell culture media as NP stock suspensions. Experiments were performed in triplicate. Viability was assessed after the removal of cell culture media and washing of cells with DPBS in order to eliminate possible NP interferences (Kroll *et al.*, 2012). The two assays used were: MTS assay and ATP assay were performed according to manufacturer's instructions. The MTS assay analyzes the conversion of a tetraziolium salt 3-(4,5-dimethylthiazol-2-yl)-5-(3-carboxymethoxyphenyl)-2-(4-sulfophenyl)-2H] (MTS) into its reduced and soluble formazan form by mitochondrial

enzyme of metabolically active cells and was evaluated by recording absorbance at 490 nm. ATP assay is based on light production caused by the reaction of ATP with added luciferase and D-luciferin and quantify the ATP content. Both absorbance and luminescence were recorded with the Synergy4 microplate reader (Bio-Tek Instruments).

3.4.3 Analysis of the bimodal dose-response curves of NiNPs

In order to discriminate the contribution of Ni ions in NiNP cytotoxicity, we performed the ATP content analysis on the three cell lines after a 24 h (A549 cells) or 48 h treatment (A549, L929 and HepG2 cells) with NiNP in presence of L-cysteine and L-histidine, as Ni^{2+}chelating agents. In particular, cells were treated with different concentration of NiNPs and L-cysteine or L-histidine 6.8mM. This concentration is calculated on the basis of NiNP dissolution experiments and correspond to the twofold equimolar highest concentration of Ni^{2+}found to be released at 48 h (Forgacs *et al.*, 2001).

3.4.4 Late effects

Possible late effects induced by of NiNPs and Ni^{2+} exposure were analyzed by incubating cells with each nickel compound for 6 h, removing treatments and replacing with fresh culture media, after washing cells twice with DPBS, and finally analyzing ATP content at 24 and 48 h post treatment.

3.5 Analysis of cellular uptake

Cellular uptake of NiNPs and Ni^{2+} was quantitatively analyzed by ICP-MS (NexION 300D, Perkin Elmer). Cells were seeded in 24-well plate at densities 10 times higher compared to those used in 96-well plate experiments. After 24 h from seeding, cells were treated for 24 h with 10 µg/mL of NiNPs or Ni^{2+} obtained from stock suspensions prepared similarly to cytotoxicity tests. At the end of exposure, cells were washed three-times with PBS to remove NPs and ions not internalized. Cells were then detached with 200 µL of Trypsin-EDTA and collected with 800 µL of PBS to be analyzed for protein quantification and uptake. Samples dedicated to protein quantification were centrifuged at 16000 g for 5 minutes. Then, supernatants were discarded and cell pellets

were lysed with a lysis solution containing PBS 1X, 1% Triton X-100 and 1% SDS. Protein quantification was conducted using the microBCA assay. Bovine Serum Albumin (BSA) provided by the kit was diluted to prepare different standards in the linear concentration range of 10-40 µg/mL and manufacturer's instructions were followed. To analyze uptake, samples were centrifuged at 400 g for 15 minutes. Once supernatants were discarded pellets were digested with 1mL of HNO_3. After an overnight incubation at room temperature, samples were incubated 12 h at 70°C in Thermoblock (FALC Instruments; Treviglio, IT) and finally diluted in ultrapure H_2O (18,3 $M\Omega \cdot cm^{-1}$). The obtained solutions were quantitatively analyzed by ICP-MS (NexION 300D, Perkin Elmer; Waltham, MA, USA) by using Dynamic Reaction Cell (DRC) method with a standard calibration curve and a rhodium solution as internal standard.

3.6 Statistical analyses

Statistical analyses were performed using Origin Pro 8.0 software (OriginLab; Northampton, MA, USA). Cytotoxicity results were fitted by sigmoid functions and EC50 values were calculated. Where bimodal dose-response curves appeared more appropriate, F-tests were performed to compare unimodal and bimodal models. Statistical significance was determined by ANOVA analysis (P value < 0.05).

4 Results

4.1 NiNP characterization

Chemical purity analysis showed that NiNPs had three main chemical contaminations: cobalt (Co), copper (Cu) and germanium (Ge) (Table 1).

TABLE 1. Elemental contaminations of NiNPs.

Element	Concentration	
	μg/g [a] ± SD	% [b] ± SD
Co	19.4 ± 0.1	0.002 ± 0.000
Cu	25.1 ± 0.2	0.003 ± 0.000
Ge	3.3 ± 0.7	0.0000 ± 0.0000

a: dry weight
b: % expressed as w/w (dry weight)
SD: standard deviation (mean of three determinations).

NiNPs did not display microbiological contaminations and the endotoxin levels were below 0.01 EU/mL (corresponding to levels found in sterile water).

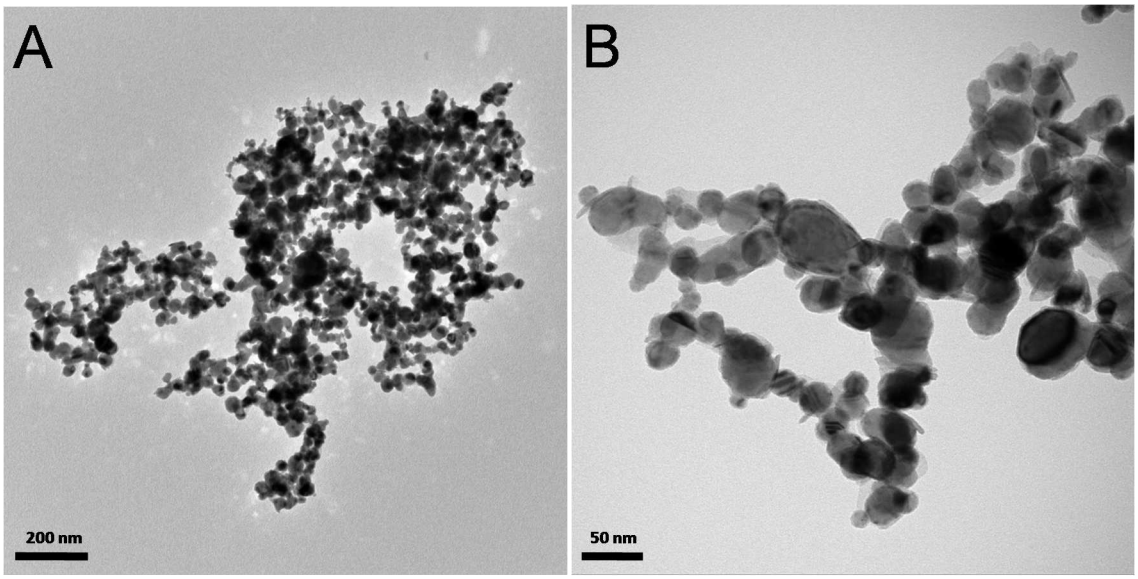

FIGURE 1. TEM images of NiNPs at different instrumental magnifications: A) 57000 ×; B) 195000 ×.

NiNPs appeared in a crystalline form, aggregated and mainly spheroidal in shape (Fig.1). No isolated, individual particles were found in the sample. Since the borders of individual particles could not be easily determined, a manual selection of apparent particle diameters was used for particle size distribution determination, resulting in a mean particle diameters of 22.7 ± 9.8 nm. However, size was found to range between 4.8 and 71.9 nm (Fig. 2).

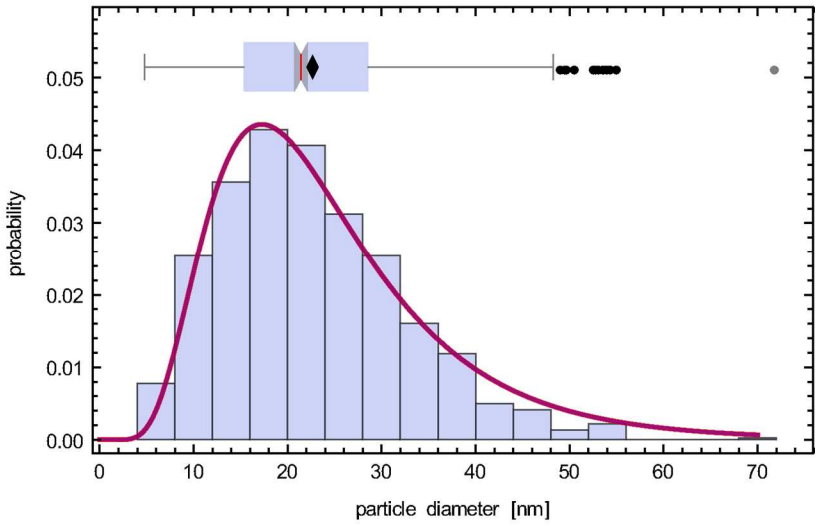

FIGURE 2. NiNP size-distribution.

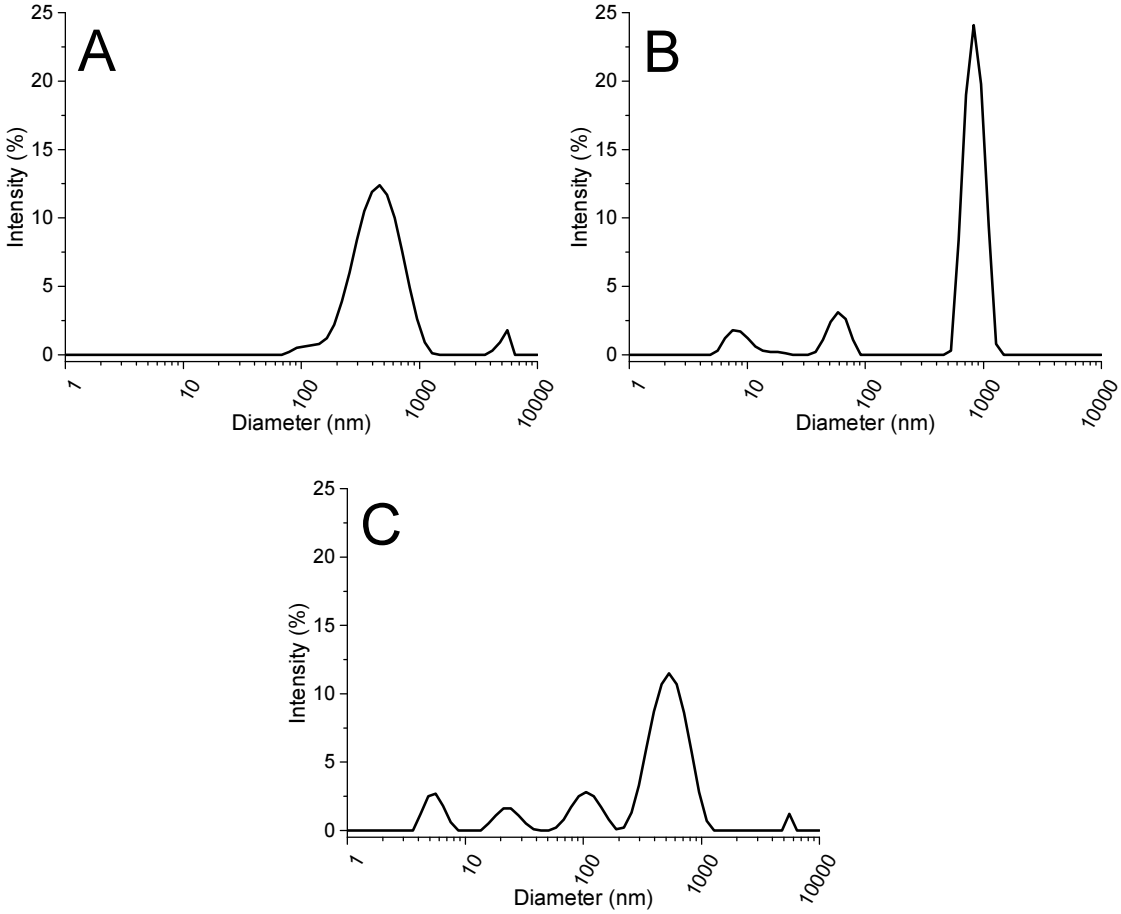

FIGURE 3. DLS size distribution performed in A) water (PdI = 0.279), B) Ham's F-12K medium (PdI = 0.765) and C) EMEM (PdI = 0.592).

DLS analysis of NiNP suspensions showed an aggregated and highly polydisperse system, as can be observed by Polidispersity Index (PdI) and by the presence of different peaks in DLS size distribution graphics (Fig. 3).

4.2 NiNP dissolution

Ultracentrifugation was performed to separate NiNPs from potentially released ions for determining NP dissolution rate under our experimental conditions. Before the analysis, the possible precipitation of Ni ions after ultracentrifugation was evaluated. In the presence of EMEM, a slight but significant decrease (about 20%) in nickel content was observed (Fig.4). However, no ion precipitation occurred over time (Fig. 5).

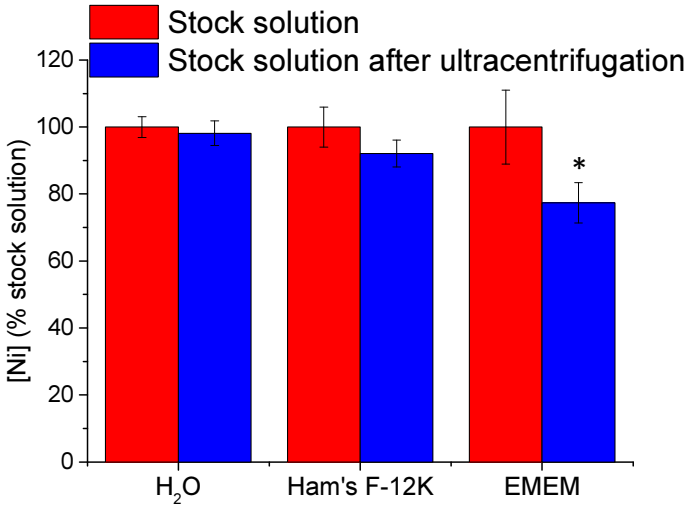

FIGURE 4. Analysis of concentrations Ni^{2+} before and after ultracentrifugation in water and cell culture media. Data are expressed as mean of three different measurements, each of them expressed as % of stock solution concentrations. Error bars represent standard deviations of three different measurements. * Significant different from stock solution (P value < 0.05)

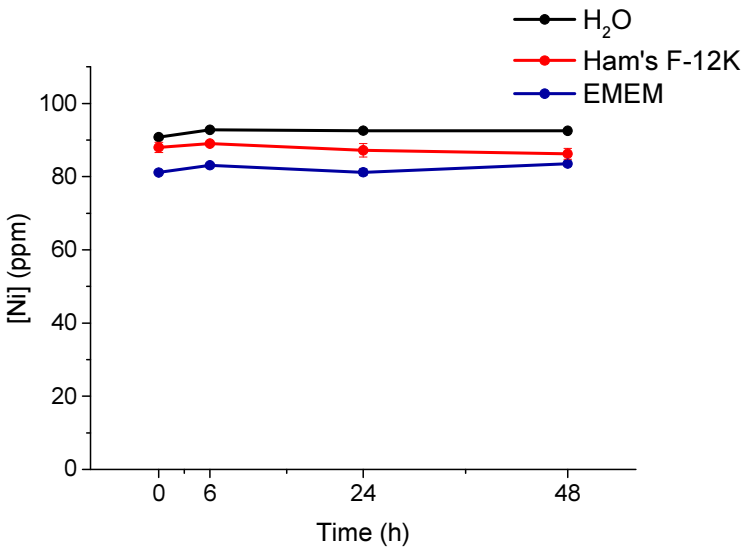

FIGURE 5. Ni^{2+} in solutions over time in water and cell culture media (Ham's F-12K and EMEM). Data are expressed as means of three measurements and error bars represents standard deviations.

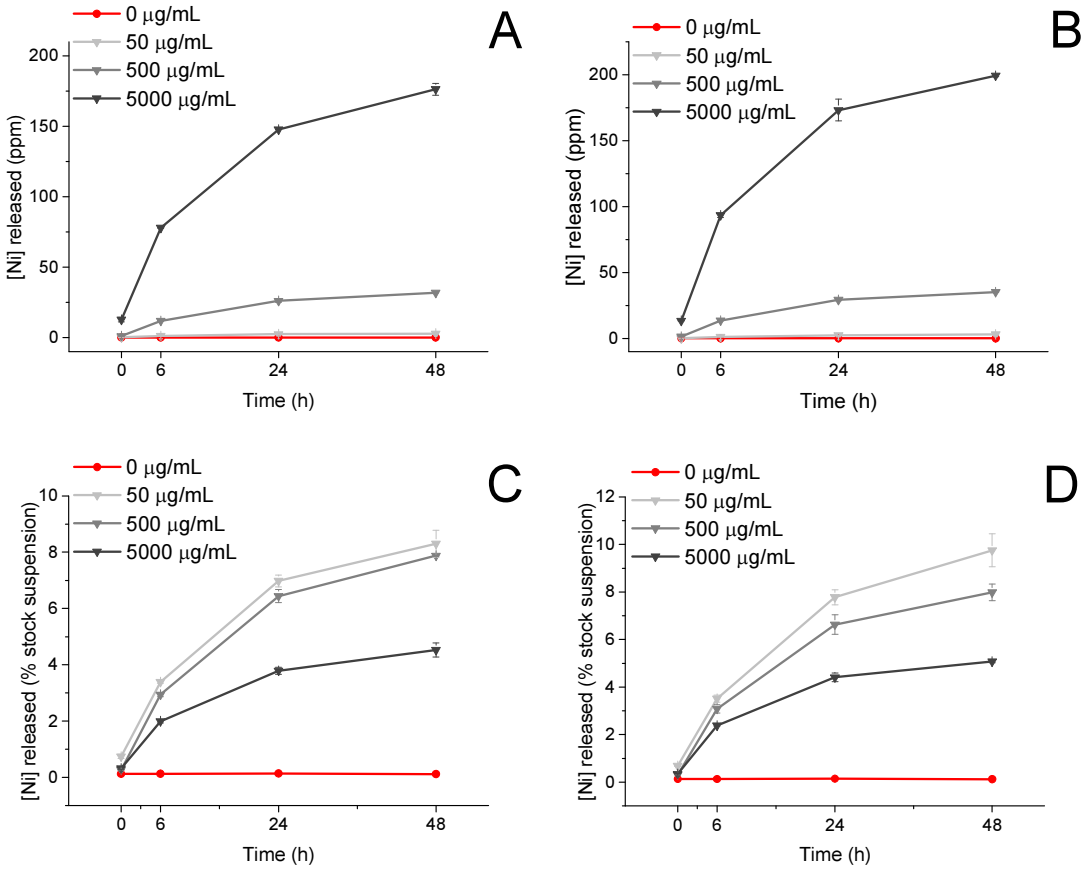

FIGURE 6. Ions released from NiNPs in Ham's F-12K (A, C) and EMEM (B, D) media overtime. Data are expressed as mean of three measurements and error bars represents standard deviations.

The ion release from NiNPs appeared to be dependent on both time and NP concentration, whereas it was not related to the type of cell culture medium (Fig. 6). Although the total amount of released nickel is proportional to the amount of NiNPs in suspension (Fig. 6A, 6B), dissolution rate is higher at low NP concentration (Fig. 6C, 6D).

4.3 NiNP and Ni^{2+} toxicity

After exposure of the three cells models to NiNPs and Ni^{2+} ions, cell viability was evaluated by MTS and ATP assays and dose-response curves were fitted (Fig. 7, 8, 9) and EC50 values were calculated (Table 2). Both NiNPs and Ni^{2+}showed a dose- and time-dependent toxicity in all the *in vitro* models used (Fig. 7, 8, 9 and Table 2). Interestingly, NiNP dose-response curves displayed a bimodal trend in A549 and HepG2 cells, respectively at 24 h and 48 h or only at 48 h (Fig. 7, 9). Exposure of L929 cells produced unimodal dose-response curves in L929 (Fig. 8). The calculated EC50 values (Table 2) were different among the three cell models. In particular, when ATP assay was performed to assess toxic effects, the A549 cells were the most susceptible cells, followed by HepG2 and then L929 cells. Cell viability determined by MTS assay showed a different ranking in terms of susceptibility (L929 > A549 > HepG2).

TABLE 2. EC50 values of NiNPs and Ni^{2+} in the three cell models at 6, 24 and 48 h.

	EC50 (μg/mL)								
	A549			L929			HepG2		
Compound	6 h	24 h	48 h	6 h	24 h	48 h	6 h	24 h	48 h
	ATP assay								
NiNP	N.D.	3/1200*	2.8/161.7*	N.D.	94.6	59	249.5	49.5	10.3/303.1*
Ni^{2+}	N.E.	49.5	24.6	222.6	85.8	26.3	127.6	33.2	19.5
	MTS assay								
CoNP	N.E.	44.6/2170*	6.3/641.5*	N.D.	174.5	49.4	N.D.	917.3	11.4/349.9*
Ni^{2+}	N.E.	122.9	33.7	258.4	82.2	12.3	N.D.	136.7	61.6

N.E.: no effect.
N.D.: not determined.
* Double EC50 values calculated from bimodal dose-response curves.

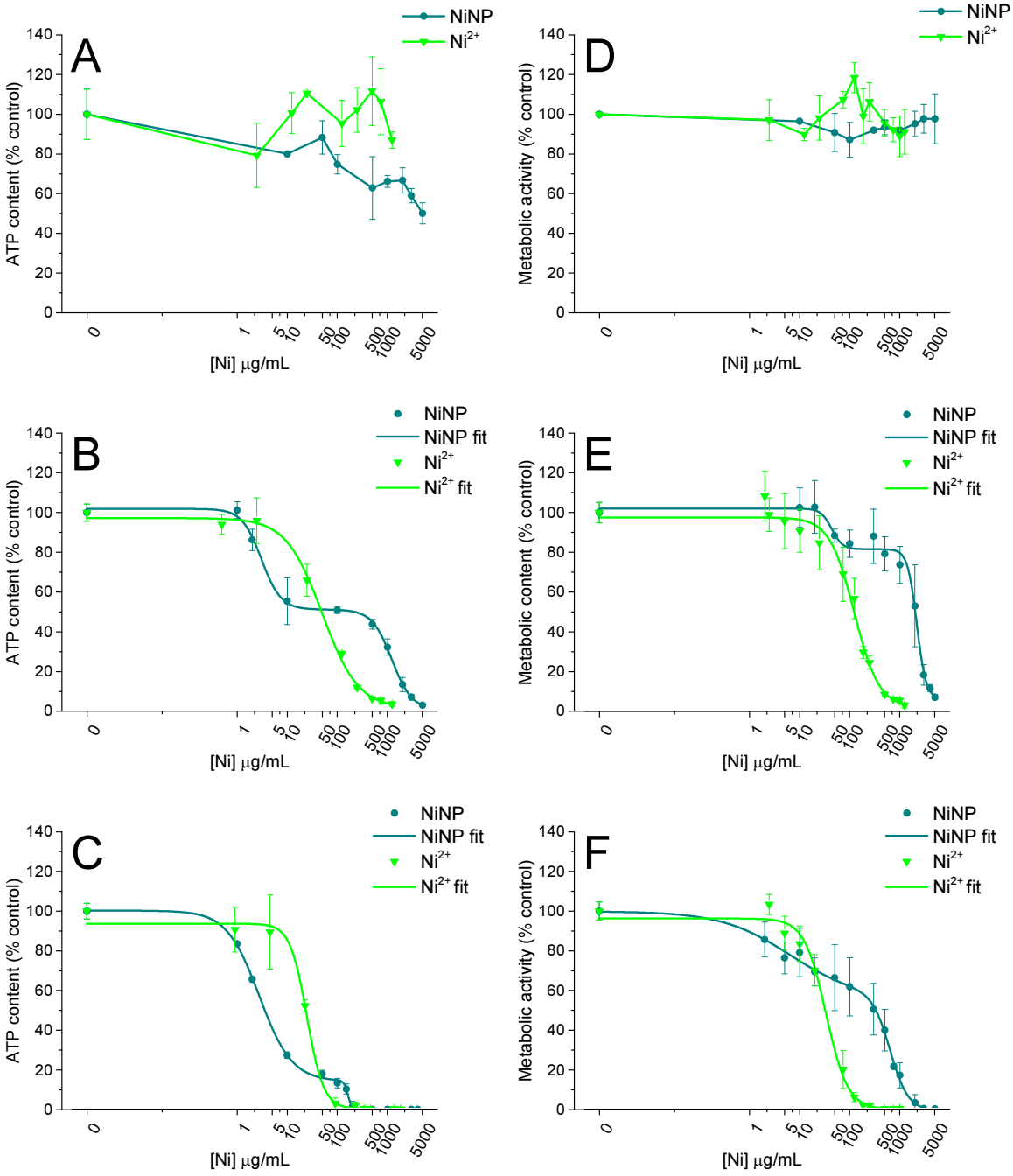

FIGURE 7. Dose-response curves obtained by treating A549 cells with NiNPs and Ni^{2+} for 6 (A, D), 24 (B, E) and 48 h (C, F). Panels A, B, C refer to ATP assay, while panels D, E, F refer to MTS assay. Data are expressed as mean of three independent experiments and error bars represent standard deviations.

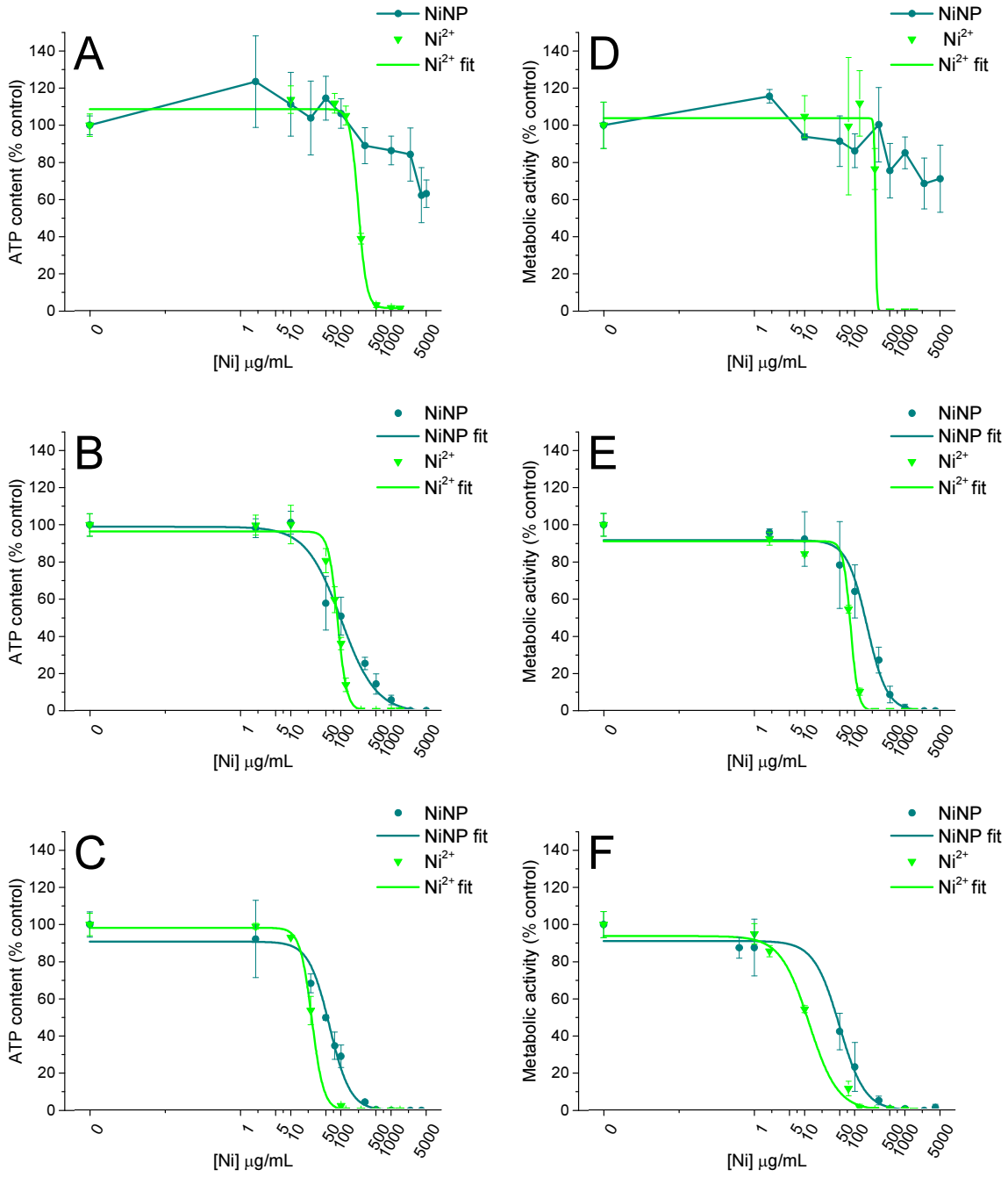

FIGURE 8. Dose-response curves obtained by treating L929 cells with NiNPs and Ni^{2+} for 6 (A, D), 24 (B, E) and 48 h (C, F). Panels A, B, C refer to ATP assay, while panels D, E, F refer to MTS assay. Data are expressed as mean of three independent experiments and error bars represent standard deviations.

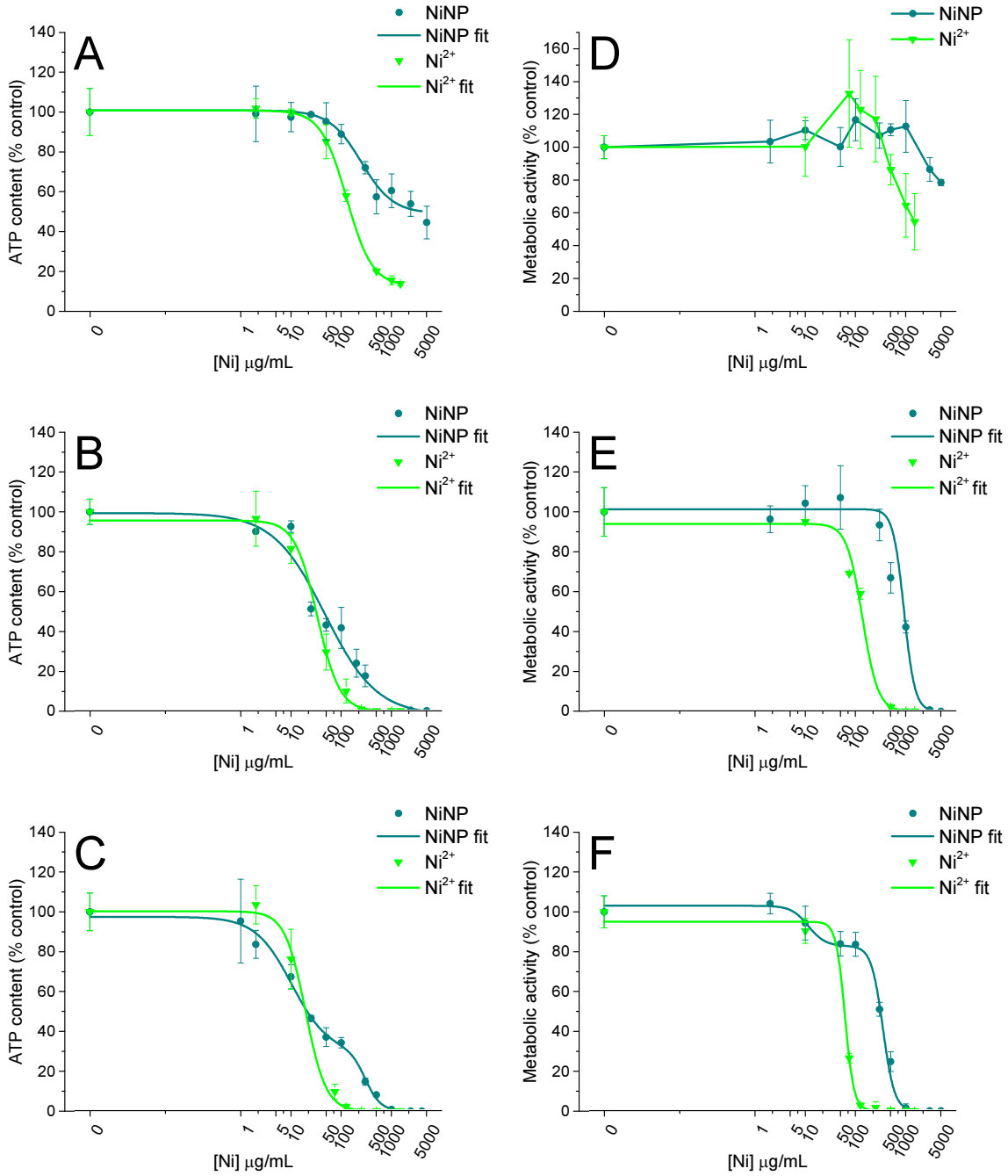

FIGURE 9. Dose-response curves obtained by treating HepG2 cells with NiNPs and Ni^{2+} for 6 (A, D), 24 (B, E) and 48 h (C, F). Panels A, B, C refer to ATP assay, while panels D, E, F refer to MTS assay. Data are expressed as mean of three independent experiments and error bars represent standard deviations.

4.4 Analysis of the bimodal NiNP dose-response curves

In order to explain the bimodal trend of NiNP dose-response curves in A549 and HepG2, two chelators with high affinity for Ni^{2+} (L-cysteine (L-Cys) and L-histidine (L-His))

were used to complex free Ni^{2+} released by NPs. In presence of L-Cys and L-His the second transition was prevented, and the maximum effect corresponded to the that ot the first plateau observed in the bimodal dose-response curves (Fig.10). Therefore, the observed bimodal trend would reflect the dual effect of NiNPs and the corresponding released ions. In L929 cells, for which no bimodal dose-response was observed, L-Cys and L-His only reduced NiNP toxicity (Fig. 10D) and the protective effect of L-Cys resulted more pronounced compared to L-His, as can be observed form EC50 values (Table 3).

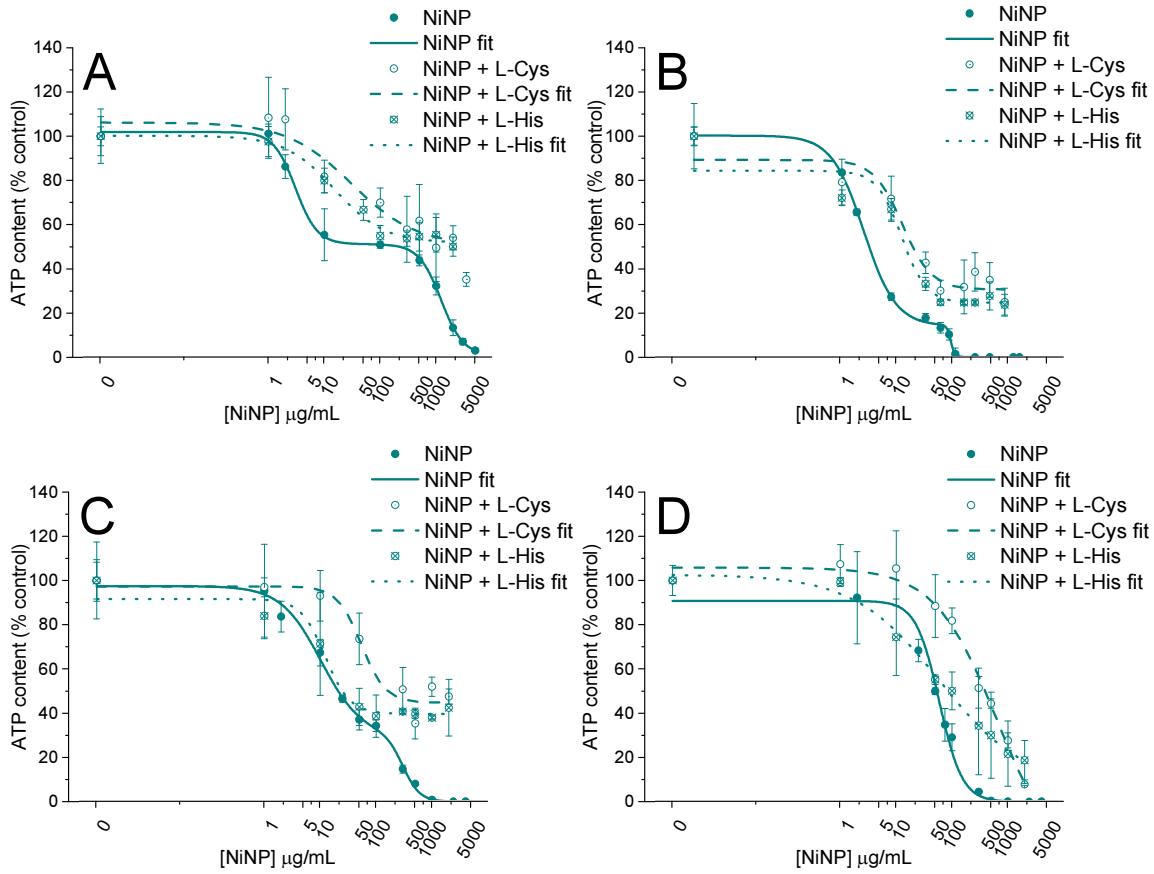

FIGURE 10. Toxicity of NiNPs in absence or presence of L-Cys or L-His assessed by ATP assay. A) Analysis on A549 after 24 h of treatment; B) Analysis on A549 after 48 h of treatment; C) Analysis on HepG2 after 48 h of treatment and D) Analysis on L929 after 48 h. Data are expressed as means of three independent experiments and error bars represent standard deviation.

TABLE 3. EC50 values and maximum effects of A549, L929 and HepG2 cells treated with NiNPs and L-Cys or L-His.

	A549		L929	HepG2
Chelator	24 h	48 h	48 h	48 h
	Max effect (% control)			
L-Cys	50.6	30.7	0	44.8
L-His	51.8	44.8	6.8	39.7
	EC50 (μg/mL)			
L-Cys	30.9	17	342	54.5
L-His	15.2	11.8	59.9	12.3

N.D: not determined

4.5 Late effects

To investigate the effects of internalized NiNPs reducing extracellular ion release, a short time exposure experiment was performed. Cells were exposed to NiNP and Ni^{2+} for 6 h, and their viability measured after 24 and 48 h recovery. Short-time incubation with NiNPs induced a dose- and time-dependent impact on cells (Fig. 11A, 11B, 12A, 12B), though the maximum effect does not change over time (Table 4). Ni^{2+} toxicity resulted to be only slightly time-dependent in HepG2 cells (Fig. 12C, 12D), whereas in L929, where no dose-response curves were obtained, it appeared independent of time (Fig. 11C, 11D).

TABLE 3. Maximum effect and EC50 values of L929 and HepG2 cells after 6 h of exposure with Ni compound and 24 and 48 h of recovery.

	L929		HepG2	
Compound	**24 h**	**48 h**	**24 h**	**48 h**
	Max effect (% control)			
NiNP	42.2	40.8	17.3	32
Ni^{2+}	0	0	37.6	20
	EC50 (μg/mL)			
NiNP	22.1	7.8	26	23
Ni^{2+}	N.D.	N.D.	46.5	N.D.

N.D: not determined

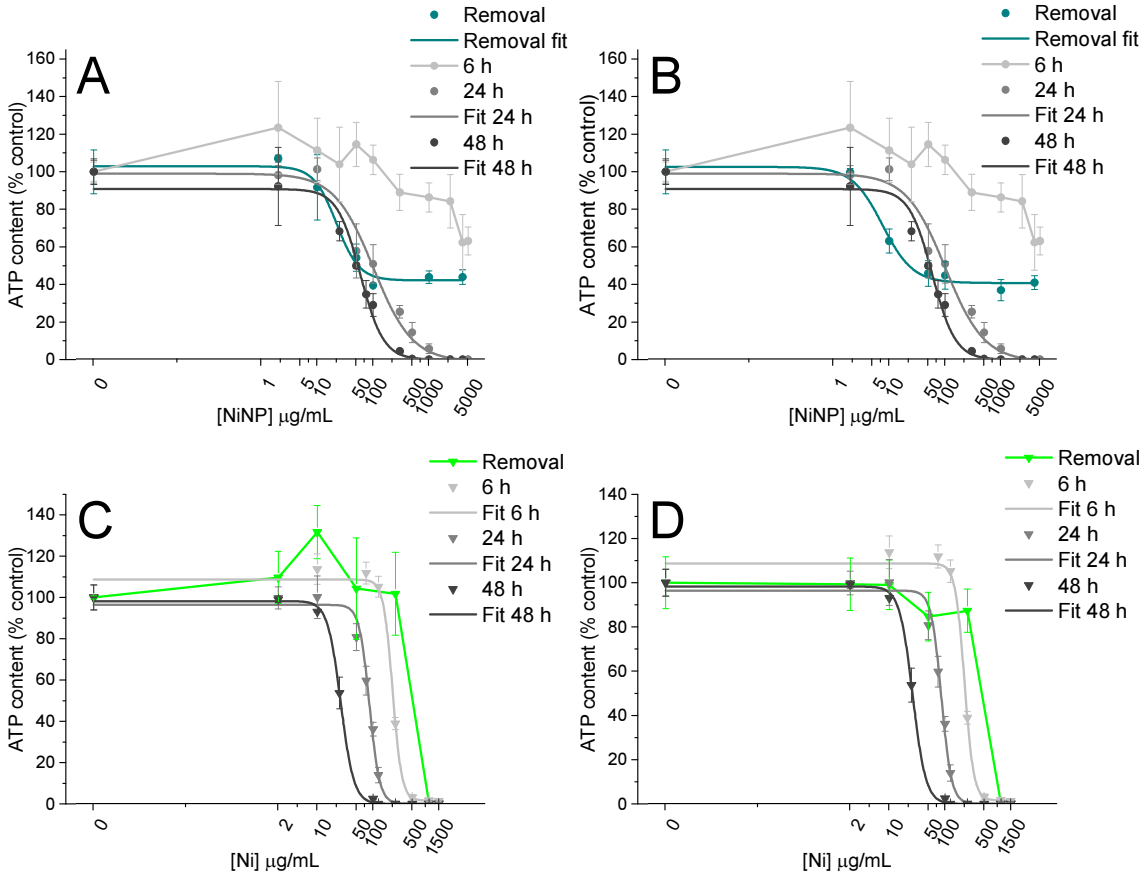

FIGURE 11. NiNP (A, B) and Ni^{2+} (C, D) toxicity on L929 cells measured by ATP assays after the removal of treatments (6 h post treatments). ATP assay were performed after 24 h (A, C) and 48 h (B, D) from treatment. Dose-response curves obtained by treating cells with NiNPs and Ni^{2+} for 6, 24 and 48 h were also reported. Data are expressed as means of three independent experiments and error bars represent standard deviation.

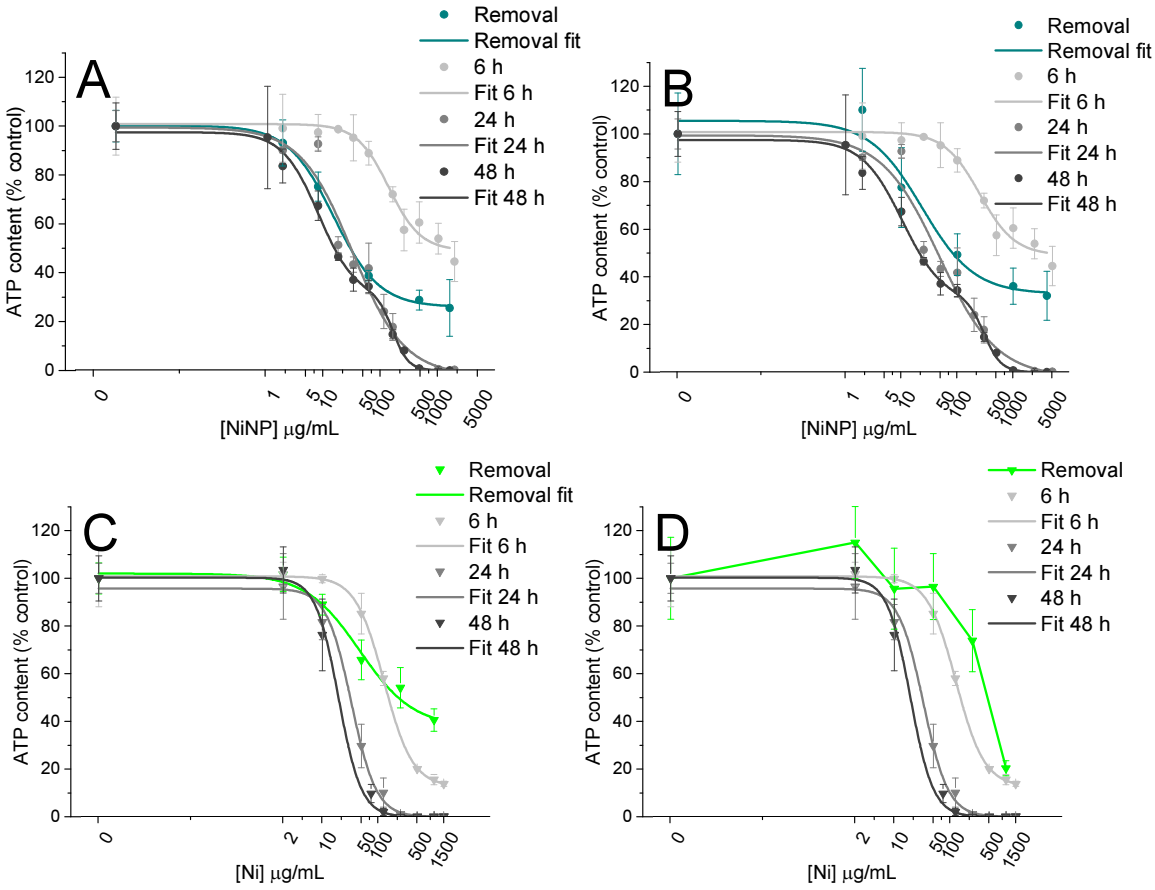

FIGURE 12. NiNP (A, B) and Ni^{2+} (C, D) toxicity on HepG2 cells measured by ATP assays after the removal of treatments (6 h post treatments). ATP assay were performed after 24 h (A, C) and 48 h (B, D) from treatment. Dose- response curves obtained by treating cells with NiNPs and Ni^{2+} for 6, 24 and 48 h were also reported. Data are expressed as means of three independent experiments and error bars represent standard deviation.

4.6 Cellular uptake

To understand NP toxicity in *in vitro* studies the knowledge of the uptake is a fundamental aspect. With this respect, the quantification of NiNP and Ni^{2+} internalized by the three cell models was determined. A higher intracellular Ni concentration was found in NiNPs-treated cells than compared to the those treated with nickel ions (Fig. 13). Furthermore, the cellular uptake of NiNP-treated cells were cell-type dependent; indeed. A549 cells showed the higher nickel concentration followed by L929 and HepG2 ($P < 0.05$).

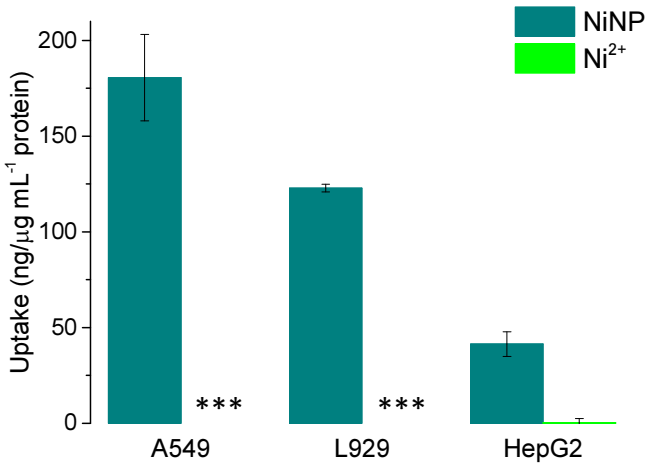

FIGURE 13. Uptake of NiNP and Ni^{2+}in A549, L929 and HepG2 cells. Data are expressed as ng of Ni for protein concentrations and error bars are standard deviations. *** Under detection limit (0.47µg/mL).

5 Discussion

Size distribution analysis showed that NiNPs dimension is heterogeneous with a size range from 4.8 to 71.9 nm, i.e. in the nano-size range. NiNP tendency to aggregate does not depends on the medium since DLS measurements showed that aggregation is present both in water and cell culture media. As different authors suggested a role of ions released by NiNPs in inducing NP toxicity (Griffitt et al., 2008; Pietruska et al., 2011; Muñoz and Costa, 2012), we analyzed the release of soluble Ni. A time- and concentration-dependent NP dissolution rate was observed. Despite higher concentration of NPs results into a higher concentration of ions, the observed dissociation rate is higher in the presence of low NiNPs concentration. This observation could be related to the different aggregation states of NiNPs as a function of their concentration (Misra *et al.*, 2012).

In vitro viability assays show that NiNPs are less toxic than the corresponding ionic form. Dose-response curves obtained treating A549 and HepG2 cells with increasing NiNPs concentrations are characterized by a bimodal trend. The bimodal trend could indicate the presence of different mechanisms of action, of the superimposition of multiple effects or of a heterogeneity of the cellular population (i.e. the presence of different cell subpopulation in the assay) (Derelanko and Auletta, 2014). Considering the

kinetic of ion release (strongly related to the NP concentration) and the NiNP bimodal dose-response curves, we hypothesize that the first transition is probably due to the toxicity of NP itself while the second one is probably due to the released ions. In order to discriminate the specific contribution of the presence of ions from that of the NiNPs, a co-treatment of cells with both NiNPs and two Ni^{2+}chelators (such as L-Cys and L-Hys) was performed. In the presence these two chelators, NiNPs showed a unimodal dose-response curve with the maximum effect corresponding to the viability reduction of the first transition obtained in the absence of nickel chelators. Furthermore, L-Cys resulted to be more efficient than L-His in reducing NiNP toxicity, probably because of its antioxidant property; in fact, it has been demonstrated that ROS generation could be involved in NiNP toxicity (Morel and Barouki, 1999; Ahamed, 2011; Kang *et al.*, 2011). Late effect experiments indicated that toxicity mediated by internalized NiNPs is not time-dependent. Taking into consideration dissolution kinetics, the time-independency is compatible with a low amount of internalized NiNPs after 6 h of exposure and the reduced ion release in intracellular compartments.

Cellular uptake of NiNPs and nickel ions indicated that NiNPs enter more readily into cells than Ni^{2+} ions in all the three cell models. This difference may be related to the different uptake mechanisms involved in internalization of the different forms of Ni. While NiNPs are internalized via endocytic mechanisms (Muñoz and Costa, 2012), Ni^{2+} uptake is associated to membrane transporters, such as DMT1 (divalent metal transporter 1) or calcium channel, competing with other physiological divalent cations, such as iron and calcium (Denkhaus and Salnikow, 2002). Moreover, the cell lines used in this work showed a different degree of Ni internalization following NiNP exposure. This could partially explain the degree of toxicity induced by NiNPs in the three cell models. A549 cells internalize more efficiently NiNPs than L929 and HepG2 cells and they are more sensitive to the treatment. Considering L929 cells, the unimodal trend of dose-response curves can be explained by the high NiNP toxicity that prevents the effect of release the ions.

In conclusion, NiNP toxicity is mediated by NPs themselves and nickel released ions in an independent manner, as summarized in Fig.14. At low NiNP concentrations the effect

on viability depends only on NPs, whereas at high concentrations, NiNP toxicity is mainly due to the released Ni^{2+}.

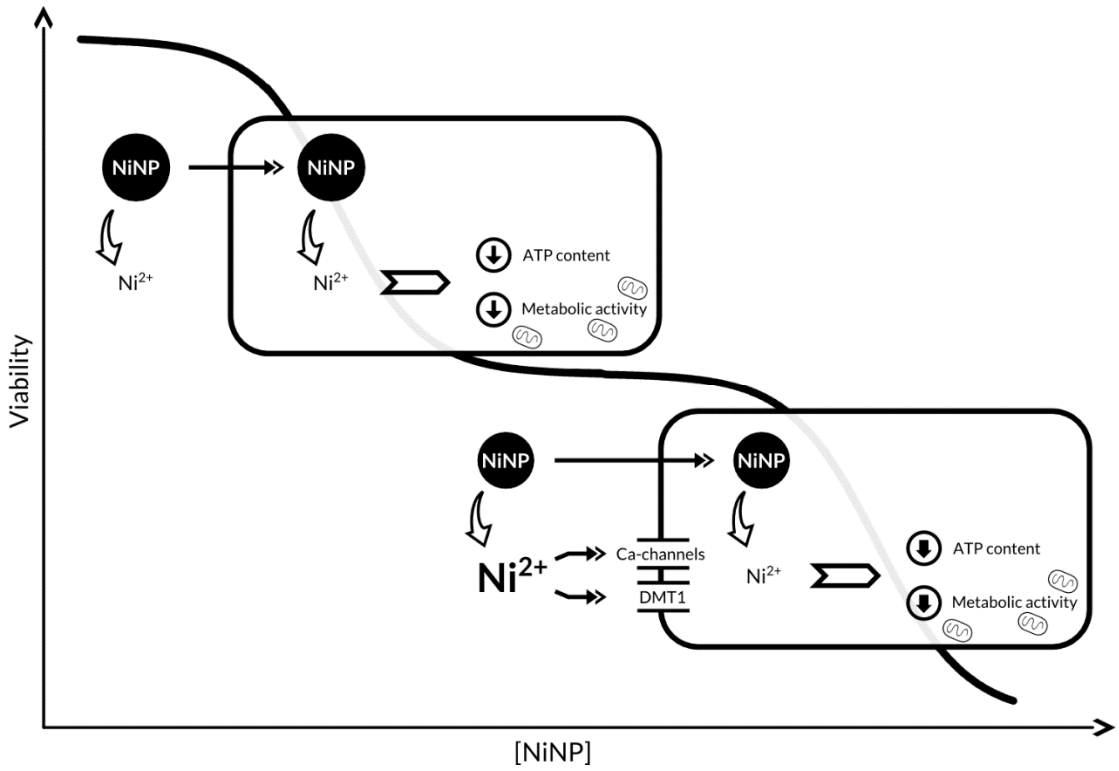

FIGURE 14. Putative mechanism of NiNP toxicity. At low NiNP concentration, the amount of ions released into the culture media is limited, suggesting that the effect on cell viability (i.e. ATP content and mitochondrial metabolic activity) is related only to NP internalization and the release of Ni^{2+} inside cells. On the contrary, at high concentrations of NiNPs, there are higher levels of free Ni^{2+} released by NPs that could enter into the cells through the DMT1 (divalent metal transporter 1) or calcium channels. This induces a large toxic effect as described by the bimodal dose-response curve shown in the scheme.

6 References

Ahamed M. (2011). Toxic response of nickel nanoparticles in human lung epithelial A549 cells. *Toxicol. In Vitro* 25(4): 930-936.

Cotton F. A. and Wilkinson G. (1972). Advanced inorganic chemistry. A comprehensive text. *John Wiley & Sons, Inc.*, New York. pp.1145.

Da Silva J. F. and Williams R. (2001). The biological chemistry of the elements: the inorganic chemistry of life. *Oxford University Press*, Oxford. pp.561.

Denkhaus E. and Salnikow K. (2002). Nickel essentiality, toxicity, and carcinogenicity. *Crit. Rev. Oncol. Hematol.* 42(1): 35-56.

Derelanko M. J. and Auletta C. S. (2014). Handbook of toxicology. *CRC press*, Boca Raton. pp.1022.

Forgacs Z., Nemethy Z., Revesz C. and Lazar P. (2001). Specific amino acids moderate the effects on Ni^{2+} on the testosterone production of mouse leydig cells in vitro. *J. Toxicol. Environ. Health A* 62(5): 349-358.

Griffitt R. J., Luo J., Gao J., Bonzongo J. C. and Barber D. S. (2008). Effects of particle composition and species on toxicity of metallic nanomaterials in aquatic organisms. *Environ. Toxicol. Chem.* 27(9): 1972-1978.

Ispas C., Andreescu D., Patel A., Goia D. V., Andreescu S. and Wallace K. N. (2009). Toxicity and developmental defects of different sizes and shape nickel nanoparticles in zebrafish. *Environ. Sci. Technol.* 43(16): 6349-6356.

Kang G. S., Gillespie P. A., Gunnison A., Rengifo H., Koberstein J. and Chen L.-C. (2011). Comparative pulmonary toxicity of inhaled nickel nanoparticles; role of deposited dose and solubility. *Inhal. Toxicol.* 23(2): 95-103.

Kang J., Zhang Y., Chen J., Chen H., Lin C., Wang Q. and Ou Y. (2003). Nickel-induced histone hypoacetylation: the role of reactive oxygen species. *Toxicol. Sci.* 74(2): 279-286.

Kroll A., Pillukat M. H., Hahn D. and Schnekenburger J. (2012). Interference of engineered nanoparticles with in vitro toxicity assays. *Arch. Toxicol.* 86(7): 1123-1136.

Magaye R. and Zhao J. (2012). Recent progress in studies of metallic nickel and nickel-based nanoparticles' genotoxicity and carcinogenicity. *Environ. Toxicol. Phar.* 34(3): 644-650.

Misra S. K., Dybowska A., Berhanu D., Luoma S. N. and Valsami-Jones E. (2012). The complexity of nanoparticle dissolution and its importance in nanotoxicological studies. *Sci.Total Environ.* 438: 225-232.

Morel Y. and Barouki R. (1999). Repression of gene expression by oxidative stress. *Biochem. J.* 342 Pt 3: 481-496.

Muñoz A. and Costa M. (2012). Elucidating the mechanisms of nickel compound uptake: a review of particulate and nano-nickel endocytosis and toxicity. *Toxicol. Appl. Pharmacol.* 260(1): 1-16.

Pietruska J. R., Liu X., Smith A., McNeil K., Weston P., Zhitkovich A., Hurt R. and Kane A. B. (2011). Bioavailability, intracellular mobilization of nickel, and HIF-1α activation in human lung epithelial cells exposed to metallic nickel and nickel oxide nanoparticles. *Toxicol. Sci.*: kfr206.

Zhao J., Bowman L., Zhang X., Shi X., Jiang B., Castranova V. and Ding M. (2009). Metallic nickel nano-and fine particles induce JB6 cell apoptosis through a caspase-8/AIF mediated cytochrome c-independent pathway. *J. Nanobiotechnol.* 7(2).

CONCLUSIONS

CONCLUSIONS

The growing development of nanotechnology and the subsequent increasing use of NMs lead to an increase human and environmental exposure. Therefore, the safety evaluation of NM toxicity is needed. This work focuses on the toxicological effects of zerovalent FeNPs, CoNPs and NiNPs, whose three constituent elements belong to the main transition group and share ferromagnetic properties. In relation to the specific objectives of this study, the following conclusions can be drawn.

I. Physico-chemical characterization of FeNPs, CoNPs, NiNPs.

Fe-, Co- and NiNPs have similar nominal average diameters. TEM and DLS analysis indicated that all the metallic NPs aggregate in suspension, making difficult to relate their toxic effects to the primary size. Data on chemical and biological contaminations, revealed the absence of endotoxins and mycoplasma, suggesting that artifacts due to the presence of such contaminants can be reasonably excluded under our experimental conditions.

II. Dissolution of NPs in culture media.

NP dissolution was different and depending on the constituent element of the nanoparticles. No free Fe ions released by FeNPs were found, whereas CoNP and NiNP dissolution was dose- and time-dependent. However, CoNP suspensions showed higher ion concentrations compared to those of NiNPs. In relation to the high soluble Co content, our results would tend to exclude the effect of sonication on NP dissolution.

III. *In vitro* toxicity induced by NPs on the three cell models.

Toxic effects were observed in all case, i.e. when the three different NPs were used to treat each of the three cell line models used. However, in all the *in vitro* models NP toxicity degree was different: CoNPs were the most toxic, followed by NiNPs and FeNPs. The same toxicity ranking was observed also when the corresponding ions were considered; this rank is probably related to the physiological role of these elements. Although the similar NP toxicity ranking, the three different cell lines showed different susceptibility. In particular, lung epithelial cells (A549) were more

susceptible compared to dermal fibroblast (L929), the latter being more sensitive than hepatocytes (HepG2). A direct relation between toxicity and dissolution degree of NP was found. Furthermore, a peculiar bimodal trend in NiNP dose-response curves was observed. We demonstrated that this behaviour ensue from two simultaneous but independent mechanisms responsible for NiNP toxicity that involve both NPs themselves and Ni ions released from the particles. This further confirms the great importance of chemical form in nanotoxicology research. During toxicological studies, high concentrations of NPs and ions were tested. These concentrations can be compatible with the high local NP concentrations following *in vivo* exposure, due to both their internalization and biopersistence. Furthermore, the wide range of concentrations allowed us to obtain dose-response curves and toxicity benchmarks (i.e. EC50 values) that can be used to identify sub-lethal doses useful for investigate NP toxicity mechanisms.

IV. Cellular uptake of NPs and their corresponding ions.

We found that NPs are internalized more easily than relative ions. The exposure of the three types of cells to Fe-, Co- and Ni NPs led to a large increase in the concentration of the metal constituent of the particles, confirming the ability of NPs to enter cells. Such increase was much less pronounced for the corresponding ionic forms. The different levels of uptake do not explain differences in their toxicity. Indeed, despite the highest toxicity of CoNPs, they are internalized less than NiNPs and FeNPs. Under our experimental conditions, it was not possible to establish whether the intracellular metal was still in the form of particles or ions or both. In addition, cell susceptibility is partially related to internal dose, as shown by the high susceptibility of lung epithelial cells (A549) and the low sensitivity of hepatocytes (HepG2) which internalize huge and low amount of NPs respectively. Moreover, study of the subcellular distribution of the internalized metals would be necessary to establish whether their metabolic fate are similar for the metallic NPs considered.

Overall, the present *in vitro* research comparing metallic NPs constituted by elements with similar physico-chemical properties suggests that the evaluation of NPs toxicity should be performed on a case by case basis, being very difficult to predict the metallic

NP toxicological properties on the basis of their chemical affinity. Our results represent the basis for future investigations concerning the assessment of toxicity of metal-based nanoparticles. This study rises some concerns related to the development of new nanotechnologies and their impact on human health and the environment. Among several chemical elements with similar physico-chemical properties, as ferromagnetism of *Iron Triad*, it could be useful to select the most physiological elements for a well-defined biological target. This allows to take advantage from nanotechnology permitting the biological systems to manage it safely.